DOCUMENT NO. SM-TM 8156-202

X67-39967

RE-ENTRY F SPACECRAFT STRUCTURAL MECHANICS
STAGE 3 RELEASE

CONTRACT NAS-1-6039

MARCH 17, 1967

AEROMECHANICS AND MATERIALS LABORATORY
SYSTEMS AND TECHNOLOGIES SECTION

Approved by:

Bachert FOR A.M GARBER

A. M. Garber, Manager
Structural Mechanics Technology Component

GENERAL ELECTRIC
RE-ENTRY SYSTEMS DEPARTMENT
A Department Of The Missile and Space Division
3198 Chestnut Street, Philadelphia 4, Penna.

CONTENTS

CONTENTS (Cont'd)

CONTENTS (Cont'd)

I. INTRODUCTION

This report represents the Stage 3 structural analysis of the Re-entry F Spacecraft (Turbulent Heating Experiment), and demonstrates the structural integrity of the spacecraft. The report includes structural design loads and criteria, the structural environments and the stress analysis. The inboard profile of the spacecraft is as shown in Figure 1.

The report represents the combined efforts of the following personnel:

W. Castle

G. Kachadourian

J. Marron

J. McMullen

B. Resnick

G. Ritchie

II. SUMMARY

The structural adequacy of the design to date is demonstrated by the following list of the critical margins of safety:

Item	Load Condition	Type of Loading	M.S.	Ref. Page
<u>Calorimeter</u>				
Calorimeter Shell	J	Thermal & Inertial	HIGH	
Bolted Joint 45.0	J	Joint Separation	+0.01	
Bolted Joint 68.0	J	Joint Separation	+0.26	
Field Joint 93.4	C	Joint Separation	AMPLE	
Bolted Joint 115.0	C	Joint Separation	AMPLE	
Bolted Joint 139.2	C	Joint Separation	AMPLE	
Interface Joint	C	Pin Bending	+0.27	
Expansion Joint	J	Bearing	HIGH	
Breech Joint	J	Bending	HIGH	
Antenna Windows	J	Thermal Stress	HIGH	
<u>Fwd. Substructure</u>				
Fwd. Shell Segment	C	Buckling	HIGH	
Mid Shell Segment	C	Buckling	HIGH	
Aft Shell Segment	J	Tension	HIGH	
Ring, Stat. 48.0	J	Rivet Shear	+0.10	
Ring, Stat. 60.8	J	Bolt Tension	+0.04	
Ring, Stat. 70.1	J	Rivet Shear	+0.23	
Ring, Stat. 90.0	G	Rivet Shear	HIGH	
Expansion Joint Pins	J	Pin Bending	HIGH	
Ballast Tube Ass'y	A	Tension	HIGH	
Ballast Fitting	J	Bending	HIGH	
Ballast Retainer	G	Bearing	HIGH	
<u>Aft Substructure</u>				
Support Bracket	J	Bending	+0.40	
Rails	J	Crippling	+0.35	
Aft Rail Angles	J	Bending	+0.98	
Support Clips	J	Crippling	HIGH	
Aft Bulkhead	J	Crippling	AMPLE	

Item	Load Condition	Type of Loading	M.S.	Ref. Page
Miscellany				
Payload Retent. Stud	J	Bearing	+0.07	
Antenna Frames	J	Pin Bending	+0.13	
Umbilical Disconnect	K	Bending	+0.05	
Aft Cover				
Beam	J	Crippling	+0.23	
Disc. Phen. Glass	J	Bending & Membrane	+0.23	
Circular Stiffener	J	Bending	HIGH	
Equipment Package				
Battery Fitting	J	Bending	HIGH	
Mounting Tee	J	Bending	HIGH	
Rivets, Tee-to-Bulkhd.	J	Shear	+0.02	
Panel	J	Bending	HIGH	
Guide	A	Bending	+0.68	
Fwd Bulkhead	J	Bearing	HIGH	
Aft Bulkhead	G	Bending	+0.11	

The following additional information is brought out in the analysis:

Beryllium shell distortions at the scalloped joints are

Joint Station	Radial Distortion, Inches
45	0.011
68	0.027
115	0.032
139	0.033

The preload for the bolts at the beryllium joints is

2800 ± 300 pounds

at room temperature. This is obtained with a torque of 140 ± 10 inch-lbs on the 1/4-inch diameter bolts.

Nose tip belleville springs preload is 470 ± 175 pounds.

For the nose tip low temperature (482°F) cure of the C-10 bond, the analysis shows some risk of bond or porous carbon failure, due to wide variance of Material properties . . . data is still rather undefinitive. Margins range from -.26 using worst mechanical properties and minimum strengths to +1.90 using average mechanical properties and minimum strengths.

For the C-10 bonding at high temperatures (1560°F), higher risk of nose tip scrappage is involved since even use of average mechanical properties and minimum strengths give negative margins of -.42 and -.39.

Bonding of the PD-162A presents no problem for the nose tip.

Powered flight loads on the nose tip produced HIGH or AMPLE margins of safety, even with assumptions of 25% bond efficiency for C-10 and 50% for the PD-162A. Conditions C and L were critical.

Thermal expansion problems are negligible now that the composite ATJ-PG nose plug (Figure 47) is part of the design. Maximum stress calculated due to plug expansion within its cavity is only 250 psi.

The minimum margin in the nose tip during flight is +.03 due to bearing of the nose plug in its cavity at maximum loads time, where all axial load is assumed to pass through the plug region. A small area in bearing was considered after compression of the graphite felt.

Thermal stresses show a minimum margin at station 3.55 in the ATJ shell transition area but are still quite HIGH, M.S. = 2.27 for tension.

With a manufactured gap of 0.100 inch between nose tip and beryllium calorimeter, the calculated minumum gap at re-entry is still .017

The required radial step at the nose tip-beryllium calorimeter interface is .042 inch.

III. GROUND RULES

A. CRITERIA

The structural design criteria is based on that of the Scout Booster vehicle, Reference 12, and is summarized below:

Limit load	=	Maximum load on structure
Yield load	=	1.15 x limit load
Ultimate load	=	1.50 x limit load

For stress criteria, there shall be no yielding at limit load and no failures at ultimate load; for stability, there shall be no elastic buckling at ultimate load; and for deflections, clearances between calorimeter and substructure shall also be maintained. Exception to this criteria is that certain structural components may be allowed to yield, providing the system can be shown to operate properly, with no failure of structure or function. Margins of safety between 0 and 0.99 are indicated numerically, those between 1.0 and 1.99 are listed as "AMPLE" and those greater than 2.0 are listed as "HIGH".

B. DRAWINGS

The spacecraft drawings are shown on the drawing tree, ER47R197812.

C. LOADS

The structural loads are obtained from Reference 10 and are summarized in Table I. In two instances, however, the loads have been covered in more detail or changed to meet design analysis requirements in the nose tip area and for the internal structure. This expansion on the loads information is shown in Figures 18 thru 24, 32 thru 34, and 43 thru 48.

1. NOSE TIP LOADS

The nose loads in Figure 48 have been calculated for re-entry using the pressure distribution given in Figure 49 (reproduced from Figure 15 of Reference 10). The loads are based on a C-10 bond failure between the ATJ graphite skirt and the porous carbon insulation. The net axial load on the ATJ nose is reacted at station 3.547 while the net lateral loads were assumed to act at stations 5.5 and 8.0 as point loads on the porous carbon.

TABLE 1. LIMIT LOAD CONDITIONS

Ltr.	Load Condition Description	Load Factors G_x Static	G_x Dyn. Equiv.	G_n Static	G_n Dyn. Equiv.	G_{spin} g's/inch	Notes*
A	Ground Handling	±3.0		3.0			6
B	Launch	-2.0	±19.2	-	±4.8		1,2,6
C	Max Qα	-4.8	±19.2	1.6	±4.8		1,2,5,6
D	First Stage Burnout	-5.2		-			1,5
E	Second Stage Ignition	-3.2	±20.0	-			1,3
F	Second Stage Burnout	-10.4		3.0			1,8
G	Third Stage Ignition	-5.2	±20.0	-			1,3
H	Third Stage Burnout	-12.8		-			1
I	Spin-up to 70 RPM	-		-	-	0.047	7
J	Re-entry	+23.0		7.0	-	0.139	1,5
K	Miscellany						
	• Separation						
	• Preloads						
	• Disconnect	-	-	-	-	-	800 lbs
	• Spin Test (300 RPM)	-	-	-	-	2.55	
L	Dynamic Axial	-	±13.0				4

*1. Acceleration
2. Random
3. Shock
4. Sinusoidal Test
5. Air Loads
6. Axial & Lateral Dynamic are not to be Combined
7. Tangential - Lateral
8. Also present are pitching G's per inch of 0.028 acting to decrease G_n aft

2. INTERNAL STRUCTURE LOADS

The internal structure loads have been recalculated, since those shown in Reference 10 are unfortunately largely based on an obsolete design used in the first dynamic model (this was the only information available at that time). Accordingly, the weight distributions for the forward substructure, aft substructure and equipment package were revised. The load factors of Conditions C, G, and J (obtained from Table 1) were used to obtain the diagrams shown in Figures 18 thru 24 (forward substructure), 32 thru 34 (aft substructure) and 43 (equipment package).

D. STRUCTURAL ENVIRONMENTS

1. EXTERNAL LOADS

Tables 2 and 3 show the latest interface loads obtained from References 13 and 15. These loads, used for both system testing and for inputs to the dynamic loads analysis, are considered "external loads". For sinusoidal, random and shock environments, they are considered to act at station 156.0 on the spacecraft.

2. INTERNAL LOADS

Table 4 shows the recommended component qualification levels. The components will survive the system testing (and, ergo, the flight environment) to the levels of Tables 2 and 3 if they receive these component test levels. The levels were agreed to as being within NASA philosophy at a January 26, 1967 meeting at NASA/LRC.

The stated levels are to be monitored in the EDM system test to check the actual component responses. If they are predicted to be too high, the following five alternatives are being considered:

Component equipment shelf isolation

Individual component isolation

Incorporation of damping in the shelf design

Obtain buy-off for narrow-band resonant peaks

Employing notching or cutting-back input (interface) levels to limit component responses to their component qualification levels

TABLE 2. REVISED INTERFACE QUALIFICATION VIBRATION, SHOCK AND ACOUSTIC NOISE REQUIREMENTS

Type Test	Axis	Input Level	Frequency Range, cps	Test Time
Sinusoidal	Thrust	0.075 in. D. A. ±1.5g ±3g	5-20 20-50 50-2000	Log sweep 2 oct/min
		±3g	50-70	24 sec
Random	Thrust	0.00405g^2/cps 5.32db/oct 0.0488g^2/cps overall level 7.5g rms	20-330 330-1350 1350-2000	2 min
	Transverse & Normal	0.00101g^2/cps 5.32db/oct 0.01216g^2/cps overall level 3.75g rms	20-330 330-1350 1350-2000	2 min
Shock	Axial	One half-sine pulse, 10-15 ms, 30 g's, Applied 3 times.		
Acoustic Noise	Powered Flight	154 db		
	Re-entry	Later		

TABLE 3. REVISED INTERFACE ACCEPTANCE VIBRATION, SHOCK AND ACOUSTIC NOISE REQUIREMENTS

Type Test	Axis	Input Level	Frequency Range, cps	Test Time
Sinusoidal	Thrust	±1.0g ±2.0g	20-50 50-2000	Log sweep 4 oct/min
		±2.0g	50-70	12 sec
Random	Thrust	$0.0018g^2$/cps 5.32db/oct $0.0217g^2$/cps overall level 5.0g rms	20-330 330-1350 1350-2000	1 min
	Transverse & Normal	$0.00045g^2$/cps 5.32db/oct $0.0054g^2$/cps overall level 2.5g rms	20-330 330-1350 1350-2000	1 min
Shock	Axial	One half-sine pulse, 10-15 ms, 20 g's, applied three times.		
Acoustic Noise	Powered Flight	150 db		
	Re-entry	Later		

TABLE 4. COMPONENT TEST REQUIREMENTS

Type of Excitation	Direction	Frequency Range, cps	Qualification Amplitude	Qualification Time	Acceptance Amplitude	Acceptance Time
Sinusoidal	Axial Transverse and Normal	10-200	5.0 g (0-peak) 0.5 inch d.a. limited	1 oct. per min each axis	3.33 g (0-peak) 0.5 inch d.a. limited	2 oct per min each axis
		200-2000	10.0 g (0-peak)		6.67 g (0-peak)	
Random	Axial Transverse and Normal	20-80 80-200 200-1200 1200-2000	0.02 g^2/cps +5.7 db/octave 0.12 g^2/cps -12.0 db/octave 12.4 grms overall	2 minutes per axis	0.0089 g^2/cps +5.7 db/octave 0.053 g^2/cps -12.0 db/octave	
Shock	Axial Transverse and Normal		Peak terminal sawtooth, 10-15 milliseconds. 60 g's		None	

Two schemes presently under study are:

To waive sinusoidal component qualification for those components already qualification tested to 0.4 to 0.6 g^2/cps random environments.

A single qualification test of the entire equipment package.

3. DYNAMIC ANALYSIS

The response of the Re-entry F vehicle to sinusoidal vibration, random vibration and shock was examined by the use of a dynamic model and several computer programs. This design is similar to the design shown on present drawings. The results of this analysis at mass-point 13 (a representative location on the equipment package) for the revised interface loads are listed in Reference 13 and shown in Figures 59, 60 and 61. Mass point 13 represents the environment for the majority of the components.

These figures show both the computer results and the recommended component qualification levels. In Figure 59, the sinusoidal levels are compared. The peak of 3.8 g's over the 10-200 frequency band is raised to 5.0 g's and the 20.8 peak in the 200-2000 band is resolved to 10.0 g's. The latter decision was made because:

The 10.0 g level matches other similar re-entry programs

The components probably will not all withstand 20.8 g's

Any troublesome responses found in the system test can be "fixed" using the methods listed in Section III. D. 2

Axial and lateral random environments for typical components are shown in Figures 60 and 61. Figure 60 shows both the present recommended levels and those previously recommended in Kachadourian's Reference 34, a document which was based on flight test data from Reference 14. It should be noted that present recommended levels are at least 1.2 times as high as Kachadourian's (which were already admittedly conservative). Also in both Figures, qualification levels efficiently clip or contain the two resonant axial peaks and the four lateral peaks of spectral density.

There are then on Figures 60 and 61 five contributors to establishment of the required component qualification random vibration levels:

Axial response curves of a representative spacecraft location

Lateral response curves

Separately derived component response levels by Kachadourian

Customer tentative agreement

Actual levels that components are historically tested to

Shock testing recommendations in Table 4 are taken from the maximum levels given in Reference 34, which stated that on the basis of shock spectrum data from the Scout vehicle flight data Re-entry F components should be shock tested to:

Longitudinal - 50g - 10ms terminal peak saw-tooth

Transverse - 60g - 10ms terminal peak saw-tooth

It is concluded, therefore, that the present component qualification levels (listed in the internal environment specification) should be revised to the levels shown in Table 4 of this report.

E. TEMPERATURES

Room temperature material properties are used for all load conditions except re-entry.

During re-entry, prior to initial calorimeter melt, it has been shown (Figure 3.12.2, Reference 19) that the forward and aft substructure assemblies will have a negligible increase in temperature. Consequently, except for the parts which attach to the calorimeter, the assemblies are assumed to be at room temperature during re-entry.

During re-entry, the beryllium calorimeter is most critical (structurally) at the time of initial calorimeter melt. This occurs at about station 48 (inches) for natural transition at an altitude of about 49,000 feet and at time 35.26 seconds from 300,000 feet (Figures 3.9.1 and 3.10.4, Reference 19). For the tripped transition condition initial melt occurs at about station 9 (inches) at about 60,000 feet at about time 33.91 seconds from 300,000 feet (Figures 3.9.2 and 3.10.9, Reference 19). The natural transition condition is more critical and the temperature distributions used in the analysis are shown in Figure 7.

The temperature distributions in the calorimeter which are used for the thermal strain distortion of the outer surface of the calorimeter are those shown in Figure 2 (Figures 3.10.4, 3.10.5 and 3.10.8, Reference 19) and in Figures 3 thru 6 (obtained from Thermodynamics computer runs of 8/15/66 and 11/17/66).

Temperature distributions in the old beryllium oxide VHF and C-band antenna windows are given in Figure 15 (Figures 3.13.1 and 3.13.2, Reference 19). For the fuzed silica (present design) windows, the temperatures are as shown in Figure 16. The aft cover temperatures during the re-entry period were obtained from Reference 18 and are shown in Figure 41.

The nose temperature distributions were taken from Reference 19 (Figures 4.1.1 thru 4.1.5) and unpublished data provided by Thermodynamics. These temperature distributions are shown in Figure 50.

IV. CALORIMETER ANALYSIS

A. BERYLLIUM SHELL DISTORTIONS

1. GENERAL

During re-entry, the calorimeter joints will have different (cooler) temperature distributions than those in the shell away from the joints. This will cause distortion along the meridians of the conical shell. Since the joints will have lower average temperatures than the shell between joints, the joints will not expand as much as the "free" shell. The maximum distortions will occur at the end of the experiment at the time the beryllium shell just reaches melting temperature.

2. TEMPERATURES

The temperature distributions, in the shell away from the joints are given in Figures 3.10.1 through 3.10.8 of Reference 19 and are the distributions used for the analysis. They are reproduced in Figure 2, and are those which exist at the time of initial calorimeter melt (at station 48) at 49,000 feet altitude (at time 35.3 seconds after 300,000 feet altitude).

Temperature distributions in the bolted joint regions are shown in Figures 3 through 6 for two designs - scalloped (current design) and unscalloped. These temperatures are taken from the results of computer programs (Program THTB) run on 11/15/66 and 11/17/66 by the Thermodynamic Technology Component (V. Hann). Although the joint locations used in the thermodynamic analysis do not coincide with actual locations on the spacecraft, it is assumed that the resulting joint deflections will be approximately linear between stations 68 and 139.25 such that the deflections at the true joint locations can be obtained by linear interpolation.

3. SUMMARY

Both the solid and scalloped joint designs were studied with the following calculated results for radial distortion:

SOLID

Joint Station	Distortion
45	0.023
68	0.040
115	0.061
139	0.069

SCALLOPED

45	0.011
68	0.027
115	0.032
139	0.033

4. ANALYSIS

The following procedure is used in this analysis. The radial thermal expansion of the "free" (i.e., no joints or other discontinuities) calorimeter shell is calculated at various points along a meridian. Also, the radial thermal expansion of "free" (i.e., no cylinder) ring joints are calculated. Using linear extrapolation to find the radial deflections for points at which no temperatures are available, the shell distortions due to thermal stresses can be calculated by taking the difference between the radial deflections for the free shell and the free ring joints.

Poisson's ratio is assumed to be constant in all directions for both elastic and inelastic stresses. Radial stresses thru the calorimeter thickness are neglected. Using stress-strain diagrams for different temperatures for beryllium (Figures 2-22 and 2-23 of Reference 21) and the thermal expansion coefficient (Reference 20) for different temperatures, the hoop strain in a free shell can be calculated for any temperature distribution through the shell thickness using the method given in section IV.B. (Beryllium Shell Strains). In the same way, the hoop strain in a joint can be calculated. The hoop strain is equal to the radial strain; consequently, the radial distortion of the shell from the "free" shell position at any joint will be about

$$\Delta_s = r\left[(e_s)_{shell} - (e_s)_{joint}\right]$$

It has been found that for the "free" shell, the hoop strain can be closely approximated without going through a lengthy analysis, such as shown in section IV B. The hoop strain was determined subject to the condition that the outer surface of the calorimeter is at least 2000^{o}F or above. If this condition has been met, the hoop strain can be determined as follows:

$$(e_s)_{shell} = \alpha_1 (T_1 - 70^{o})$$

where α_1 (coefficient of thermal expansion in inch/inch/^{o}F) and T_1 (temperature in ^{o}F) are evaluated at the temperature given at t_1 = 0.39 inch from the outer surface. For time 35.3 seconds (at 49,000 feet altitude) the following temperatures (Reference 19) and strains exist in the free shell:

Station, x (inches)	T_1 (^{o}F)	α_1 (10^{-6} in/in/^{o}F)	$(\epsilon_s)_{shell}$ (in/in)
48	1060	8.50	0.00841
72	1140	8.59	0.00919
144	1020	8.46	0.00805

It has been found that for the scalloped joints, the hoop strain can be closely approximated without lengthy analysis provided the computer element #102 is above 1700^{o}F. If $T_{153} \geq 1700^{o}$F then the strain is given by the following:

$$(e_s)_{joint} = \alpha_1 (T_1 - 70^{o}F)$$

where α_1 and T_1 are evaluated at the temperature of element #502. For time 35.3 seconds (49,000 feet altitude) the following temperatures and strains exist in the scalloped joint areas:

Station, x (inches)	T_1 (^{o}F)	α_1 (10^{-6} in/in/^{o}F)	$(\epsilon_s)_{joint}$ (in/in)
72	759^{o}F	8.07	0.00555
144	748^{o}F	8.05	0.00545

It is estimated that the strain of scalloped joint at station 48 would be about 0.00550 in/in. Using linear interpolation the following deflections from the free shell position can be calculated:

Station (inches)	Radius, r (inches)	$(e_s)_{shell}$	$(e_s)_{joint}$	Δ_s (inches)
45	3.94	0.00831	0.00549	0.011
68	5.95	0.00906	0.00554	0.027
115	10.07	0.00851	0.00549	0.032
139	12.17	0.00813	0.00546	0.033

For the non-scalloped joint design it has been found that the hoop strain at the joints can be approximated (provided computer element #102 is above 1700°F) by the following:

$$(e_s)_{joint} = \alpha_1 (T_1 - 70^{\circ}F)$$

where α_1 and T_1 are evaluated at the temperature of element #703. For time 35.3 seconds (47,000 feet altitude) the following temperatures and strains exist in the joints:

Station (inches)	T_1 (°F)	α_1 (10^{-6} in/in/°F)	$(e_s)_{joint}$ (in/in)
72	411	7.09	0.00242
144	420	7.12	0.00249

For the non-scalloped joint design it is estimated that the strain at station 45 will be about 0.000242 in/in. Using linear interpolation the following deflections from the free shell position are calculated for the non-scalloped joints:

Station (inches)	Radius, r (inches)	$(e_s)_{shell}$	$(e_s)_{joint}$	Δ_s (inches)
45	3.94	0.00831	0.00242	0.023
68	5.95	0.00906	0.00242	0.040
115	10.07	0.00851	0.00247	0.061
139	12.17	0.00813	0.00249	0.069

Due to the complexity of the problem, all of the calculated deflections can only be approximate and it is recommended that more detailed analyses be performed if accuracy to more than one significant figure is desired.

B. BERYLLIUM SHELL STRAINS

1. GENERAL

The calorimeter consists of seven conical shell frustums mechanically attached together. The material is beryllium (2% BeO) and the normal thickness of the shell is 0.600 inch. The cone angle is 5^{o}.

This analysis is primarily concentrated on the strains which occur in the shell away from any discontinuities such as the mechanically attached joints.

2. LOADS

The beryllium calorimeter is most critical during Load Condition J, re-entry, at the time the outer surface just reaches melting temperature. The spacecraft loads are as shown in Figure 12, 13 and 14 of Reference 10. The stresses and strains in the calorimeter due to the loads given in figures named above are negligible compared with thermal stresses and strains.

3. TEMPERATURES

The most critical temperature distributions through the calorimeter shell are taken from Reference 19 and are shown in Figure 7.

4. ANALYSIS - THERMAL STRAINS

The thermal strain distribution through the shell thickness is calculated based on the following assumptions and conditions:

a. The shell is assumed to act the same as a flat plate. This implies that the radius/thickness ratio is large. It is estimated that the results are sufficiently accurate for $R/t > 6$. This region would extend aft of station 45.

b. Discontinuities in the calorimeter are not considered.

c. A biaxial state of stress is assumed to exist and the radial stress component is neglected. The stresses and strains in the meridional and hoop directions are assumed to be equal.

d. Poisson's ratio is assumed to be constant for all temperatures and for any stress or strain.

The "free" thermal strain at each point through the plate thickness is calculated using the coefficient of thermal expansion for the temperature at that point by the following:

$$\epsilon_t \quad = \quad \alpha\,(T-T_o) \text{ where } T_o = 70^{o}F$$

The actual strain distribution through the thickness will be nearly a constant, ϵ_o. The strain due to thermal stress is the important result and is given by the following:

$$\epsilon_s \quad = \quad \epsilon_o - \epsilon_t$$

An iterative procedure is required to solve for the value of ϵ_o. This is accomplished as described below. A value for ϵ_o is assumed as a first approximation. Using the equation $\epsilon_s = \epsilon_o - \epsilon_t$, an approximate strain distribution due to thermal stress is determined. With the aid of stress-strain data for beryllium at various temperatures from Reference 21, an approximate thermal stress distribution is determined. Now, in order to have the sum of the forces about an element equal to zero, the following must be true:

$$\int_{o}^{0.6} f_t\,dt \quad = \quad 0$$

where f_t is thermal stress. If the integral is not zero, then the assumed value for ϵ_o is not correct. The above procedure must be iterated until the desired accuracy is obtained.

The calculated thermal strain distributions due to thermal stress are presented in Figure 8. A comparison of the calculated thermal strains (multiplied by 1.5 to give ultimate values) with the ultimate strains at failure is given in Figure 9. Assuming the compression strain at failure is at least as high as that for tension, the minimum margin of safety occurs at about $T = 1500^{o}F$ where $\epsilon_s = 0.8\%$ compression, ultimate and the allowable is at least 4.0%:

$$\text{M.S.} \quad = \quad \frac{4.0}{0.8} - 1 = \text{High}$$

5. ANALYSIS - SPACECRAFT LOADS

The maximum combined meridional load per unit of circumference in the calorimeter shell due to spacecraft loads during re-entry occurs at about station 65:

$$P = -1260 \text{ pounds, limit}$$

$$M = 34,200 \text{ inch-pounds, limit}$$

$$A = 20.5 \text{ sq. inches, area}$$

$$I/C = 55.0 \text{ inches}^3\text{, section modulus}$$

$$a = f\,t_o = t_o \left[\frac{P}{A} \pm \frac{Mc}{I}\right] = 0.600 \left[61.5 + 622.0\right]$$

$$= -410 \text{ pounds/inch, limit}$$

From the thermal strain analysis it was found that this load would cause a strain of less than 0.05% (ultimate). Thus, the spacecraft loading can be safely neglected and the results of the previous section are sufficiently accurate.

6. COMPUTER CHECK

A computer analysis was also performed for the beryllium shell thermal strains to back-up the hand calculations described in sections IV. B. 1 through IV. B. 5. It also provides a solution forward of Station 45, where the hand calculation, using flat plate theory becomes inaccurate.

An analysis was performed at stations 29.5 and 72.0 at time 35.5 seconds. The analysis was done using the plain strain assumption for the isotropic thick cylinder program (Reference 17). Then a secant - modulus iteration (Reference 30) was performed to determine the modulus in the plastic range.

A second thick cylinder was run using the plastic values of modulus and the final strains were extracted from this second run. The resulting thermal strains are shown in Figure 58 for stations 29.5 and 72.0. Comparison with the results of the hand solution of Figure 8 shows good agreement between the two.

Station 72 is a representative temperature profile for stations 96.0, 120.0, 144.0, and 156.0. Therefore, an analysis was not required at these stations. An investigation into higher altitudes showed lower thermal gradients at all stations and therefore no analyses were needed at these higher altitudes.

The scheme used to calculate the final strain utilizes the stress-strain relationships of Beryllium versus temperature and accurately predicts the iterative modulus in the plastic range. It is a valid analysis and shows the actual thermal strain throughout the shell.

C. FRUSTUM BOLTED JOINTS

1. GENERAL

The calorimeter conical shell sections are mechanically attached at five stations. NAS 1586 tension bolts, 1/4 diameter, are used as shown in Figure 10. The number of bolts and the locations are given below. The bolted field joint at station 93.44 is included in this analysis since the geometry is nearly identical with the other joints.

Station	Number of Bolts, N	Bolt Circle Radius, r (inches)	Bolt Spacing (inches)
45.00	12	3.02	1.56
68.00	16	5.03	1.96
93.44	24	7.27	1.90
115.00	30	9.14	1.91
139.25	36	11.26	1.96

2. LOADS

The two critical load conditions are load condition C (Max Q α, lateral) and load condition J (re-entry). During load condition C the parts are all at room temperature while during load condition J the joint temperature distributions at the time when the outer surface of the calorimeter just reaches melting temperature are given in Figure 3 (Station 72) and Figure 4 (Station 144) as examples.

3. ANALYSIS

Due to the relatively high stiffness of the clamped parts, the maximum bolt loads will be those due to preload and differential thermal expansion provided the net preload is greater than the maximum applied inertial and/or external pressure loads.

The allowable tension loads for the NAS 1586-4 bolts (Unitemp 212) are given below (linear interpolation is used for 500°F values):

			Load (pounds)	
Temperature	F_{ty} (ksi)	F_{tu} (ksi)	Yield	Ultimate
Room Temp.	130	185	4340	6180
500°F	126	168	4210	5610
1200°F	120	140	4000	4670

(Reference: NAS 1597)

Assuming the bolts are torqued at assembly to a preload of 2800 ± 300 pounds, the margin of safety for the bolts in tension at assembly will be

$$M.S._{ty} = \frac{4340}{3100(1.15)} - 1 = 0.22$$

The above margin of safety is valid only if the equivalent external limit load per bolt is less than the preload. Thus, for load condition C the maximum allowable limit bending moment for each of the four attachment stations can be expresses as

$$M_{max} = \frac{2500Nr}{2} = 1250\ (Nr)\ \ldots\ \text{limit}$$

For load condition J, the preload may be reduced because of differential thermal expansion. The strain in the beryllium "lugs" due to thermal stress is conservatively neglected to find the margin of safety for joint separation. It is conservative to assume both the bolts and the beryllium "lugs" are at 500°F. The calculated net preload for the above conditions will be about

$$T_1 = AE_1\ (y_o - y_1)/L$$

where A = 0.049 sq. in. (cross-section area of bolt)

$E_1 \cong 26.5 \times 10^6$ psi at 500°F for bolt (estimated)

$E_o \cong 29.0 \times 10^6$ psi at 80°F for bolt (estimated)

L = 1.30 inches (effective bolt length)

T_o = 2800-300 = 2500 lbs. (minimum initial preload)

and $$Y_o = \frac{T_o L}{AE_o} = \frac{2500\ (1.30)}{0.049\ (29.0 \times 10^6)} = 0.00229 \text{ inch}$$

$$Y_1 = L(T_1 - T_o)(\alpha_{bolt} - \alpha_{cal}) = 1.30\ (500 - 80)\ (\Delta\alpha) = 546\ \Delta\alpha$$

$\alpha_{bolt} \cong 9.5 \times 10^{-6}$ in/in/°F (80°F to 500°F, estimated)

$$\alpha_{Be} \cong 7.4 \times 10^{-6} \text{ in/in/}^{o}\text{F} \quad (80^{o}\text{F to } 500^{o}\text{F})$$

$$T_1 = 0.049\ (26.5 \times 10^{-6})(0.00229 - 0.00115)/1.45 = 1020 \text{ lbs. net preload (conservative)}$$

To avoid joint separation during re-entry, the maximum allowable combined limit loads for each of the five stations is given by

$$R_{max} = \left(P + \frac{2M}{r}\right)_{max} = 1020 \text{ N} \ldots \text{ limit}$$

It is probable that the bolt temperature will be somewhat lower than the beryllium temperature; thus, the true bolt preload may be much higher than previously calculated for re-entry. The maximum value would probably be not greater than the yield load at room temperature of 4340 pounds. This yield condition is not considered to be a failure for the bolts since the bolts will still function properly.

It is conservative to assume the calorimeter internal loads must be transfered across the joints by shear at the barrel nuts. The resulting calculated principal compressive stress (yield) is as follows:

$$f_{c_{max}} \cong \sqrt{f_c^{\,2} + f_s^{\,2}} \quad \text{(conservative)}$$

where $f_c \cong T/(d\,L - A)$

$f_s = (P + 2M/r)/dhN$

$d = 0.50$ inch, nut diameter

$L \cong 0.50$ inch, barrel nut length

$A = .0616$ sq. in. bolt hole area

$h = 0.465$ inch, shear length

For load condition C compression yield is critical and the maximum allowable limit moment will be

$$M_{max} = \frac{rdhN}{2(1.15)}\left[F_{cy}^{\,2} - f_c^{\,2}\right]^{1/2}$$

$$= rN\left[\frac{0.50(0.465)}{2(1.15)}\right]\left[(27.000)^2 - \left(\frac{3100}{0.250-0.0616}\right)^2\right]^{1/2}$$

$$M_{max} = 2165\ (Nr) \ldots \text{limit} \qquad \text{(Reference 4)}$$

For load condition J it is assumed that the maximum temperature at the point of maximum principle compressive stress is 500°F. Compression yield is critical with

$$F_{cy} \cong 21{,}600 \text{ psi} \qquad \text{(Reference 4)}$$

Assuming T_1 = 4340 lb preload, the maximum allowable combined limit load will be about

$$R_{max} = \left(P + \frac{2M}{r}\right)_{max} = \frac{2hN}{1.15}\left[F_{cy}^{\ 2} - f_c^{\ 2}\right]^{1/2}$$

$$= N\ \frac{(0.50)(0.465)}{1.15}\left[(21600)^2 - \left(\frac{4340}{0.2284}\right)^2\right]^{1/2}$$

$$= 2080\ (N) \ldots \text{limit}$$

4. SUMMARY AND MARGINS OF SAFETY

It has been shown that load condition C is most critical for joint separation at room temperature and the maximum allowable limit moment at any of the four joints is given by

$$M_{max} = 1250\ Nr$$

Using the actual loads given in Figure 8 of Reference 10, the following margins of safety result:

Station	M_{max} (kip)	M(kip)P Load Condition C	M.S.
45.00	45.3	20	AMPLE
68.00	100.5	50	AMPLE
93.44	218	95	AMPLE
115.00	342	145	AMPLE
139.25	506	205	AMPLE

Load condition J is most critical for joint separation at elevated temperature. The maximum combined limit load is given by the following equation:

$$R_{max} = \left(P + \frac{2M}{r}\right)_{max} = 1020N$$

The actual loads and margins of safety are as follows:

Station	R_{max} (lb)	Load Condition J			M.S.
		P (lb)	M (kip)	R (lb)	
45.00	12,230	-560	19	12,040	+0.01
68.00	16,300	-1400	36	12,920	+0.26
93.44	24,400	2650	40	8,350	AMPLE
115.00	30,600	1850	46.5	8,350	HIGH
139.25	36,700	-100	30	5,230	HIGH

D. FIELD JOINT

The field joint consists of twenty-four NAS 1586 tension bolts (1/4 diameter) located at station 93.44. This joint is nearly identical to the other four frustum bolted joints (shown in Figure 10). Thus, the analysis of the field joint is included in section IV.C. (Frustum Bolted Joints).

$$M_{allow} = \frac{119.5\,(0.196)(0.25)F_{ty}}{1.15\,(4)(0.45)} = 2.83\,F_{ty} \quad \text{or}$$

$$M_{allow} = 2.83\left(\frac{1.15}{1.50}\right)F_{tu} = 2.17\,F_{tu}$$

The shear pins are made of 17-4 PH (H 1025) with $F_{tu} = 155$ ksi and $F_{ty} = 140$ ksi.

$$M_{allow} = 2.17\,(155,000) = 336,000 \text{ in.-lb., limit}$$

The allowable limit load based on the peak bearing stress in the beryllium calorimeter hole is given below.

$$f_{br}(max) = \frac{Q}{DL} + \frac{6Q\,(x + L/2)}{DL^2} = \frac{4Q}{DL}\,(1 + 3x/2L)$$

$$Q_{allow} = \frac{DL}{4(1 + 3x/2L)}\;\frac{F_{bru}}{1.5} \qquad M_{allow} = 119.5\,Q_{allow}$$

$$M_{allow} = \frac{119.5\,DL\,F_{bru}}{1.5\,(4)(1 + 3x/2L)} = \frac{119.5\,(0.50)(0.70)(110,000)}{1.5\,(4)\;\;1 + 3[(0.15)/2\,(0.70)]}$$

$$= 579,000 \text{ in.-lb., limit}$$

Based on the average tension stress in the beryllium calorimeter acting as a "lug" at the pin hole, the maximum allowable limit load is calculated.

$$f_t = \frac{f_{br}\,D/2}{t_{eff}} = \frac{2Q}{L\,t_{eff}}\left(1 + \frac{3x}{2L}\right)$$

$$Q = \frac{f_t\,L\,t_{eff}}{2\left(1 + \frac{3x}{2L}\right)} \qquad M_{allow} = 119.5\,Q_{allow}$$

$$M_{allow} = \frac{119.5\,F_{ty}\,L\,t_{eff}}{2(1 + 3x/2L)\,(1.15)} = \frac{119.5\,(27,000)(0.70)(1.12 - 0.50)}{1.15\,(2)\,[1 + 3\,(0.15)/2\,(0.70)]}$$

$$= 460,000 \text{ in.-lb., limit}$$

The allowable limit load based on bearing in the shear pin hole in the closure ring is given below.

$$f_{br} = \frac{Q}{dt} \qquad M = 119.5\,Q$$

$$M_{allow} = 119.5\,dt\,F_{bry}/1.15 = 119.5\,(0.50)(0.20)\,88,000/1.15$$

E. INTERFACE JOINT

1. GENERAL

The calorimeter is attached to the aft closure ring by twenty 0.500 diameter steel shear pins at station 154.5 as shown in Figures 11 & 12. The aft closure ring is attached to the spacecraft interface ring by twenty-four tension bolts (NAS 1304). The interface ring is not analyzed in this report, since it is designed by Ling-Temco-Vought Corp.

2. LOADS

All parts of the joint are most critical during load condition C (Max $Q\alpha$, lateral). All parts are at room temperature for this condition. Material properties are taken from Reference 4.

3. ANALYSIS

The peak load per shear pin is given by

$$Q = \frac{2M}{Nr} = 0.00836M \text{ or } M = 119.5Q$$

where N = 20 shear pins

r = 11.95 inches radius

M is the bending moment at station 154.5

The allowable limit load based on pin ultimate shear is given by

$$Q_{allow} = F_{su}A/1.5$$

$$M_{allow} = \frac{119.5}{1.5} F_{su}A = \frac{119.5}{1.5}(0.196)F_{su} = 15.6\ F_{su}$$

The allowable limit loads based on pin bending for yield and ultimate are as follows:

$$f_b = \frac{M'c}{I} = \frac{4M'}{AR} = \frac{4}{AR}QK$$

$$Q = \frac{AR\ f_b}{4K} \qquad M_{allow} = 119.5\ Q_{allow}$$

$$M_{allow} = \frac{119.5\ AR}{4K}\ \frac{F_{ty}}{1.15} \quad \text{or} \quad \frac{119.5\ AR}{4K}\ \frac{F_{tu}}{1.5}$$

= 915,000 in.-lb., limit

The maximum tension stress at the net section of the closure ring at the shear pin hole is given by the following:

$$f_t = \frac{Q}{bh} + \frac{6Q\,(h/2-L)}{bh^2} = \frac{4Q}{bh} - \frac{6QL}{bh^2} = \frac{4Q}{bh}\left(1 - \frac{3L}{2h}\right)$$

$$M_{allow} = 119.5\ bh\ F_{tu}/1.5\ (4)(1 - 3L/2h)$$

$$= 119.5\ (1.00 - 0.56)(0.70)(60,000)/6\ [1 - 3(0.1)/2(0.7)] = 467,000 \text{ in.-lb. limit}$$

The maximum compressive bending stress in the closure ring (away from the four VHF window areas) will result in the following allowable limit load:

$$M_R = T_o K_M \qquad T_o = 0.448\ Q \qquad M = 119.5\ Q$$

$$K_M = 3.80 \quad \text{(based on ring analysis)}$$

$$f_b = M_R c/I$$

$$M_{allow} = 119.5\ I\ F_{cy}/1.5\ (0.448)K_M c$$

$$= 119.5\ (0.56)(55,000)/1.5\ (0.448)(3.60)(1.625)$$

$$= 886,000 \text{ in.-lb., limit}$$

In the closure ring at the VHF window areas, the maximum tensile stress due to bending results in the following allowable limit load:

$$M_{allow} = 119.5\ I\ F_{tu}/1.5(0.448)K_M c$$

$$= 119.5(0.294)(63,000)/1.5(0.448)(3.80)(0.81)$$

$$= 1,070,000 \text{ in.-lb., limit}$$

The maximum shear stress in the closure ring (away from the four VHF window areas) results in the following allowable limit load

$$V_{max} = \frac{T_o}{\pi r} K_s \qquad T_o = 0.448\ Q \qquad M = 119.5\ Q$$

$$K_s = 8.44 \quad \text{(based on ring analysis}$$

$$f_s \approx \frac{V_{max}}{A_{web}}$$

$$= 119.5\,(40{,}000)\,\pi\,(11.95)\left[0.060\,(2.3)\right]/1.5\,(0.448)(8.44)$$

$$= 4{,}380{,}000 \text{ in.-lb., limit}$$

All other sections of the closure ring are less critical for shear than the calculations given above.

The peak load for the tension bolts is given by:

$$Q_T = \frac{2M}{Nr} = 0.00877\ M$$

where N = 20 effective bolts

r = 11.5 inch radius of bolt circle

M is the moment at station 156

The allowable tensile load for NAS 1304 bolts (1/4 diameter) is 5340 pounds, ultimate. The allowable limit moment is given by:

$$M_{allow} = \frac{5340}{0.00877(1.5)} = 409{,}000 \text{ in.-lb., limit}$$

4. SUMMARY

The minimum margin of safety at the interface joint in the beryllium calorimeter occurs at the shear pin hole for tensile stress in the effective "lug":

$$M_{allow} = 460{,}000 \text{ in.-lb., limit}$$

The shear pin is most critical in bending:

$$M_{allow} = 336{,}000 \text{ in.-lb., limit}$$

The closure ring (2014-T6 hand forging) is most critical for the maximum tensile stress in the net section at the shear pins:

$$M_{allow} = 467{,}000 \text{ in.-lb., limit}$$

The tension bolts give

$$M_{allow} = 409{,}000 \text{ in.-lb., limit}$$

The maximum moment at station 156 for load condition C is obtained from Figure 8 of Reference 10:

$$M = 265{,}000 \text{ in.-lb., limit}$$

The minimum margin of safety is

$$MS = \frac{336,000}{265,000} - 1 = +0.27$$

F. EXPANSION JOINT

1. GENERAL

The expansion joint at station 90 consists of six pins which fit into steel bushings. The bushings (17-4PH, H1025) are located in the beryllium calorimeter with an interference fit. This analysis applies only to the bushings and calorimeter.

2. ANALYSIS

Load condition J, Re-entry, results in the maximum loads acting on the bushings. It is assumed that the average bushing temperature is about 500°F. The allowable compression yield stress for 17-4PH (H 1025) at 500° F is approximated by the following (2. 7. 4. 1, Reference 4):

$$F_{cy} \cong 178,000\left(\frac{155,000}{190,000}\right)(0.77)$$

$$\cong 112,000 \text{ psi}$$

The bushing diameter is 0. 50 inch and has a pin bearing area of about A = 0. 50 x 0. 125 = 0. 0625 sq. in. The maximum allowable limit load per pin is given by

$$Q_{allow} = A\frac{F_{cy}}{1.15} = (0.0625)\frac{112,000}{1.15} = 6090 \text{ lbs., limit}$$

The actual maximum load is obtained from Figure 12 of Reference 10 for which P = 5350 pounds:

$$Q = \frac{P}{6} = \frac{5350}{6} = 895 \text{ lbs. per pin}$$

$$M.S. = \frac{6090}{895} - 1 = \text{HIGH}$$

G. BREECH JOINT

1. GENERAL

The breech joint at station 24. 5 is shown in Figures 13 and 14. The joint consists of a 2. 75 inch diameter, 0. 25 pitch, one inch long Acme 4C thread with 8 longitudinal slots machined through the threads on both parts. A small metallic gasket is used to control the joint preload.

2. LOADS

At room temperature the joint is most critical for loads occurring during load condition C (Max $Q\alpha$ - lateral). The joint is also checked for the loads which occur during load condition J (re-entry). The maximum temperature of the threads during re-entry is taken to be 1000°F (this is estimated to be very conservative).

3. ANALYSIS

It is assumed that only 3 threads are effective which give $N = 3x8 = 24$ effective thread segments.

The maximum allowable limit load per segment can be found from the following:

$$f_b = \frac{6\ FhK}{Lb^2}$$

$$F_{max} = \frac{F_{ty} Lb^2}{1.15(6hK)}$$

where $K = 0.22 + \left(\frac{b}{r}\right)^{1/5} \left(\frac{b}{h}\right)^{2/5}$ (page 378, Ref. 5)

$L = 0.451$
$b = 0.159$ inch
$h = 0.073$ inch
$r = 0.030$ inch
F_{ty} is the allowable tensile yield stress for beryllium

At room temperature, $F_{ty} = 27,000$ psi (Reference 4).

F_{max} 287 pounds - limit

At 1000°F, $F_{ty} = 11,600$ psi (Reference 4).

$F_{max} = 123$ pounds - limit

The maximum applied load per thread segment is given by

$$F = CF_1 + F_o$$

$$F_1 = \frac{P}{N} + \frac{4M}{ND}$$

where P is the axial load at station 24.5
M is the bending moment at station 24.5
N = 24 effective thread segments
D = 2.625 inches - thread pitch diameter
F_o is the joint preload (lbs.)
C $\cong$ 1 (joint stiffness factor)

When the total joint preload is to be 1050 ± 300 pounds (limit), then the maximum preload per segment will be

$$F_o = \frac{1350}{N} = 56.2 \text{ pounds}$$

For load condition C the maximum allowable moment at station 24.5 will be approximately:

$$M_{max} = \frac{ND}{4}(F_{max} - F_o) = \frac{24(2.625)}{4}(287 - 56.2)$$

$$= 3640 \text{ in.-lb., limit}$$

For load condition J the maximum allowable combined load at station 24.5 is given by

$$(P_{eq})_{max} = \left(P + \frac{4M}{D}\right)_{max} = N(F_{max} - F_o)$$

$$\left(P_{eq}\right)_{max} = (P + 1.525\ M)_{max} = 24(123 - 56.2) = 1600 \text{ lbs., limit}$$

4. THERMAL EXPANSION

The radial thermal strain is conservatively taken to be 0.010 inch/inch during load condition J for the forward calorimeter section. Assuming the calorimeter section with the external threads is at room temperature, the radial differential thermal expansion will be about

$$\Delta R = 0.010\ R = 0.010\left(\frac{2.625}{2}\right) = 0.01325 \text{ inch}$$

The preload will be reduced since the threads are machined with 14.5° slopes. The forward calorimeter section will be "pushed" by the gasket a distance of

$$X = \Delta R \tan 14.5^\circ = 0.0034 \text{ inch}$$

Thus, the gasket will be "unloaded" by this amount of deflection. Note that the meridional differential thermal expansion will be negligible since an 0.010 inch gap is provided between the two calorimeter sections at station 24.5

The preload gasket should have the capability of maintaining some preload after the above calculated differential thermal expansion occurs.

5. SUMMARY AND MARGINS OF SAFETY

For a joint preload of 1350 pounds (maximum) limit combined with the spacecraft loads at station 24. 5, the margins at safety are given below for thread bending:

Load Condition	P (lb)	M (in. -lb.)	P_{eq} (lb)	P_{max} (lb)	M_{max} (in. -lb.)	M. S.
C	-	165	-	-	3640	HIGH
J	-120	140	94	1600	-	HIGH

The loads are obtained from Figures 12 and 14 of Reference 10 and from unpublished data provided by the Optimization and Synthesis Component.

H. ANTENNA WINDOWS

The analyses for both the Beryllium Oxide windows and Fuzed Silica antenna windows (latest design) are given here to show the rationale for the change in design. The analysis for the antenna window frames is given in Section V. D.

1. BERYLLIUM OXIDE WINDOWS

Four thicknesses of window were analyzed and negative margins of safety were obtained for both tension and compression for all four thicknesses:

BeO Thickness	Predicted Max. Stress	Allowable Stresses	Temp. °F	M. S.
1. 24	+ 80, 000 - 130, 000	+ 15, 000 - 40, 000	870 2200	- 0. 88 - 0. 80
0. 80	+ 47, 400 - 93, 600	+ 14, 000 - 35, 000	990 2315	- 0. 81 - 0. 76
0. 40	+ 34, 000 - 61, 700	+ 12, 000 - 30, 000	1400 2420	- 0. 77 - 0. 68
0. 20	+ 19, 870 - 15, 700	+ 6, 150 - 785	2150 3800	- 0. 80 - 0. 97

It will be noted that a factor of safety of 1. 50 was applied here in calculating margins of safety.

Temperature gradients from Figures 3.13.1 and 3.13.2 of Reference 19 and unpublished data generated by the Thermodynamics Technology Component were used for the analysis. Typical gradients are reproduced in Figure 15 of this report. A computer program (References 29 & 31) was used for determining stresses, treating the window as a free-free beam and using mechanical properties from Reference 25. The results are also shown in Figure 15. As can be seen, the shape of the stress distribution is such (compression-tension-compression) that no mechanical preload can be used to lower the stress level.

The influence of creep in alleviating the stresses in the BeO windows was investigated but proved to be of negligible help. Creep time is too long compared to the seconds available during re-entry.

2. FUZED SILICA ANTENNA WINDOWS

The present design of antenna window, shown in Figures 38 and 39, is a fuzed silica glass type 7941 construction (quartz). For the analysis, two thicknesses of window were studied, a 0.80 inch size and a 1.24 inch size, thus neatly bounding the present thicknesses of 1.19 inch for the VHF and 1.10 inch for C-Band window. Positive margins of safety are demonstrated by use of the results shown in Figure 16 and and the following tabulation:

Quartz Thickness	Predicted Max. Stresses	Allowable Stresses	Temp. °F	M. S.
1.24	+ 846 - 2781	5200 36800	115 1048	HIGH HIGH
0.80	+ 998 - 1774	5250 35900	158 1172	HIGH HIGH

Temperature gradients were obtained from unpublished data generated by the Thermodynamics Technology Component and these are shown in Figure 16. The computer program discussed in References 29 and 31 was again used with mechanical properties inputted from Reference 33 (which gives conservative elastic moduli and coefficients of thermal expansion). To obtain the allowable stresses, Reference 16 was consulted. . . Page No. 30.3.2.2.1.

V. INTERNAL STRUCTURE

A. FORWARD SUBSTRUCTURE

1. GENERAL

As shown in Figure 17, the forward substructure consists of a ring-stiffened shell type assembly. The shell consists of three segments all of which are made of 0.063 inch thick 2024-T3 aluminum alloy. Each shell segment of the substructure is described and analyzed below, using the loads shown in Figures 18 to 24.

2. FORWARD SHELL SEGMENT

The forward shell segment is conical in shape and extends from station 48.67 to 60.34. The shell has radii of 3.55 and 4.55 inches at its forward and aft ends, respectively. The maximum compression loads in the shell are due to limit load condition C, Maximum $Q\alpha$, where from Figures 18, 19 and 20 it is found that the axial, shear and bending limit loads are

$$P = -3800 \text{ lbs}$$

$$V = 110 \text{ lbs}$$

$$M = 11000 \text{ in-lbs}$$

The allowable axial load is determined by:

$$\rho = \frac{R}{\cos \phi} = \frac{3.55}{\cos 4^{\circ}54'} = 3.56 \text{ inches}$$

$$\frac{\rho}{t} = \frac{3.56}{0.063} = 56.5$$

$$\frac{L}{\rho} = \frac{60.34 - 48.67}{\cos 4^{\circ}54' (3.56)} = \frac{11.72}{3.56} = 3.29$$

$$\frac{F_c \times 10^3}{E} = 9 \qquad \text{(Reference 22)}$$

$$F_c = 9 (10.7 \times 10^6)(10^{-3}) = 96,300 \text{ psi}$$

$$\text{Use } F_c = F_{cy} = 45,000 \text{ psi}$$

$$P_c = F_{cy} (2\pi Rt) = 45,000 (1.4) = 63,000 \text{ lbs}$$

35

The allowable bending load is:

$$\frac{F_b \times 10^3}{E} = 10 \qquad \text{(Reference 22)}$$

$$F_b = 10\ (10.7 \times 10^6)(10^{-3}) = 107,000 \text{ psi}$$

$$\text{Use } F_b = F_{cy} = 45,000 \text{ psi}$$

$$M_{cr} = F_b\ \pi R^2 t = 45,000\ (2.49) = 112,000 \text{ in-lbs}$$

The allowable shear load is:

$$F_s = 1.4\ F_{st}$$

$$\frac{F_{st}}{E} = 0.0027 \quad \text{(Reference 22)}$$

$$F_{st} = 0.0027(10.7 \times 10^6) = 28,900 \text{ psi}$$

$$F_s = 1.4\ (28,900) = 40,400 \text{ psi}$$

$$V_s = F_s\ (\pi R t) = 40,000\ (0.702) = 28,100 \text{ lbs}$$

Using the following interaction equation the margin of safety is shown to be positive.

$$(R_c + R_b + R_v)^{1.2} = 1 \qquad \text{(Reference 22)}$$

$$R_c = \frac{3800 \times 1.5}{63000} = 0.0905$$

$$R_b = \frac{11000 \times 1.5}{112000} = 0.1470$$

$$R_v = \frac{110 \times 1.5}{28100} = 0.00588$$

$$[0.0905 + 0.1470 + 0.0059]^{1.2} = .183$$

This is less than 1.0, thus the section will not buckle under the given combined loading.

M.S. HIGH

The maximum tension loads in the shell are due to limit Load Condition J, Re-entry, where G_x and G_n are +23.0 and 7.0, respectively. From Figures 21, 22 and 23 the limit loads are found to be

$$P = 3580 \text{ lbs}$$

$$V = 140 \text{ lbs}$$

$$M = 12{,}200 \text{ in-lbs}$$

The equivalent tensile load in the shell is:

$$P_{eq} = \frac{2M}{R} + P = \frac{2(12{,}200)}{3.55} + 3580$$

$$= 6870 + 3580 = 10{,}450 \text{ lbs}$$

$$A = 2\pi Rt = 6.28\ (3.55)(0.063) = 1.40 \text{ in.}^2$$

$$f_{eq} = \frac{10{,}450 \times 1.5}{1.40} = 11{,}200 \text{ psi, ultimate}$$

$$F_{tu} = 63{,}000 \text{ psi}$$

$$M.S. = \frac{63{,}000}{11{,}200} -1 = \text{HIGH}$$

The shear stress in the shell is:

$$f_s = \frac{V}{\pi Rt} = \frac{140 \times 1.5}{\pi\,(3.55)(0.063)} = 265 \text{ psi}$$

$$F_{su} = 40{,}000 \text{ psi}$$

$$M.S. = \frac{40{,}000}{265} -1 = \text{HIGH}$$

3. MID SHELL SEGMENT

The mid shell segment is cylindrical in shape and extends from station 61.3 to 69.78 and has a radius of 4.62 inches. The maximum compression loads in the shell are due to Load Condition C, where from Figures 18, 19 and 20 the axial, shear and bending loads are:

$$P = 3900 \text{ lbs}$$

$$V = 310 \text{ lbs}$$

$$M = 9200 \text{ in-lbs}$$

The allowable axial load is:

$$\frac{R}{t} = \frac{4.62}{0.063} = 73.2$$

$$\frac{L}{R} = \frac{69.78 - 61.3}{4.62} = \frac{8.48}{4.62} = 1.84$$

$$\frac{F_{c_{cr}}}{E} = 0.0078$$

$$F_{b_{cr}} = 0.0078\,(10.7 \times 10^{6}) = 83{,}500 \text{ psi}$$

$$\text{Use } F_c = F_{cy} = 45{,}000 \text{ psi}$$

$$P_c = F_{cy}\,(2\pi Rt) = 45{,}000\,(1.83) = 82{,}500 \text{ psi}$$

The allowable bending load is:

$$\frac{F_{b_{cr}}}{E} = 0.007 \qquad \text{(Reference 22)}$$

$$F_{b_{cr}} = 0.007\,(10.7 \times 10^{+6}) = 74{,}900 \text{ psi}$$

$$\text{Use } F_{b_{cr}} = F_{cy} = 45{,}000 \text{ psi}$$

$$M_{b_{cr}} = F_{b_{cr}}\,\pi R^2 t = 45{,}000\,(4.21) = 190{,}000 \text{ in-lbs}$$

The allowable shear load is assumed to be 1.25 times that for torsion.

$$\frac{F_{st}}{E} = 0.0022$$

$$F_s = 1.25\,F_{st} = 1.25(0.0022)(10.7 \times 10^{6})$$

$$= 29{,}400 \text{ psi}$$

$$V_{cr} = F_s\,\pi Rt = 29{,}400\,(0.91) = 26{,}800 \text{ lbs}$$

The interaction equation for combined axial, shear and bending loads is:

$$R_c + \left[(R_s)^3 + (R_b)^3\right]^{1/3} = 1 \qquad \text{(Reference 22)}$$

$$R_c = \frac{3900 \times 1.5}{82,500} = 0.071$$

$$R_s = \frac{310 \times 1.5}{26,800} = 0.0173$$

$$R_b = \frac{12200 \times 1.5}{190,000} = 0.0965$$

$$0.071 + \left[(1.73 \times 10^{-2})^3 + (9.65 \times 10^{-2})^3\right]^{1/3} = 0.167$$

This is less than 1.0, thus the cylinder will not buckle.

$$M.S. = \text{HIGH}$$

The maximum tension loads in the shell are due to limit Load Condition J, Re-entry, where G_x and G_n are +23.0 and 7.0, respectively. From Figures 21, 22 and 23 the limit loads are found to be

$$P = 3750 \text{ lbs}$$

$$V = 340 \text{ lbs}$$

$$M = 10,300 \text{ in-lbs}$$

The equivalent tensile load in the shell is

$$P_{eq} = \frac{2M}{R} + P = \frac{2(10,300)}{4.62} + 3750$$

$$= 4470 + 3750 = 8220 \text{ lbs}$$

$$A = 2\pi Rt = 6.28\,(4.62)(0.063) = 1.83 \text{ in}^2$$

$$f_{eq} = \frac{8220 \times 1.5}{1.83} = 6730 \text{ psi}$$

$$F_{tu} = 63,000 \text{ psi}$$

$$M.S. = \frac{63,000}{6730} - 1 = \text{HIGH}$$

The shear stress in the shell is:

$$f_s = \frac{V}{\pi Rt} = \frac{340 \times 1.5}{\pi\,(4.62)(0.063)} = 558 \text{ psi}$$

$F_{su} = 40,000$ psi

$M.S. = \frac{40,000}{558} - 1 = \text{HIGH}$

4. AFT SHELL SEGMENT

The aft shell segment is conical in shape and extends from station 70.67 to 87.72. The shell has radii of 4.62 and 6.54 inches at its forward and aft ends, respectively. The maximum compression loads in the shell are due to Load Condition C, Maximum $Q\alpha$, where from Figures 18, 19, and 20 it is found that the axial, shear and bending loads are

$P = 4050$ lbs

$V = 340$ lbs

$M = 6300$ in-lbs

The allowable axial load is:

$$\rho = \frac{R}{\cos \phi} = \frac{4.62}{\cos 6^{\circ}45'} = \frac{4.62}{0.993} = 4.65$$

$$\frac{\rho}{t} = \frac{4.65}{0.063} = 74.0$$

$$\frac{L}{\rho} = \frac{87.72 - 70.67}{\cos 6^{\circ}45'(4.65)} = \frac{17.05}{0.993(4.65)} = 3.69$$

$$\frac{F_c \times 10^3}{E} = 5.3 \qquad \text{(Reference 22)}$$

$$F_c = 5.3(10.7 \times 10^6)(10^{-3}) = 56,800 \text{ psi}$$

$$\text{Use } F_c = F_{cy} = 45,000 \text{ psi}$$

$$P_c = F_{cy}(2\pi Rt) = 45.000\ (1.82) = 81,800 \text{ lbs}$$

The allowable bending load is:

$$\frac{F_b \times 10^3}{E} = 6.8 \qquad \text{(Reference 22)}$$

$$F_b = 6.8\,(10.7 \times 10^6)(10^{-3}) = 72{,}700 \text{ psi}$$

$$\text{Use } F_b = F_{cy} = 45{,}000 \text{ psi}$$

$$M_{cr} = F_b\,\pi R^2 t = 45{,}000\,(4.2) = 189{,}000 \text{ in-lbs}$$

The allowable shear load is:

$$F_s = 1.4\,F_{st}$$

$$\frac{F_{st} \times 10^3}{E} = 1.9 \qquad \text{(Reference 22)}$$

$$F_{st} = 1.9\,(10.7 \times 10^6)(10^{-3}) = 20{,}300 \text{ psi}$$

$$F_s = 1.4\,(20{,}300) = 28{,}400 \text{ psi}$$

$$V_s = F_s\,(\pi R t) = 28{,}400\,(0.912) = 25{,}900 \text{ lbs}$$

Using the following interaction equation the margin of safety is shown to be positive.

$$[R_c + R_b + R_v]^{1.2} = 1 \qquad \text{(Reference 22)}$$

$$R_c = \frac{4050 \times 1.5}{81{,}800} = 0.0742$$

$$R_b = \frac{6300 \times 1.5}{189{,}000} = 0.0500$$

$$R_v = \frac{340 \times 1.5}{25{,}900} = 0.00197$$

$$[0.0742 + 0.0500 + 0.0020]^{1.2} = 0.084$$

This is less than 1.0, therefore the section will not buckle under the given combined loading.

M.S. = HIGH

The maximum tension loads in the shell are due to limit Load Condition J, Re-entry, where G_x and G_n are +23.0 and 7.0, respectively. From Figures 21, 22, and 23, the limit loads are found to be

·//

$$P = 3900 \text{ lbs}$$

$$V = 370 \text{ lbs}$$

$$M = 7200 \text{ in-lbs}$$

The equivalent tensile load in the shell is:

$$P_{eq} = \frac{2M}{R} + P = \frac{2(7200)}{4.62} + 3900$$

$$= 3120 + 3900 = 7020 \text{ lbs}$$

$$A = 2\pi Rt = 6.28\ (4.62)(0.063) = 1.825 \text{ in}^2$$

$$f_{eq} = \frac{7020 \times 1.5}{1.825} = 5770 \text{ psi}$$

$$F_{tu} = 63,000 \text{ psi}$$

$$M.S. = \frac{63,000}{5770} - 1 = \text{HIGH}$$

The shear stress in the shell is:

$$f_s = \frac{V}{\pi Rt} = \frac{370 \times 1.5}{0.915} = 606 \text{ psi}$$

$$M.S. = \frac{40,000}{606} - 1 = \text{HIGH}$$

5. RING AT STATION 48.0

a. General

The station 48 ring is made of 7079-F aluminum alloy heat treated to the -T6 condition after forming. The cross-section, shown in Figure 25, has radial and axial legs that are 0.125 and 0.120 inch thick, respectively. The ring provides a structural tie between the steel ballast fitting and the shell portion of the substructure. The ballast fitting is attached to the forward axial leg of the ring by 12 NAS 583-5 screws (#10). The aft leg of the ring is attached to the substructure by 22 FF-200 steel rivets (3/16 dia.).

b. Loads

The critical load condition is J, Re-entry, where the applied limit loads obtained from Figures 21, 22 and 23 are

$P = 3580$ lbs

$V = 140$ lbs

$M = 12{,}200$ in-lbs

c. Analysis

1. Substructure to Ring Attachment

From Reference 4 the maximum allowable limit and ultimate loads for a 3/16 inch diameter FF-200 (NAS 1670-3) steel rivet in machined countersunk aluminum alloy are 610 and 1000 lbs, respectively. The number of rivets required is

$$N = \frac{2M/R + P}{P_{allow}} = \frac{\left[2(12200)/3.49 + 3580\right]1.15}{610}$$

$$= \frac{\left[7000 + 3580\right]1.15}{610} = 20$$

$$M.S. = \frac{22}{20} - 1 = +0.10$$

2. Ballast to Ring Attachment

The allowable shear strength of a NAS 583-5 screw is 3062 lbs. The allowable bearing strength in the 0.120 inch thick ring is 1200 lbs. The number of rivets required is

$$N = \frac{2M/R + P}{P_{allow}} = \frac{\left[2(12200)/3.30 + 3580\right] 1.15}{1200}$$

$$= \frac{\left[7400 + 3580\right] 1.15}{1200} = 10.5$$

$$M.S. = \frac{12}{10.5} - 1 = +0.14$$

3. Ring Analysis

The ring at station 48 carries most of the load from the ballast fitting to the substructure skin in its axial legs. However, due to the "flare-out" of the aft leg of the ring there are induced kick loads in the ring. This load is equal to the axial load component times the tangent of the "flare-out" angle ϕ.

In order to calculate the kick loads it is first necessary to calculate all the fastener loads, P_a. The individual limit loads and the resulting "kick loads" are

Fast.	y	y^2	$P_M = \frac{My}{y^2}$	$\frac{P}{N}$	P_a	P_k
1	0	0	0	+298	+298	+26.0
2	-1.65	2.72	-308	+298	- 10	- 0.875
3	-2.86	8.18	-533	+298	-235	-20.6
4	-3.30	10.90	-615	+298	-317	-27.7
5	-2.86	8.18	-533	+298	-235	-20.6
6	-1.65	2.72	-308	+298	- 10	- 0.875
7	0	0	0	+298	+295	+26.0
8	1.65	2.72	308	+298	606	+53.0
9	2.86	8.18	533	+298	831	+72.7
10	3.30	10.90	615	+298	913	+80.0
11	2.86	8.18	533	+298	831	+72.7
12	1.65	2.72	308	+298	606	+53.0
		65.40				

Shown below is the limit load diagram for the ring at station 48.

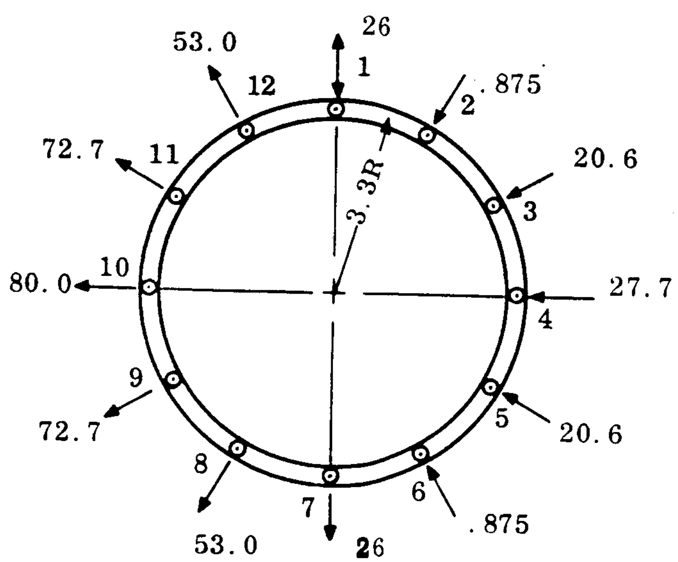

The maximum ring stress occurs at load point 10. The ring is solved using ring coefficients from Reference 27.

$$M = K_m P_k R = [-0.239\ (+80) -0.02\ (+72.7) +0.09\ (+53.0) +0.09\ (+26.0)$$
$$+0.025\ (-0.875) -0.049\ (-20.6) -0.079\ (-27.7) -0.049\ (-20.6)$$
$$+0.025\ (-0.875) +0.090\ (+26.0) +0.09\ (+53.0) -0.02\ (+72.7)]\ R$$

$$= [-19.1 - 1.45 + 4.77 + 2.34 - 0.022 + 1.06 + 2.19 + 1.06 - 0.022$$
$$+ 2.34 + 4.77 - 1.45]\ R$$

$$= [-3.51]\ 3.3 = -11.6 \text{ in-lbs, limit}$$

$$N = K_n \cdot P_k = 0.24\ (+80) +0.41\ (+72.7) +0.41\ (+53.0) +0.25\ (+26.0)$$
$$+0.025\ (-0.875) - 0.16\ (-20.6) -0.24\ (-27.7) -0.16\ (-20.6)$$
$$+0.025\ (-0.875) +0.25\ (+26.0) +0.41\ (+53.0) +0.41\ (+72.7)$$

$$= +19.2 + 29.8 + 21.7 + 6.5 - 0.0219 + 3.3 + 6.65 + 3.3 - 0.0219$$
$$+6.5 +21.7 + 29.8$$

$$= +148.4 \text{ lbs}$$

A positive bending moment, M, denotes compression in the outer fiber of the ring while a positive axial load, N, denotes tension in the ring. The ring section properties, from Figure , are:

$A = 0.269 \text{ in}^2$

$\bar{y} = 0.404$ in (from inside fiber)

$I_{c.g.} = 0.0032 \text{ in}^4$

The maximum stress is compressive in nature and occurs in the outer fiber of the ring.

$$f_b = \frac{Mc}{I} + \frac{P}{A} = + \frac{11.6\ (0.106)}{0.0032} + \frac{148.4}{0.269}$$

$$= 384.0 + 553 = 937 \text{ psi}$$

$$F_{cy} = 66{,}000 \text{ psi}$$

$$M.S. = \frac{66{,}000}{937 \times 1.15} - 1 = \text{HIGH}$$

6. RING AT STATION 60.8

a. General

The station 60.8 ring is made of 7079-T652 aluminum alloy. The ring cross-section, shown in Figure 26, is made up of two angles forming a tee. The axial legs of the ring are fastened to the 0.063 inch thick substructure skin by 3/16 inch diameter aluminum rivets while the radial legs are fastened together using 18 AN 173C6 hex head bolts and NAS 1068C3 nut plates.

b. Loads

The critical load condition is J, Re-entry. From Figures 21, 22, and 23 the limit loads are

$$P = 3750 \text{ lbs}$$

$$V = 340 \text{ lbs}$$

$$M = 10300 \text{ in-lbs}$$

c. Analysis

1. Substructure Shell to Ring Attachment

The forward leg of ring is attached to the skin using 30 CR 2248 countersunk aluminum rivets, 3/16 inch in diameter. The allowable yield and ultimate loads for this rivet are 388 and 606 lbs, respectively. The aft leg of the ring is attached to the skin using 28 NAS 1398D protruding head rivets, 3/16 inch in diameter. The allowable ultimate strength of this rivet is 816 lbs. The CR 2248 rivets are critical and the number of rivets required is:

$$N = \frac{2M/R + P}{P_{allow}} = \frac{\left[2(10,300)/4.54 + 3750\right]1.15}{388}$$

$$= \frac{\left[4540 + 3750\right]1.15}{388} = 24.6$$

$$M.S. = \frac{30}{24.6} - 1 = +0.22$$

2. Ring and Bolt Stresses

In calculating the ring bending stresses and bolt load, the load distribution shown below is used.

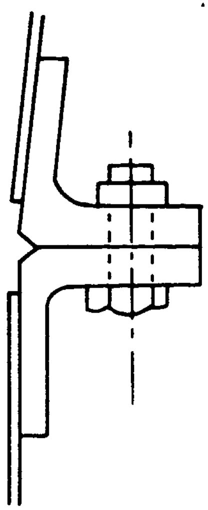

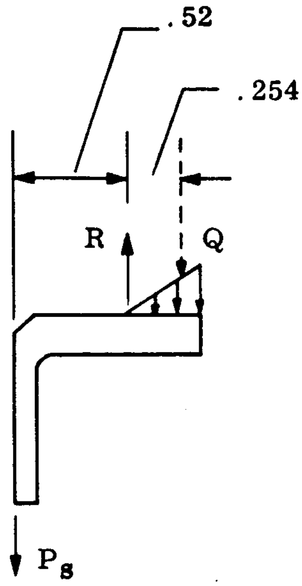

With this type of joint there is prying action on the bolt. Because of this the bolt load is greater than the applied load P_s. As the applied load begins to "open up" the angles, the bolt feels an increasing load, R, and the "toes" of the rings bear more on each other. For a AN 173C6 bolt the ultimate tensile strength is 2210 lbs. By taking moments about the center of pressure of the "toe" pressure the bolt load is calculated. The maximum bolt load is

$$P_s = \frac{8290}{30} = 276 \text{ lbs, limit}$$

$$\Sigma M_Q = 0 = -P_s\left(\frac{30}{18}\right)(0.52 + 0.254) + 0.254\,R$$

$$R = \frac{276\ (1.67)(0.774)}{0.254} = 1410 \text{ lbs, limit}$$

$$\text{M.S.} = \frac{2210}{1410 \times 1.5} - 1 = +0.04$$

The bending stress in the axial leg of the ring is calculated assuming a beam width b, one end fixed the other end free to deflect but not to rotate

$$M_{max} = \frac{P\ell}{2} = \frac{276(1.67)(0.52)}{2} = 120 \text{ in-lbs}$$

$$f_b = \frac{6M}{bt^2} = \frac{6\ (120)(1.5)}{1.04(0.0156)} = 66{,}500 \text{ psi}$$

$$F_{tu} = 71,000 \text{ psi}$$

$$M.S. = \frac{71,000}{66,500} - 1 = +0.07$$

The bending stress in the "toe" section of the angle is

$$M_{max} = 0.254\ Q = 0.254\ (950) = 241 \text{ in-lbs}$$

$$f_b = \frac{6M}{bt^2} = \frac{6\ (241)(1.5)}{0.800\ (0.04)} = 67,800 \text{ psi}$$

$$M.S. = \frac{71,000}{67,800} - 1 = +0.05$$

In additi on to the out of plane loads due to substructure bending and axial loads, the ring also reacts in-plane loads due to the equipment package. Loads at the forward end of the equipment package are transferred to the ring at station 60 by four shear pins located at 45°, 135°, 225° and 315°. The maximum loads occur in the ring when the orientation of the shear is such that only two attachment points react to the load.

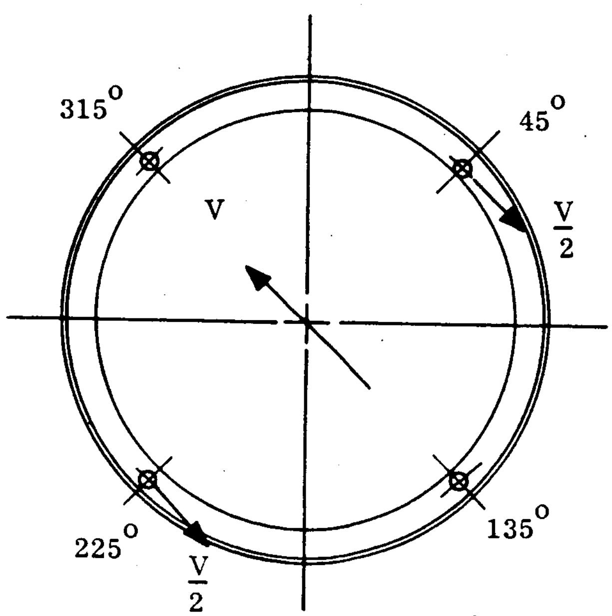

The total shear load reacted by the two pins is 35.56 lbs, limit. Therefore, each pin carries

$$\frac{V}{2} = \frac{35.56}{2} = 17.8 \text{ lbs}$$

Transferring the applied load in the ring to the center of gravity of the cross-section, a moment is induced.

$$M_a = \frac{35.56}{2} \left(\frac{8.191-7.00}{2} \right) = 10.6 \text{ in-lbs}$$

The maximum internal moment and axial load occurs at the load point and are

$$M = M_a K_m = 10.60 (0.50) = 5.3 \text{ in-lbs}$$

$$N = P_a K_n = 17.8 (0.50) = 8.9 \text{ lbs}$$

The section properties of the ring are

$$A = 0.640 \text{ in}^2$$

$$\bar{y} = 0.983 \text{ in (from inside fiber)}$$

$$I_{c.g.} = 0.108 \text{ in}^4$$

The maximum ring stress occurs in the radial leg and is

$$f_b = \frac{Mc}{I} + \frac{P}{A} = \frac{5.3 (0.983)}{0.108} + \frac{8.9}{0.640}$$

$$= 48.3 + 13.9 = 62.2 \text{ psi}$$

$$M.S. = \frac{71,000}{62.2 \times 1.5} - 1 = \text{HIGH}$$

7. RING AT STATION 70.1

a. General

The 7079-T652 aluminum alloy ring at station 70 has a tee shaped cross-section as shown in Figure 27. The axial legs of the ring are fastened to the 0.063 inch thick substructure skin by 16 NAS 1398D 3/16 inch diameter rivets.

b. Loads

The critical load condition is J, Re-entry. The limit loads obtained from Figures 21, 22 and 23 are

$P = 3900$ lbs

$V = 370$ lbs

$M = 7200$ in-lbs

c. Analysis

From Reference 4, the maximum allowable ultimate load for a 3/16 inch diameter NAS 1398D aluminum rivet is 816 lbs. The number of rivets required is

$$N = \frac{2M/R+P}{P_{allow}} = \frac{[2(7200)/4.53 + 3900]1.50}{816}$$

$$= \frac{[3180 + 3900]1.5}{816} = 13.0$$

$$M.S. = \frac{16}{13} - 1 = +0.23$$

The ring at station 70 carries most of the load axially in the legs of the section. However, due to the "flare-out" of the aft leg of the ring ($6^{o}19'$) there is induced a kick load in the ring. This radial load is equal to the axial load component times the tangent of the angle. The individual kick loads, P_k, are calculated below.

No.	y	y^2	$P_M = \frac{My}{y^2}$	$P_a = \frac{P}{N}$	P_t	P_k
1	0	0	0	+244.00	+244.00	+27.00
2	1.74	3.03	76.50	+244.00	+320.50	+35.40
3	3.20	10.20	140.50	+244.00	+384.00	+42.50
4	4.18	17.50	184.00	+244.00	+428.00	+47.40
5	4.53	20.60	199.00	+244.00	+443.00	+49.20
6	4.18	17.50	184.00	+244.00	+428.00	+47.40
7	3.20	10.20	140.50	+244.00	+384.00	+42.50
8	1.74	3.03	76.50	+244.00	+320.50	+35.40
9	0	0	0	+244.00	+244.00	+27.00
10	-1.74	3.03	- 76.50	+244.00	+167.50	+18.50
11	-3.20	10.20	-140.50	+244.00	+103.50	+11.45
12	-4.18	17.50	-184.00	+244.00	+ 60.00	+ 6.65
13	-4.53	20.60	-199.00	+244.00	+ 45.00	+ 4.98
14	-4.18	17.50	-184.00	+244.00	+ 60.00	+ 6.65
15	-3.20	10.20	-140.50	+244.00	+103.50	+11.45
16	-1.74	3.03	- 76.50	+244.00	+167.50	+18.50
		164.12				

Shown below is the limit load diagram for the ring at station 70. The applied axial load is in the aft direction while the moment is as shown.

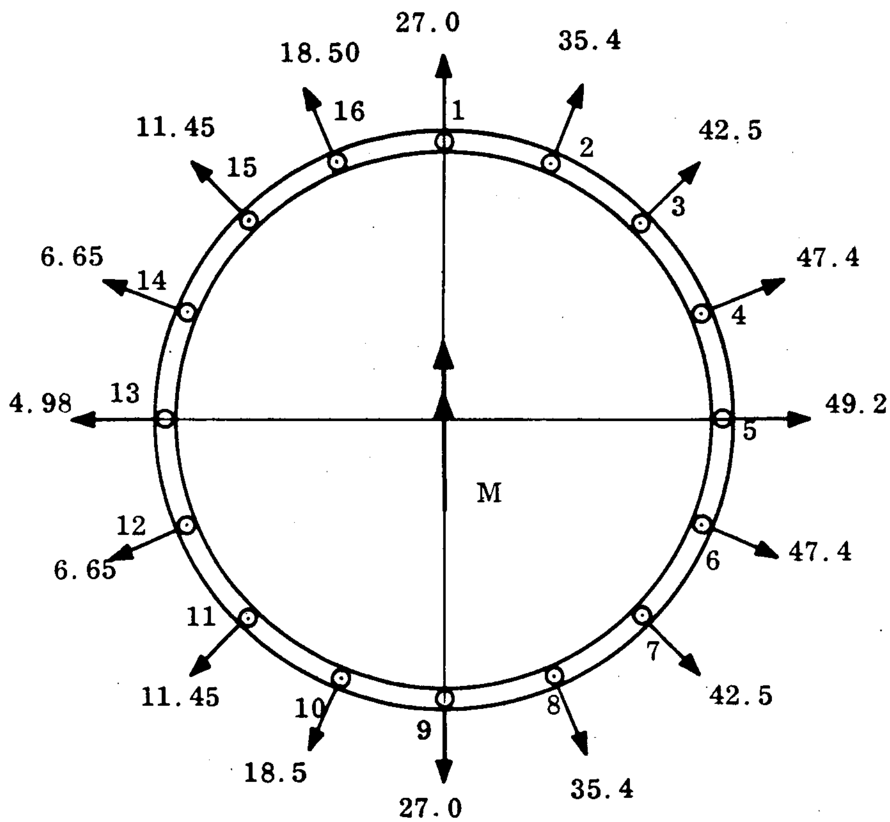

The maximum in-plane ring stresses occur at load point 5. The ring is solved using the ring coefficients from Reference 27.

$$
\begin{aligned}
M &= K_m PR = [-0.239\ (49.2) - 0.065\ (47.4) + 0.05\ (42.5) \\
&\quad + 0.10\ (35.4) + 0.09\ (27.0) + 0.045\ (18.5) - 0.013\ (11.45) \\
&\quad - 0.041\ (6.65) - 0.080\ (4.98) - 0.041\ (6.65) - 0.013\ (11.45) \\
&\quad + 0.045\ (18.50) + 0.090\ (27.0) + 0.100\ (35.4) + 0.050\ (42.5) \\
&\quad - 0.065\ (47.4)]\, 4.53 \\
&= [-11.75 - 3.08 + 2.12 + 3.54 + 2.43 + 0.83 - 0.149 - 0.272 \\
&\quad - 0.399 - 0.272 - 0.149 + 0.83 + 2.43 + 3.54 + 2.12 - 3.88]\, 4.53 \\
&= [-2.11]\, 4.53 = -9.55 \text{ in-lbs}
\end{aligned}
$$

$$N = K_nP = 0.24\,(49.2) + 0.39\,(47.4) + 0.435\,(42.5) + 0.38\,(35.4) + 0.25\,(27.0) + 0.08\,(18.5) - 0.08\,(11.45) - 0.20\,(6.65) - 0.24\,(4.98) - 0.20\,(6.65) - 0.08\,(11.45) + 0.08\,(18.50) + 0.25\,(27.0) + 0.38\,(35.4) + 0.435\,(42.5) + 0.39\,(47.4)$$

$$= 11.8 + 18.5 + 18.5 + 13.45 + 6.75 + 1.48 - 0.915 - 1.33 - 1.20 - 1.33 - 0.915 + 1.48 + 6.75 + 13.45 + 18.5 + 18.5$$

$$= +133.47 \text{ lbs}$$

A positive bending moment denotes compression in the outer fiber of the ring while a positive axial load denotes tension in the ring. The section properties of the ring are

$$A = 0.165 \text{ in}^2$$

$$\bar{y} = 0.0777 \text{ in (from inner flange)}$$

$$h = 0.438 \text{ in}$$

$$I_{c.g.} = 0.0018 \text{ in}^4$$

The maximum stress is compression in nature and occurs in the outer fiber of the ring.

$$f_b = \frac{Mc}{I} + \frac{P}{A} = \frac{+9.55(0.405)}{0.0018} + \frac{133.47}{0.165}$$

$$= +2150 + 809 = 2959 \text{ psi}$$

$$M.S. = \frac{61{,}000}{2959 \times 1.50} - 1 = \text{HIGH}$$

8. RING AT STATION 90.0

a. General

The 7079-T652 aluminum alloy ring at station 90 is shown in Figures 28 and 29. The ring basically has the shape of a 90° angle reinforced locally with bosses at points where the ring is pinned to the calorimeter. These pins transfer all the mid-section axial loads and a portion of the mid-section shear loads to the calorimeter. The equipment package assembly is attached to the underside of the local bosses. The axial and radial legs of the ring section have lightning holes as indicated in Figure 28.

b. Substructure to Ring Attachment

The substructure skin is riveted to the ring at station 90 using 36 1398B 5/32 inch diameter rivets. The ultimate strength of this rivet is 596 lbs. The critical load condition is Third Stage Ignition. From Figure 24 the maximum axial load is 4500 lbs. The number of rivets required is

$$N = \frac{4500}{596} = 7.56 \text{ rivets}$$

$$M.S. = \frac{36}{7.56 \times 1.5} - 1 = \text{HIGH}$$

c. Ring Analysis

The ring is analyzed as a ring on multiple supports (6 pins) subjected to a transverse uniformly distributed load, w, due to the substructure weight. The equipment package weight is not included since it acts at the pin locations.

The critical load condition is Third Stage Ignition and from Figure 24 the maximum limit load of 4500 lbs is obtained. The uniform transverse load, w, is

$$w = \frac{4500}{2\pi (6.42)} = 112 \text{ lbs/inch}$$

The maximum internal moment about a radial axis occurs at the pin location and is equal to

$$M_o = w R^2 m_2$$

where: $m_2 = 1 - \frac{\pi}{n} \quad (\sin \phi + \text{ctn} \frac{\pi}{n} \cos \phi)$

$$= 1 - \frac{\pi}{6} \quad (\sin 0^o = \text{ctn} \frac{\pi}{6} \cos 0^o)$$

$$= 1 - 0.523 (1.73) = 0.095$$

w = 112 lbs/inch, limit

R = 6.4 inches

$$M_o = 112 (6.4)^2 (0.095) = 680 \text{ in-lbs, limit}$$

The maximum torsion about an axis tangent to the ring occurs at a section midway between the pins and is equal to:

$$T_o = w R^2 n_2$$

where:

$$n_2 = \phi - \frac{\pi}{n} + \frac{\pi}{n} \left(\cos\phi - \text{ctn}\frac{\pi}{n}\sin\phi\right)$$

$$= \frac{\pi}{12} - \frac{\pi}{6} + \frac{\pi}{6} \left(\cos\frac{\pi}{12} - \text{ctn}\frac{\pi}{6}\sin\frac{\pi}{12}\right)$$

$$= 0.262 - 0.524 + 0.524 \left[0.966 - 1.73\,(-0.259)\right]$$

$$= 0.262 - 0.524 + 0.524\,(0.518)$$

$$= 0.262 - 0.524 + 0.271 = 0.009$$

$$T_o = 112\,(6.4)^2(0.009) = 41.2 \text{ in-lbs, limit}$$

The minimum section properties of the ring are

$$A = 0.496 \text{ in}^2$$

$$h = 3.42 \text{ in}$$

$$\bar{y} = 1.53 \text{ in (from aft end)}$$

$$I_{c.g.} = 0.628 \text{ in}^4$$

The maximum bending stress in the ring due to M_o is:

$$f_b = \frac{Mc}{I} = \frac{680\,(1.89)}{0.628} = 2050 \text{ psi}$$

$$F_{tu} = 71,000 \text{ psi}$$

$$M.S. = \frac{71,000}{2050} - 1 = \text{HIGH}$$

The maximum torsional stress in the ring is calculated assuming a rectangular cross-section, 0.36 inches wide and 2.35 inches high.

$$f_{max} = \frac{T\,(3a + 1.8b)}{8a^2 b^2}$$

$$= \frac{41.2\,[3(1.175) + 1.8(0.18)]}{8(1.175)^2\,(0.18)^2}$$

$$= \frac{158}{0.358} = 442 \text{ psi}$$

$$F_{su} = 43{,}000$$

$$M.S. = \frac{43{,}000}{442 \times 1.5} - 1 = \text{HIGH}$$

9. EXPANSION JOINT PINS

a. General

The expansion joint at station 90 consists of six pins which fit into radial holes in the calorimeter shell and are fixed in the ring at station 89.44. These pins allow the calorimeter to grow in size radially without inducing stresses in the forward substructure. There is a 17-4PH steel bushing on the calorimeter end of the pin to prevent pin fixity, as shown in Figure 29.

b. Loads

The pins are critical for either Load Condition G (room temp pin) or Condition J (pin at an estimated $400^{\circ}F$).

c. Analysis, Condition G

The maximum pin shear and bending loads are calculated below. The shear per pin is assumed to be equal to V. With a moment arm equal to 0.1625 inches (Figure 29). the moment is 0.1625 V. Using beam in a socket theory to analyze the pin

$$M_{max} = K_M (V)(L) = 0.25\,(V)(1.2) = 0.3V$$

The pin is made of CRES 17-4 PH, H1025 steel which has properties at room temperature of

$$F_{tu} = 155{,}000 \text{ psi}$$

$$F_{su} = 100{,}000 \text{ psi}$$

$$\text{Pin Area} = \pi R^2 = \pi (0.25)^2 = 0.196 \text{ in}^2$$

$$I = 0.25\pi R^4 = 0.25 (\pi)(0.25)^4 = 30.8 \times 10^{-4} \text{ in}^4$$

$$V_{allow} = \frac{F_{su} \cdot A}{1.5} = \frac{100,000\ (0.196)}{1.5} = 13,060 \text{ lbs, limit}$$

$$M_{allow} = \frac{F_{tu}\ (I)}{1.5\ c} = \frac{155,000\ (30.8 \times 10^{-4})}{1.5\ (0.25)}$$

$$= 1272 \text{ in-lbs, limit}$$

The pin is obviously critical in bending. Using Figure 24, we obtain, for Load Condition G:

$$P = 4500 \quad \text{lbs limit}$$

$$V = \frac{4500}{6} = 750 \text{ lbs}$$

$$M = 0.3V = 226 \text{ inch-lbs, limit}$$

$$M.S. = \frac{1272}{226} - 1 = \text{HIGH}$$

d. Analysis, Load Condition J

From Figure 21, the axial load for Condition J is 4150/4500 = 0.923 of that for Condition G. At a temperature of 400°F, the material ultimate tensile drops to 0.90 of its room temperature value. Accordingly, we have:

$$M.S. = \frac{1272 \times 0.90}{226 \times 0.923} - 1 = \text{HIGH}$$

10. BALLAST TUBE ASSEMBLY

The 304L steel ballast tube assembly is checked for ground handling where $G_x = 3.0$. The maximum ballast weight possible is 85.0 lbs.

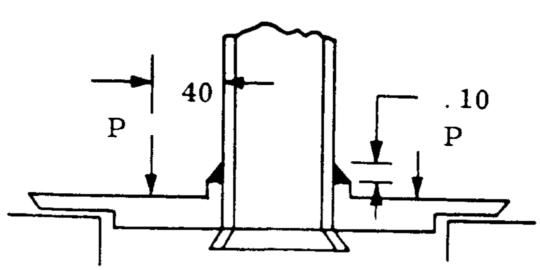

The maximum shear stress in the weld, assuming a class III weld is:

$$A = 2\pi R \ell = 6.28\,(0.25)(0.10) = 0.157 \text{ inch}$$

$$f_s = \frac{3\,(85.0)}{0.157} = 1620 \text{ psi}$$

$$M.S. = \text{HIGH}$$

The maximum bending stress is obtained using Reference 5, Table X, Case 22.

$$S_r = \frac{3w}{2\pi t^2}\left[\frac{2a^2(m+1)\log\frac{a}{b} + a^2(m-1) - b^2(m-1)}{a^2(m+1) + b^2(m-1)}\right]$$

where:

$w = 255$ lbs

$t = 0.185$ inch

$m = 3$

$a = 0.40$

$b = 0.25$

$$S_r = \frac{3(255)}{6.28(0.0342)}\left[\frac{0.32(4)(0.204) + 0.16(2) - 0.0625(2)}{0.16(4) + 0.0632(2)}\right]$$

$$= 3540\left[\frac{0.26 + 0.32 - 0.1350}{0.64 + 0.1264}\right]$$

$$= 3540\left[\frac{0.445}{0.7664}\right] = 2050 \text{ psi, limit}$$

Tube stress away from support plate is:

$$f = \frac{P}{A}$$

where: $A = 2\pi R t = 6.28(0.22)(0.06)$

$= 0.083 \text{ inch}^2$

$$f_T = \frac{3(85)}{0.083} = 3070 \text{ psi, limit}$$

$$M.S. = \text{HIGH}$$

11. BALLAST FITTING

The ballast fitting is made of 4130 alloy steel and extends from spacecraft stations 26.281 to 48.03. The design is shown in drawing number 47E190430. The maximum bending stress in the fitting occurs at station 46.0 where for re-entry conditions the loads are obtained from Figure 21, 22 and 23.

$$P = 3100 \text{ lbs}$$
$$V = 0$$
$$M = 12,200 \text{ in-lbs}$$

The fitting section properties at station 46 are:

$$A = 12.67 \text{ in}^2$$
$$r = 2.62 \text{ in}$$
$$I = 30.88 \text{ in}^4$$

The fitting bending stress is:

$$f_b = \frac{Mc}{I} + \frac{P}{A} = \frac{12,200\ (2.62)}{30.88} + \frac{3100}{12.67}$$

$$= 1035 + 245 = 1280 \text{ psi}$$

For 4130 alloy steel

$$F_{tu} = 90,000 \text{ psi}$$

$$M.S. = \frac{90,000}{1280 \times 1.5} - 1 = \text{HIGH}$$

12. BALLAST RETAINER

a. General

The variable ballast is held in the steel ballast fitting by means of a steel screw type retainer, located at the aft end of the ballast fitting as shown in Figure 30. The plug has a maximum diameter of 3.625 inches, is 1.0 inch thick and has 3-5/8 -16 UNF threads. The ballast rests on a 0.185 inch wide ring, 3.07 inches in diameter. The retainer is machined from 301, 302 or 316 1/4 hard or Condition A steel.

b. Analysis

The critical load is due to Third Stage Ignition where $G_x = -25.2$.

The maximum weight of the variable ballast is 85 lbs. The load per inch on the 3.07 inch diameter ring bearing surface is

$$w = \frac{85\ (25.2)}{2\pi\ (1.53)} = 223 \quad \text{lbs/inch}$$

The maximum bearing stress on the ring is

$$f_{br} = \frac{w}{t} = \frac{223}{0.185} = 1200 \quad \text{psi}$$

$$F_{bry} = 140{,}000 \quad \text{psi}$$

$$\text{M.S.} = \frac{140{,}000}{1200 \times 1.15} - 1 = \text{HIGH}$$

The shear stress in the threads is calculated assuming only 0.75 inch of the threads are effective.

$$f_s = \frac{85\ (25.2)}{2\pi\ (1.815)(0.75)} = \frac{2140}{8.53} = 251 \quad \text{psi}$$

$$F_{su} = 67{,}500 \quad \text{psi}$$

$$\text{M.S.} = \frac{67{,}500}{251 \times 1.5} - 1 = \text{HIGH}$$

B. AFT SUBSTRUCTURE

1. GENERAL

The aft substructure is located approximately between stations 94 and 139 as shown in Figure 31. The "rail" portion of the structure is made of two 0.050 inch thick 2024-T3 aluminum channel sections riveted together by their flanges. The forward support (Figure 35) at station 94.65 reacts axial and lateral loads while the aft support (Figure 31 at station 139 reacts only with lateral loads since it is slotted to allow for thermal expansion of the calorimeter.

The channel rails house wire bundles assumed to weigh 0.40 pounds per axial inch. After the wires are in place a non-structural type cover is placed over the open side of the rails to retain the wire. The loads on the rails for Condition J are shown in Figures 32 to 34.

The aft end of the rails tie to a ring bulkhead at 0° and 180° as shown in Figure 36. The ring is attached to the calorimeter at 6 locations, 0°, 60°, 120°, 180°, 240°, and 300°, by brackets fastened to the web of the channel shaped bulkhead. The web portion of the channel supports 6 lbs. of wire harness and 6 lbs. of equipment. The bulkhead is made of 0.070 inch thick 2024-T42 aluminum alloy.

2. SUPPORT BRACKET

The support bracket is a fitting which supports the forward end of the rail. It is shown in Figure 35. It is made of CRES 17-4PH (1025). The temperature of the bracket during re-entry is assumed to be $500^{\circ}F$. At station 94.65 the limit loads during re-entry are:

$P = 130$ lbs, limit

$V = 86$ lbs, limit

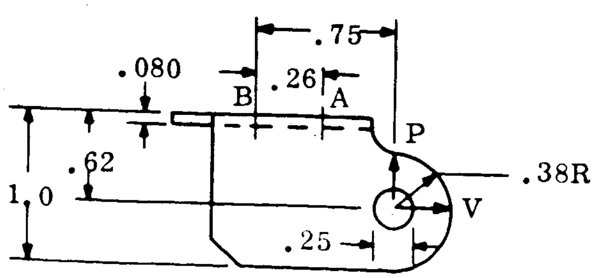

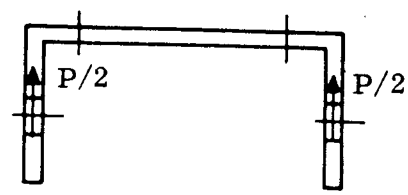

The lug portion of the bracket is checked first. For the axial load, V,

$$\frac{a}{D} = \frac{0.38}{0.25} = 1.52$$

$$\frac{W}{D} = \frac{0.76}{0.25} = 3.04$$

$$\frac{D}{t} = \frac{0.25}{0.057} = 4.4$$

$$A_{br} = Dt = 0.25\ (0.057) = 0.01425\ in^2$$

$$A_t = (W - D)\ t = (0.76 - 0.25)\ (0.057) = 0.029\ in^2$$

$$P_{bru} = K_{br}\ A_{br}\ F_{tu}$$

where:

$$K_{br} = 1.47$$

$$F_{tu} = 133,000\ @\ 500^{o}F$$

$$P_{bru} = 1.47\ (0.01425)\ (133,000) = 2780\ lbs.$$

$$P_{tu} = K_t\ A_t\ F_{tu}$$

where:

$$K_t = 0.93$$

$$P_{tu} = 0.93\ (0.029)(133,000) = 3580\ lbs.$$

For transverse load

$$\frac{A_{ave}}{A_{br}} = 1.11$$

$$P_{tru} = K_{tru} A_{br} F_{tu}$$

where:

$$K_{tru} = 1.4$$

$$P_{tru} = 1.4\ (0.01425)(133,000) = 2660\ \text{lbs.}$$

From the interaction equation the margin of safety is obtained

$$R_a^{1.6} + R_{tr}^{1.6} = 1 \quad \text{or,}$$

$$M.S. = \frac{1}{\left(R_a^{1.6} + R_{tr}^{1.6}\right)^{0.625}} - 1$$

where:

$$R_a^{1.6} = \left[\frac{43 \times 1.5}{2780}\right]^{1.6} = 0.0024$$

$$R_{tr} = \left[\frac{65 \times 1.5}{2660}\right]^{1.6} = 0.0050$$

$$M.S. = \frac{1}{\left[0.0024 + 0.005\right]^{0.625}} - 1 = \text{HIGH}$$

Check attachment to calorimeter for loads shown above. The bracket bears against the calorimeter at point A and pulls on the bolt at point B. Summing moments about A, the bolt load is found by:

$$\Sigma M_A = 0 = 65\ (0.49) + 43\ (0.62) - 0.26\ (R_B)$$

$$31.8 + 26.6 = 0.26\ R_B$$

$$R_B = 225\ \text{lbs, limit}$$

The bending stress between the lug flange and the bolt is calculated conservatively assuming a beam fixed at one end and guided at the other with no rotation. The load is assumed applied at the guided end:

$$M = \frac{PL}{2} = \frac{225\ (0.30)}{2} = 33.8 \text{ in-lbs.}$$

$$f_b = \frac{6M}{bt^2} = \frac{6\ (33.8)}{0.50\ (0.0064)} = 63,500 \text{ psi}$$

$$M.S. = \frac{133,000}{63,500 \times 1.5} - 1 = +\ 0.40$$

3. RAILS

The bending stress in the rail channels is calculated below. The section properties of the rail cross-section are:

$$A = 0.3605 \text{ in.}^2$$

$$h = 1.57 \text{ inches}$$

$$\bar{y} = 1.07 \text{ inches}$$

$$I_{c.g.} = 0.102 \text{ in.}^4$$

The maximum loads occur during re-entry and are obtained from Figures 32 and 34.

$$P = 52 \text{ lbs, limit}$$

$$M = 920 \text{ in-lbs, limit}$$

$$f_b = \frac{Mc}{I} + \frac{P}{A} = \frac{900\ (1.07)}{0.102} + \frac{52}{0.3605}$$

$$= 9430 + 144 = 9574 \text{ psi, limit}$$

The crippling strength of the section is calculated.

$$\left[\frac{F_{cy}}{E_c}\right]^{1/2} = \left[\frac{45 \times 10^3}{10.5 \times 10^6}\right]^{1/2} = 0.0655$$

$$\left[\frac{F_{cy}}{E}\right]^{1/2} \frac{b}{t} = 0.0655 \left[\frac{1.07}{0.05}\right] = 1.40$$

$$\frac{F_{cc}}{F_{cy}} = 0.43$$

$$F_{cc} = 0.43\ (45,000) = 19,350 \text{ psi}$$

$$M.S. = \frac{19,350}{9574 \times 1.5} = +\ 0.35$$

4. AFT RAIL ANGLES

At the aft end of the rail the rail is held in place by two angles as shown below.

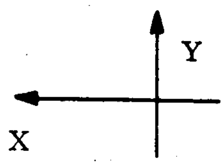

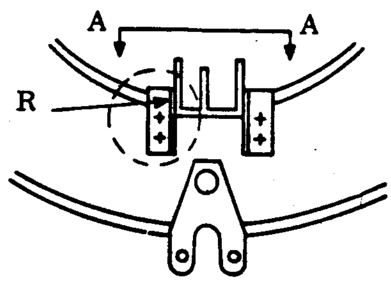

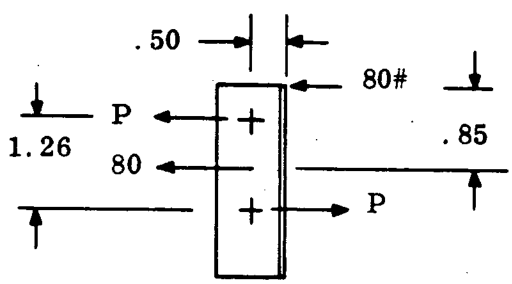

For loads in the directions indicated the bracket strength is checked. The brackets are attached to the bulkhead using #10 bolts. During re-entry the calorimeter expands approximately 0.40 inches between stations 94.65 and 139. Due to this the longitudinal expansion bracket reacts loads from the rails at a position 0.40 inches from normal. The maximum bolt shear loads are

$$P = \frac{80}{2} + \frac{80 \times 0.85}{1.26} = 40 + 54 = 94 \text{ lbs.}$$

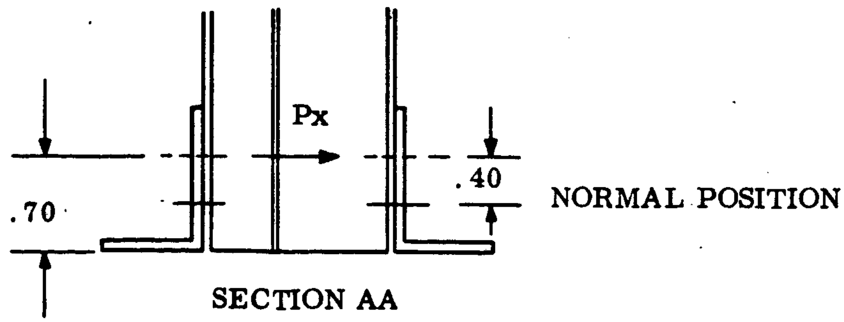

Check bending of the side walls assuming each wall carries half the load

$$M_{max} = \frac{PL}{4} = \frac{80\ (0.70)}{4} = 14 \text{ in-lbs.}$$

The bracket is made of 0.063 inch thick 2024-T3 aluminum

$$f_M = \frac{6M}{bt^2} = \frac{6\ (14)\ (1.5)}{(1)\ (0.063)^2} = 31,800 \text{ psi}$$

$$M.S. = \frac{63,000}{31,800} - 1 = +0.98$$

For a load in the "y" direction each bracket carries half the load, or

$$P_y = \frac{80}{2} = 40 \text{ lbs.}$$

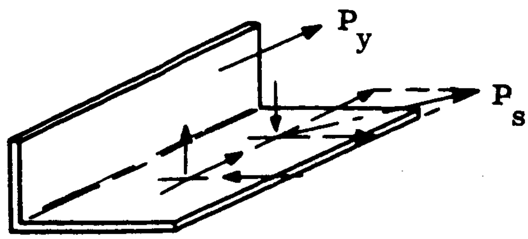

The maximum shear load in a bolt is

$$P_s = \left[\left(\frac{40}{2}\right)^2 + \left(\frac{40 \times 0.50}{1.26}\right)^2 \right]^{1/2}$$

$$P = \left[400 + 252\right]^{1/2} = 25.6 \text{ lbs.}$$

The maximum tension load per bolt is

$$P_t = \frac{P_y \times 0.5}{1.26} = \frac{40 \times 0.50}{1.26} = 15.9 \text{ lbs.}$$

M.S. = HIGH

5. SUPPORT CLIPS

The clip support connecting the bulkhead to the calorimeter is now checked. There are six clips, shown in Figure 36, and it is assumed each clip carries the same axial load while only two carry the lateral load. The clip at 180° is checked. The clip is made of CRES 17-4PH (H 1025) with the thickness being 0.062 inch.

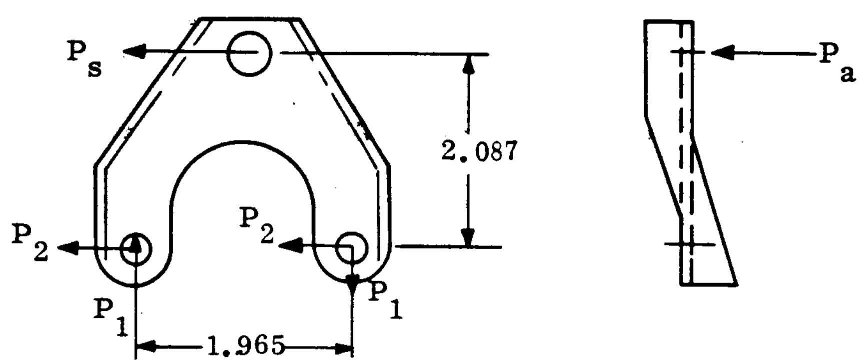

The aft bulkhead and equipment is assumed to weigh 14 lbs. Therefore, for load Condition J:

$$P_a = \frac{14 \times 23}{6} = 53.7 \text{ lbs.}$$

The shear load, P_s, is due to the 14 lbs from the bulkhead plus the reaction due to the rail.

$$P_s = \frac{14 \times 7.0}{2} + 80 = 129 \text{ lbs, limit}$$

By summing moments P_1 and P_2 are found.

$$P_1 = \frac{129 \times 2.087}{1.965} = 136 \text{ lbs, limit}$$

$$P_2 = \frac{129}{2} = 64.5 \text{ lbs.}$$

The maximum load is obtained by combining P_1 and P_2

$$P_t = \left[P_1^{\,2} + P_2^{\,2}\right]^{1/2} = \left[(136)^2 + (64.5)^2\right]^{1/2}$$

$$= \left[(1.86 \times 10^4 + 0.416 \times 10^4)\right]^{1/2}$$

$$= \left[2.276 \times 10^4\right]^{1/2} = 151 \text{ lbs.}$$

The maximum bearing stress is

$$f_{bru} = \frac{151 \times 1.5}{0.25 \times 0.062} = 14,600 \text{ psi}$$

M.S. = HIGH

The maximum "tear out" stress is

$$f_s = \frac{151 \times 1.5}{2\,(0.2)(0.062)} = 9,130 \text{ psi}$$

M.S. = HIGH

Bending of the support clip due to P_a is now calculated. Each tab carries half of the load

$$M_{max} = \frac{P_a \times 2.087}{2} = \frac{53.7 \times 2.087}{2} = 56 \text{ in-lbs.}$$

$$f_b = \frac{Mc}{I}$$

where:

$$c = 0.377$$

$$I = 0.0015$$

$$f_b = \frac{56 \times 1.5 \times 0.377}{0.0015} = 20,200 \text{ psi}$$

Check crippling of the axial leg of the support clip assuming the bracket is at 500°F

$$\left[\frac{F_{cy}}{E}\right]^{1/2} = \left[\frac{145,000\ (0.76)}{30 \times 0.90 \times 10^6}\right]^{1/2}$$

$$= [0.00407]^{1/2} = 0.0640$$

$$\frac{b}{t} = \frac{0.377}{0.062} = 6.08$$

$$\left[\frac{F_{cy}}{E}\right]^{1/2} \frac{b}{t} = 0.064\ (6.08) = 0.388$$

$$F_{cc} = 111,000\ (1.22) = 135,000 \text{ psi}$$

$$\text{Use } F_{cc} = F_{cy} = 111,000 \text{ psi}$$

$$\text{M.S.} = \frac{111,000}{20,200} - 1 = \text{HIGH}$$

6. AFT BULKHEAD

The bulkhead, Figure 36, is analyzed assuming the equipment and wire loads are transferred from the web of the channel section to the caps and then carried as a beam to the brackets attached to the calorimeter.

A typical section is at 36°. Here the equipment weight is transferred to the caps.

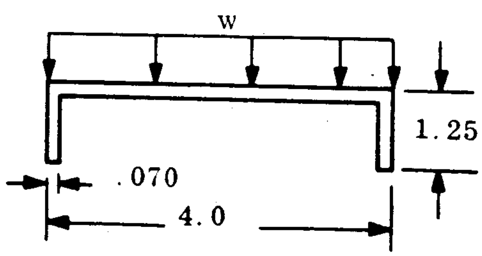

The total weight of the equipment of this section is approximately 1 lb. For load Condition J, the distributed load is

$$w = \frac{1.0 \times 23}{4.0} = 5.75 \text{ lbs/in, limit}$$

Assuming a beam 1.0 inch wide the maximum stress is

$$f = \frac{6M}{bt^2}$$

where:

$$M = 11.50 \text{ in-lbs.}$$

$$b = 1.0 \text{ inch}$$

$$t = 0.070 \text{ inch}$$

$$f = \frac{(6)(11.50)}{(1)(0.0049)} = 14,100 \text{ psi}$$

$$M.S. = \frac{63,000}{14,100 \times 1.5} - 1 = \text{HIGH}$$

Check the channel between supports. The channel is assumed to be a straight beam

$$\ell = \frac{2\pi R}{6} = \frac{6.28\ (10.75)}{6} = 11.25 \text{ in.}$$

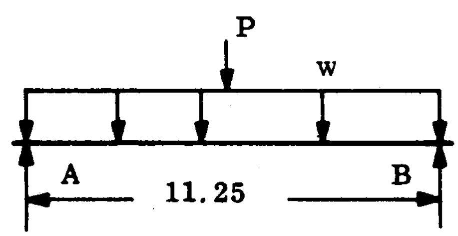

$$P = 1 \times 23 = 23.0 \text{ lbs (equipment)}$$

$$w = \frac{6 \times 23}{6 \times 11.25} = 2.05 \text{ lbs/in. (wire)}$$

$$R_A = R_B = \frac{2.05 \times 11.25}{2} + \frac{23.0}{2}$$

$$= 11.50 + 11.5 = 23 \text{ lbs.}$$

$$M_{max} = 1/2\ (11.5)(5.62) + 5.62\ (11.5)$$

$$= 32.2 + 64.4 = 96.6 \text{ in-lbs.}$$

$$f_b = \frac{Mc}{I}$$

where:

$$c = 0.98 \text{ in.}$$

$$I = 0.0632 \text{ in}^4$$

$$f_b = \frac{96.6 \times 0.98}{0.0632} = 1500 \text{ psi}$$

$$M.S. = \text{HIGH}$$

At each of the 6 bracket locations where the bulkhead is attached there are 0.040 inch stiffners attached to the web of the channel to help transmit the load from the caps to the bolt attachment. The distance from the cap to the bolt is approximately 2 inches and the cap load is:

$$P = \frac{53.7}{2} = 26.8 \text{ lbs.}$$

Assuming beam action with both ends of the beam fixed but one end guided and free to deflect the maximum moment is:

$$M = \frac{P\ell}{2} = \frac{26.8 \times 2}{2} = 26.8 \text{ in-lbs.}$$

$$f_b = \frac{Mc}{I}$$

where:

$$I = 0.000366 \text{ in}^4$$

$$c = 0.19 \text{ in.}$$

$$f_b = \frac{26.8 \times 0.19}{0.000366} = 13,900 \text{ psi}$$

The crippling allowable is:

$$\left[\frac{F_{cy}}{E}\right]^{1/2} = \left[\frac{45 \times 10^3}{10.5 \times 10^6}\right]^{1/2} = \left[4.3 \times 10^{-3}\right]^{1/2}$$

$$= 0.0655$$

$$\frac{b}{t} = \frac{0.19}{0.040} = 4.77$$

$$\left[\frac{F_{cy}}{E}\right]^{1/2} \frac{b}{t} = 0.0655\ (4.77) = 0.312$$

$$F_{cc} = 45,000\ (1.4) = 63,000\ \text{psi}$$

$$\text{Use } F_{cc} = F_{cy} = 45,000\ \text{psi}$$

$$\text{M.S.} = \frac{45,000}{13,900 \times 1.5} - 1 = \text{AMPLE}$$

C. PAYLOAD RETENTION STUD

1. GENERAL

The payload retention stud design is shown in Figure 37. The stud is made of 17-4PH (H 1025) steel. The design is such that the stud transmits shear loads only. Differential axial thermal expansion is permitted since the stud is free to move axially being guided by a bushing shrunk fit into the calorimeter. Four keys are used to transmit the shear loads from the stud to the calorimeter. The fixity of the joint is virtually eliminated by using only a small bearing area on the bushing. Axial loads induced by the substructure are reacted at station 89.4 by pins attached to the calorimeter. The analysis below indicates that a preload stud design is not required since the stud stresses are relatively low.

2. BOLT SHANK ANALYSIS

During re-entry of the spacecraft the calorimeter expands axially due to the elevated temperatures. It has been previously calculated that the calorimeter elongates at a rate of 0.01 inch per inch of spacecraft. The expansion of the calorimeter relative to the substructure between stations 24.82 and 89.4 is calculated below.

$$\Delta = 0.01\ (89.4 - 24.8) = 0.646\ \text{inch}$$

The distance ℓ, Figure 37, is equal to the initial room temperature length plus the elongation, Δ, due to temperature.

$$\ell = \ell\ (\text{Room}) + \ell\ (\text{Temp.})$$

$$= 1.45 + 0.646 = 2.10\ \text{inches}$$

For limit load Condition J, Re-entry, where G_x and G_n are + 23.0 and 7.0 respectively the limit shear load at station 24.83 is obtained from Figure 22:

$$V = 965\ \text{lbs, limit}$$

$$M = V\ell = 965\ (2.10) = 2020\ \text{in-lbs, limit.}$$

The stud is conservatively analyzed as a beam in a socket, the beam being the stud and the socket being the steel ballast fitting. The analysis neglects any bearing that may occur between the skirt of the stud and the ballast fitting at station 26.281.

The maximum stud shear, moment and bearing loads are calculated below.

$$M_{max} = K_M M = 1.02\ (2020) = 2060 \text{ in-lbs}$$

$$V_{max} = \frac{K_V M}{L} = \frac{1.66\ (2020)}{1.25} = 2680 \text{ lbs.}$$

$$W_{br} = \frac{K_{br} M}{L^2} = \frac{8.4\ (2020)}{1.56} = 10,850 \text{ lbs/in.}$$

The moment of inertia of the stud is:

$$I = \frac{\pi (R_o^4 - R_i^4)}{4}$$

where:

$$R_o = 0.375 \text{ inch}$$

$$R_i = 0.1875 \text{ inch}$$

$$I = \frac{\pi (197 \times 10^{-4} - 12.3 \times 10^{-4})}{4} = 0.0145 \text{ in}^4$$

The maximum bending stress in the stud is:

$$f_b = \frac{Mc}{I} = \frac{2060\ (0.375)}{0.0145} = 53,200 \text{ psi}$$

and the maximum shear stress is:

$$f_s = \frac{P}{A} = \frac{2680}{\pi\ (0.1405 - 0.0352)} = 8100 \text{ psi}$$

The stud material properties, 17-4PH (H 1025), at 500°F are:

$$F_{tu} = 155,000\ (0.87) = 135,000 \text{ psi}$$

$$F_{su} = 100,000\ (0.81) = 81,000 \text{ psi}$$

$$M.S.\ (bending) = \frac{135,000}{53,200 \times 1.5} - 1 = +0.69$$

$$M.S.\ (shear) = \frac{81,000}{8100 \times 1.5} - 1 = \text{HIGH}$$

The maximum bearing stress in the steel ballast fitting is:

$$f_{br} = \frac{W}{D} = \frac{10,850}{0.75} = 14,500 \text{ psi}$$

The ballast fitting is made of 4130 Condition D steel. The allowable bearing strength at 500° F is:

$$F_{bry} = 123,000\ (0.93) = 114,500 \text{ psi @ } 500°F$$

$$M.S. = \frac{114,500}{14,500 \times 1.15} - 1 = \text{HIGH}$$

The shear load at station 24.831 is transferred from the payload retention stud to a bushing (17-4PH 1025 steel) that is shrunk fit into the calorimeter. Four keys (17-PH 1025 steel) transmit the shear load. The maximum shear stress in the key, assuming only two keys effective, is:

$$f_s = \frac{V}{2lb} = \frac{965}{2\ (0.27)(0.123)} = 14,500 \text{ psi}$$

$$F_{su} = 100,000\ (0.81) = 81,000 \text{ psi @ } 500°$$

$$M.S. = \frac{81,000}{14,500} - 1 = \text{HIGH}$$

The bearing stress between the key and the bushing is:

$$f_{br} = \frac{V}{2A} = \frac{965}{2\ (0.27)(0.062)} = 28,800 \text{ psi}$$

$$F_{bry} = 123,000\ (0.93) = 114,500 \text{ psi @ } 500°F$$

$$M.S. = \frac{114,500}{28,800 \times 1.15} - 1 = \text{HIGH}$$

The key to bolt stresses are conservatively analyzed using beam in a socket theory. The maximum applied shear and moment are:

$$V_o = \frac{V}{2} = \frac{0.965}{2} = 482 \text{ lbs.}$$

$$M = V_o (0.06) = 482 (0.06) = 29.0 \text{ in-lbs.}$$

The maximum key shear, moment and bearing loads are calculated below:

$$M_{max} = K_M (V_o)(L) = 0.55 (482)(0.131) = 34.6 \text{ in-lbs.}$$

$$V_{max} = K_s (V_o) = 1.0 (482) = 482 \text{ lbs.}$$

$$W_{br} = \frac{K V_o}{L} = \frac{6.8 (482)}{0.131} = 25,000 \text{ lbs/in.}$$

The maximum bending stress is:

$$f_b = \frac{6M}{bt^2} = \frac{6 (34.6)}{0.27 (0.156)} = 4930 \text{ psi}$$

$$F_{tu} = 155,000 (0.87) = 135,000 \text{ psi @ } 500^\circ\text{F}$$

$$M.S. = \frac{135,000}{4930 \times 1.5} - 1 = \text{HIGH}$$

The maximum bearing stress is:

$$f_{br} = \frac{W_{br}}{0.27} = \frac{25,000}{0.27} = 92,500 \text{ psi}$$

$$F_{bry} = 123,000 (0.93) = 114,500 \text{ psi @ } 500^\circ\text{F}$$

$$M.S. = \frac{114,500}{92,500 \times 1.15} - 1 = +0.07$$

D. ANTENNA FRAMES

1. VHF ANTENNA WINDOW FRAME

a. General

The beryllium calorimeter has four meridional slots, measuring 10.5 inches by 2.44 inches each, located at 37.5°, 127.5°, 217.5° and 307.5° between stations 144.0 and 154.529. Into each slot is placed a VHF antenna window made of fused silica glass type 7941. The windows are secured to the internal surface of the calorimeter by an aluminum framework which is bolted to the calorimeter as shown in Figure 38. The window assembly is analyzed for the conditions listed below:

1. Differential thermal expansion loads between the aluminum window framework and the calorimeter during re-entry.

2. Structural analysis of the aluminum framework.

b. Differential Thermal Expansion

The VHF window frame design is such that large strains are not induced into the framework due to meridional and hoop expansion of the calorimeter. The meridional strains are relieved by 4 steel pins integral with the angles while the hoop strains are relieved by slotting the angles where the antenna box attaches.

The window frame is completely isolated from the calorimeter by a 0.010 inch thick glass silicone insulation layer. To conservatively calculate the length of slotted hole required the temperature of the framework will be assumed to be room temperature. The calorimeter temperature at a depth of 1.0 inch is approximately $450^{\circ}F$. The calorimeter radius at room temperature is 13.453 inches. During re-entry the change in radius, assuming a calorimeter strain rate of 0.010 in/in is

$$\Delta R = 0.01\,(R) = 0.01\,(13.453) = 0.134 \text{ inches}$$

The attachment is approximately 10° to the side of the window center line. The hoop expansion is

$$\Delta_{hoop} = \Delta R \tan \alpha = 0.134\ (0.176) = 0.0236 \text{ in.}$$

The slotted hole length must be a minimum of

$$= \text{Bolt diameter} + 0.0236 = 0.19 + 0.0236 = 0.214 \text{ in.}$$

c. Structural Analysis

Analysis of the window frame is based on the following weights for one assembly:

1.	Fused silica window	=	2.25 lbs
2.	Pyrolytic graphite	=	0.27
3.	Aluminum frame	=	0.50
4.	Aluminum plate	=	0.38
5.	Antenna box	=	2.00
6.	Aluminum angles	=	0.22
7.	Cable	=	0.63
	Total	=	6.25

Load Condition J is critical, where from Figure 15 of Reference 10, the limit loads are:

$$G_x = 23.0$$

$$G_n = 7.0$$

$$p_{windward} = 15.4 \text{ psi}$$

$$p_{leeward} = 13.0 \text{ psi}$$

The total load on the entire window assembly is due to the antenna window assembly inertia plus or minus the air pressure. The total load on the leeward side then is

$$P_o = 6.25 \times 7.0 + (10.5 \times 2.44)\ 13.0$$

$$= 43.8 + 333.0 = 376.8 \text{ lbs limit}$$

The angles are fastened to the antenna box by eight No. 10 machine screws. The load per screw is

$$P = \frac{P_o}{8} = \frac{376.8}{8} = 47.1 \text{ lbs limit}$$

In transferring the load from one leg of the angle to its supports, a bending stress is developed in the 0.090 ± 0.010 inch thick leg

$$f_b = \frac{3.05P}{t^2} = \frac{3.05 \times 47.1}{(.08)^2}$$

$$= 22450 \text{ psi, limit}$$

From verbal Thermodynamics information of February 2, 1967, the temperature of the beryllium shell at a depth of 1.0 inch is 450°F. With a glass insulating layer, the temperature of the 2024 - T4 aluminum angle will be at 300°F or less. The properties of the aluminum at 300°F and 450°F are:

Property	300°F	450°F
F_{bu}	92000 x 0.84 = 77300	92000 x 0.62 = 57000
F_{by}	48000 x 0.87 = 41700	48000 x 0.69 = 33100

The design is acceptable without the insulation:

$$M.S. = \frac{33100}{22450 \times 1.15} - 1 = +.28$$

The strength of the angle acting as a beam must be checked:

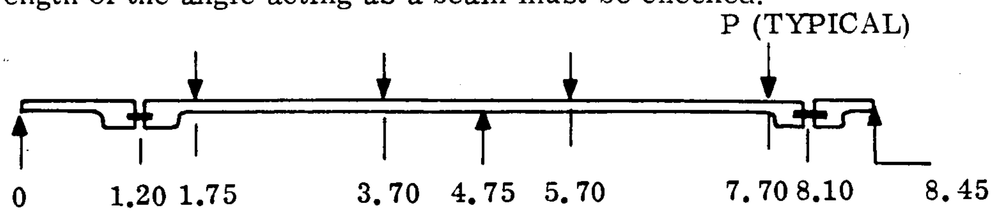

Assume the pins at stations 1.20 and 8.10 can carry moment and solve as a beam on three supports, but simplifed to treat the left hand side as a propped cantilever. Using Reference 5, Table III, Case 22:

$$R_1 = \frac{P}{2}\left[\frac{3(3.0)^2\,4.75 - (3.0)^3}{(4.75)^3} + \frac{3(1.05)^2\,4.75 - (1.05)^3}{107.2}\right]$$

$$= \frac{47.1}{2}\left[0.943 + 0.136\right] = 25.4 \text{ lbs limit}$$

$$M_2 = \frac{P}{2}\left[\frac{27 + 2 \times 3.0\,(4.75)^2 - 3 \times 9 \times 4.75}{(4.75)^2}\right.$$

$$\left. + \frac{1.158 + 2 \times 1.05\,(4.75)^2 - 3 \times 1.102 \times 4.75}{22.56}\right]$$

$$= \frac{47.1}{2}\left[1.518 + 1.459\right]$$

$$= 70.2 \text{ inch-lbs, limit}$$

$$M_{pin} = R_1\,x = 25.4 \times 1.20$$

$$= 30.5 \text{ inch-lbs}$$

Check the pin, using steel of 0.156 inch diameter

$$Z = \frac{\pi r^3}{4} = 0.785\,(.078)^3 = 372 \times 10^{-6}$$

$$f_b = \frac{M}{Z} = \frac{30.5}{372}\,10^6 = 82100 \text{ psi limit}$$

For type 4130 steel with room temperature F_{tu} of 150,000 psi, the strength at 450°F becomes:

$$F_{tu} = 150000 \times 0.93 = 139200$$

$$F_{ty} = 132000 \times 0.90 = 119000$$

$$M.S. = \frac{139200}{82,100 \times 1.5} - 1 = +0.13$$

For the .66 x .60 x .090 angle, the approximate section properties are

$$I = 0.0035$$

$$\bar{y} = 0.18$$

$$f_b = \frac{M_2 c}{I} = \frac{70.2\,(.66 - .18)}{0.0035}$$

$$= 9630 \text{ psi limit}$$

$$F_{ty} = 40,000 \times 0.69 = 27600 \text{ for 2024-T4}$$

$$M.S. = \frac{27600}{9630 \times 1.15} - 1 = \text{AMPLE}$$

The center attachment of the aluminum angle to the beryllium must be checked. The load, R_2, on this No. 10 flat-head screw is dependent on R_1 calculated above.

$$R_2 = 4P - 2R_1 = 4 \times 47.1 - 2 \times 25.4$$

$$= 137.6 \text{ lbs limit}$$

$$f_s = \frac{137.6}{0.0283} = 4860 \text{ psi limit}$$

$$F_{su} = 85000 \times 0.88 = 74700 \text{ psi}$$

$$M.S. = \text{HIGH}$$

The aluminum plate stresses will be less than those shown for the aluminum angle, since the number of effective fasteners is the same (equal to 8, even though 14 are installed). The thickness is .100 ±0.010, 0.010 greater than the angle, however, the load is not as great, since the weight of antenna box and angle do not act here.

Stresses in the aluminum frame will occur during handling, Load Condition A, when the weight of the window rests on the .060 ± .010 flange. The flange is 10 inches long and .28 inch wide

$$f_b = \frac{6M}{t^2} = 6 \frac{WG_n}{2\ell} \times \frac{w}{2} \times \frac{1}{t^2}$$

$$= \frac{1.5 \times 2.25 \times 3.0 \times .28}{10(0.05)^2}$$

$$= 113.4 \text{ psi}$$

$$\text{M.S.} = \text{HIGH}$$

2. C-BAND ANTENNA WINDOW FRAME

a. General

Two C-band antenna windows are located in cut-outs in the beryllium calorimeter at 82.5° and 262.5° at Station 150.5. The window is made of fuzed silica glass type 7941. It is held in place by an aluminum framework which is fastened to the calorimeter as shown in Figure 39. Pins and slotted or oversize screw holes have been employed to allow the framework to expand in the meridional and hoop directions during re-entry conditions. The C-band windows, with their pyrolytic graphite frames, are 2.83 inches long, 1.64 inches wide, and 1.10 inches thick.

b. Structural Analysis

The analysis is based on the following weights for one assembly:

1.	Fused silica window	=	0.394 lbs
2.	Pyrolytic graphite	=	0.065
3.	Aluminum frame	=	0.230
4.	Aluminum plate	=	0.263
5.	Antenna box	=	0.500
6.	Aluminum angles	=	0.223
7.	Cable	=	1.10
	Total		2.775 lbs

The critical condition is Load Condition J, having the same loads shown for the VHF antenna window frame. The total load on a window assembly from this condition, on the leeward side, is

$$P_o = 2.775 \times 7.0 + (2.83 \times 1.64)\ 13.0$$

$$= 19.4 + 60.4$$

$$= 79.8 \text{ lbs limit}$$

The aluminum angles are fastened to the plate by four No. 10 bolts, so that the load per bolt is

$$P = \frac{P_o}{4} = \frac{79.8}{4}$$

$$= 20.0 \text{ lbs, limit}$$

The bending stress in the angles developed in transfer of load from one leg of the angle to its supports is (in the $0.090 \pm .010$ leg):

$$f_b = \frac{3.05P}{t^2} = \frac{3.05 \times 20.0}{(.08)^2}$$

$$= 9530 \text{ psi, limit}$$

If we take the temperature of the aluminum as 450^oF, as in the VHF antenna window frame analysis, the critical parameter is $F_{by} = 33100$ psi

$$\text{M.S.} = \frac{33100}{9530} - 1 = \text{HIGH}$$

E. UMBILICAL DISCONNECT

1. GENERAL

This analysis verifies the integrity of the umbilical bracket, Drawing SK 56163-338, which is located at station 156 between the closure ring and the calorimeter shell as shown in Figure 40. The bracket is made of 7075-T6 plate material.

2. LOADS

The critical bracket loads occur for Load Condition K (Table I) where the load P is 800 pounds limit applied as shown in Figure 40. The loading occurs at spacecraft liftoff, therefore, room temperature material-properties are used.

3. END PAD ANALYSIS

The "end pad" analysis where the connector attaches assumes that the load is equally divided between two sides of the end pad. The third side is assumed to carry no load since most of the edge is cut-out to allow the interface ring to fit properly. The end pad analysis considers the end pad is free to deflect but not to rotate. Therefore, each side will be treated close to a beam fixed at one end, free but guided at other with a concentrated load at the guided end. Instead of a moment of $P\ell/4$ however, a plate analogy shows that the maximum moment (occurs at the juncture of end pad and connector) where

$$\frac{a}{b} = \frac{1.748 - .240}{.5\,(1.260 + .884)} = \frac{1.508}{1.072} = 1.405$$

$$\therefore M = \frac{P\ell}{2} \times .65 = \frac{P\ell}{3.08}$$

$$\ell = (1.748 - .240 - 1.072)\,\frac{1}{2}$$

$$= .218$$

An effective width of end pad of $b = 0.7$ inch is assumed. Thickness is $.11 \pm .01$

$$f_b = \frac{6M}{bt^2} \quad \frac{6.0\,P\ell}{3.08\,bt^2} = \frac{1.95\,P\ell}{bt^2}$$

81

$$= \frac{1.95 \times 800 \times .218}{.70\,(.10)^2}$$

$$= 48500 \text{ psi, limit}$$

For 7075-T6 plate material, $F_{tu} = 77000$ psi

$F_{ty} = 66000$ psi

$$M.S. = \frac{77000}{1.5 \times 48500} - 1 = +.05$$

4. SIDE PLATE ANALYSIS

The determination of moment on the side plate is based on length to its mid-thickness

$$\ell = (1.748 - .120 - 1.072)\frac{1}{2} = .278$$

$$M = \frac{P\ell}{2} \times .52 = \frac{800 \times .278}{3.85}$$

$$= 57.9 \text{ inch-lbs.}$$

The thickness of the side wall is $.12 \pm .01$. The maximum tensile stress is then:

$$f_t = \frac{P}{2bt} + \frac{6M}{bt^2}$$

$$= \frac{800}{2 \times .70 \times .11} + \frac{6 \times 57.9}{.70\,(.11)^2}$$

$$= 5200 + 41000$$

$$= 46200 \text{ psi}$$

For a 7075-T6 plate, $F_{tu} = 77,000$ psi

$$M.S. = \frac{77000}{1.5 \times 46200} - 1 = +.11$$

5. MOUNTING BOLTS

The shear load on each of the four mounting bolts is assumed 1/4 of the total shear load. The shear load per bolt is then:

$$V = \frac{800 \cos 28^{\circ}}{4} = 200\,(.883) = 176.6 \text{ lbs}$$

The maximum tension load, T, per fastener is determined by considering heeling about point A in Figure 32.

$$T = \frac{bdP}{2\left[a^2 + b^2\right]}$$

$$= \frac{1.60 \times .79 \times 800}{2\left[(.70)^2 + (1.60)^2\right]}$$

$$= 165.8 \text{ lbs, limit}$$

The allowable shear and tension loads for a No. 10 steel bolt are 2580 lbs and 2530 lbs respectively

M.S. = HIGH

The capability of the angle into which the bolts are mounted can be evaluated from the curves for "Flange Bending Strength of 2024-T4 Extruded Angles".

t = .080 min (conservative - one leg is .110 minimum)

eccentricity, C = .41

$$T_{allowed} = T_{2024\text{-}T3} \times \frac{F_{ty} \text{ of 7075-T6}}{F_{ty} \text{ of 2024-T3}}$$

$$= 410 \times \frac{66000}{42000}$$

$$= 645 \text{ lbs, ult}$$

$$M.S. = \frac{645}{1.5 \times 165.8} - 1 = \text{AMPLE}$$

F. AFT COVER

1. GENERAL

The aft cover is a fiberglass, aluminum beam reinforced plate and is attached to the closure ring at station 156. The cover has a radius of 10.9 inches (10.6 inches to the bolt pattern) and a minimum thickness of 0.15 inches. The plate and stiffening beams are shown in Figure 42.

2. TEMPERATURES

During re-entry the external surface of the cover is ablative at a temperature of about 2640°F. At a depth of about 0.05 inches the temperature is 740°F and remains constant at 740°F throughout the remaining depth of the cover. During the launch environment the cover is assumed to be at room temperature.

3. MATERIALS

The aft cover is made of phenolic fiberglass per NCS 3161. Room and elevated temperature mechanical and physical material properties are obtained from Reference 35.

4. LOADS

During re-entry, limit load condition J is critical where G_x and G_n are +23 and +7 respectively. Also during re-entry the base pressure on the cover is .44 psi, limit @ 40,000 ft.

During the launch environment the maximum aft cover pressures occurred at 40 seconds after launch which corresponds to limit load condition C, Maximum $Q\alpha$. The graph below describes the maximum pressure differential on the aft cover for various vent hole radii. The actual vent radius is .692 inches which gives a limit pressure differential of .175 psi.

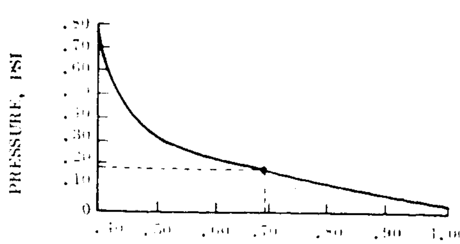

This pressure is not as critical as the base pressure which occurs during re-entry. Therefore, the re-entry condition dictates the criteria for the structural analysis of the aft cover.

5. ANALYSIS - RE-ENTRY

The cover is divided into three segments by channel shaped stiffening beams with webs of 1.5 inches and flanges of .75 inches as shown in Figure 42. During re-entry each beam is assumed to carry a portion of the total cover and equipment weight. The beam is loaded as shown below:

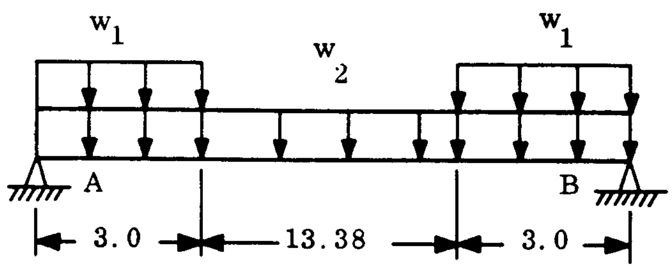

The value w_1 reflects the weight of the equipment mounted on the beams.

$$W = 4 \text{ lbs}$$

$$w_1 = \frac{4\,(23.0)}{4\,(3.0)} = 7.67 \text{ lbs/in, limit}$$

The value w_2 reflects the weight of the cover and the pressure load.

$$\text{Cover Area} = \pi (10.6)^2 = 353 \text{ in}^2$$

For G_x = 23.0 the cover weight is

$$W = A\,(t)\,(p)\,(G_x) = 353\,(.15)\,(.0632)\,(23)$$

$$= 76.8 \text{ lbs}$$

Distributing this load the equivalent "pressure" is:

$$p_o = \frac{W}{A} = \frac{76.8}{353} = .218 \text{ psi}$$

The total limit pressure is then equal to

$$p = .218 + .440 = .658 \text{ psi.}$$

Assuming the beam supports load induced by 6.5 inches of cover width, w_2 is equal to:

$$w_2 = 6.5\,(.658) = 4.28 \text{ lbs/in.}$$

Beam bending is calculated assuming the ends of the beam simply supported.

$$R_A = R_B = \frac{7.67\ (6.0) + 4.28\ (19.38)}{2} = 64.5 \text{ lbs, limit}$$

$$M_{max} = 9.69\ (64.5) - 7.67\ (8.19)\ (3) - 4.28\ (4.84)\ (9.69)$$

$$= 625 - 188 - 201 = 236 \text{ in-lbs}$$

The section properties of the channel are:

$$A = .145 \text{ inches}$$

$$h = 1.5 \text{ inches}$$

$$\bar{y} = .75 \text{ inches}$$

$$I_{c.g.} = .051 \text{ in}^4$$

$$f_b = \frac{Mc}{I} = \frac{236(.75)}{.051} = 3470 \text{ psi, limit}$$

The crippling strength of the section @ 700^oF is:

$$\left[\frac{F_{cy}}{E}\right]^{\frac{1}{2}} = \left[\frac{45,000(.2)}{10.5 \times 10^6 (.54)}\right]^{\frac{1}{2}} = \left[\frac{9000}{5670 \times 102}\right]^{\frac{1}{2}} = 3.99 \times 10^{-2}$$

For the flange, assuming $r_m = .145$

$$b_1 = .58 + .535\ (.145) = .58 + .0776 = .658$$

$$\frac{b_1}{t} = \frac{.658}{.050} = 13.2$$

$$F_{cc_1} = .70\ (9000) = 6300 \text{ psi}$$

For the web,

$$b_2 = .658$$

$$F_{cc_2} = .70\ (9000) = 6300 \text{ psi}$$

$$F_{cc} = 6300 \text{ psi}$$

$$M.S. = \frac{6300}{3470 \times 1.5} - 1 = +.23$$

The beam deflection is calculated using superposition of the deflections due to w_1 and w_2.

$$y = y_{w_1} + y_{w_2}$$

$$= \frac{w_1 a^2(\ell - x)}{12EI\ell}\left[4x\ell - 2x^2 - a^2\right] + \frac{5w_2\ell^4}{384EI}$$

where:

$$w_1 = 7.67 \text{ lbs/in}$$

$$w_2 = 4.28 \text{ lbs/in}$$

$$\ell = 19.38 \text{ inches}$$

$$x = 9.69 \text{ inches}$$

$$a = 3.00 \text{ inches}$$

$$E = 10.5 \times 10^6(.80) = 8.4 \times 10^6 \text{ psi}$$

$$y = \frac{7.67(9.0)(19.38 - 9.69)}{12(8.4 \times 10^6)(.051)(19.38)}\left[4(9.69)(19.38) - 2(9.69)^2 - (3.0)^2\right]$$

$$+ \frac{5(4.28)(19.38)^4}{384(8.4 \times 10^6)(.051)}$$

$$= .00372 + .0183 = .022 \text{ inches, limit}$$

This small deflection indicates that it is proper to analyze the phenolic fiberglass aft cover as a plate fixed on all edges neglecting the initial deflection of the plate edge attached to the beam.

The phenolic fiberglass aft cover plate is divided into 3 segments by stiffening beams. Two sections are approximately solid semi-circular plates, with all edges assumed fixed, while the third section between beams is considered as a long rectangular plate with its edges fixed. The plates are uniformly loaded with a limit pressure of .652 psi.

For a semi-circular plate with a radius of 10.6 inches and fixed on all sides, the maximum radial and tangential stresses are calculated to be:

$$S_r = \frac{.42\,wa^2}{t^2} = \frac{.42\,(.658)\,(10.6)^2\,(1.5)}{(.10)^2}$$

$$= 4670 \text{ psi, ult.}$$

$$S_t = \frac{.21\,wa^2}{t^2} = \frac{.21\,(.658)\,(10.6)^2\,(1.5)}{(.10)^2}$$

$$= 2330 \text{ psi, ult.}$$

$$\text{M.S.} = \frac{6400}{4670} - 1 = +.37$$

For a semi-circular plate with the curved boundary fixed and straight boundary simply supported, the maximum deflection is calculated.

$$y = \frac{\alpha wa^4}{Et^3} = \frac{.038\,(.658)\,(1.26 \times 10^4)\,(1.5)}{1.53 \times 10^6\,(1 \times 10^{-3})}$$

$$= .309 \text{ inches}$$

This deflection indicates that it is necessary to use large deflection theory to obtain accurate stresses and deflections. The plate is stiffer than indicated by the ordinary theory and the stresses for the applied load are less than indicated. Since large deflection theory equations for a semi-circular plate are not readily available, an equivalent rectangular plate with "a" and "b" lengths equal to 21.2 and 10.6 inches respectively will be used. This equivalent plate will yield conservative results.

$$\frac{wb^4}{Et^4} = \frac{.658\,(1.5)\,(1.26 \times 10^4)}{1.53 \times 10^6\,(1 \times 10^{-4})} = 78.0$$

From page 222 of Reference 5, the following relationships hold:

$$\frac{y}{t} = 1.07$$

$$\therefore y = 1.07\,(.10) = .107 \text{ inches, ult.}$$

$$\frac{S_d b^2}{Et^2} = 3.2$$

$$\therefore S_d = \frac{3.2\,(1.53 \times 10^6)\,(1 \times 10^{-2})}{1.125 \times 10^2} = 435 \text{ psi, ult.}$$

$$\frac{S\,b^2}{E\,t^2} = 27.8$$

$$\therefore S = \frac{27.8}{3.2}\,(435) = 3780 \text{ psi, ult.}$$

The total stress in the plate is

$$S = S_d + S = 435 + 3780 = 5215 \text{ psi}$$

$$\text{M.S.} = \frac{6400}{5215} - 1 = +.23$$

For the rectangular portion of the plate between the stiffening beams the stress and deflection are calculated. The maximum stress occurs at the centers of the long edges and is equal to:

$$S_b = \frac{.5\,wb^2}{t^2\,(1 + .623\,\alpha^6)} \qquad \text{where: } \alpha = \frac{5.1}{21.2} = .24$$

$$= \frac{.5\,(.658)\,(5.1)^2}{.01} = 855 \text{ psi, limit}$$

$$\text{M.S.} = \frac{6400}{855 \times 1.5} - 1 = \text{HIGH}$$

The maximum plate deflection is

$$\delta = \frac{.0284\,wb^4}{E\,t^3\,(1 + 1.05\alpha^5)}$$

$$= \frac{.0284\,(.658)\,(675)}{.85 \times 10^6\,(1 \times 10^{-3})} = .01485 \text{ inches}$$

The access hole in the aft cover is approximately 5.63 inches in diameter. It is attached to the basic aft cover by a splice plate as shown in Figure 42.

Assuming the plate simply supported the radial and tangential stresses are calculated. From previous calculations, the pressure on the access hole plate is:

$$p = .658 \text{ psi}$$

$$S_r = S_t = \frac{3pa^2}{8\,mt^2} \quad (3m + 1)$$

$$= \frac{3(.658)(5.63)^2}{32\,(10)\,(.010)} \quad [31] = 607 \text{ psi, limit}$$

$$M.S. = \frac{6400}{607 \times 1.5} \quad -1 = \text{HIGH}$$

The total load reacted by the splice plate is:

$$W = p\left[\frac{\pi D^2}{4}\right] = .652 \left[\frac{\pi(5.63)^2}{4}\right]$$

$$= .652 \quad [24.8] = 16.15 \text{ lbs}$$

The splice plate to access door attachment is accomplished using 6 No. 10 countersunk bolts. Therefore, the load per attachment is:

$$W/\text{attachment} = \frac{16.15}{6} = 2.7 \text{ lbs, limit}$$

This load is small relative to the fastener strength.

The 0.050 inch thick splice plate is check using plate equations from Reference 5. The splice plate is assumed fixed at both the inner and outer radii with the inner radii surface being free to deflect. Using Table X, Case 20, the maximum radial stress is calculated.

$$S_r = \frac{3W}{2\pi t^2} \left[1 - \frac{2a^2}{a^2 - b^2} \quad (\log \frac{a}{b})\right]$$

where:

$$a = 3.125 \text{ inches}$$

$$b = 2.500 \text{ inches}$$

$$t = .050 \text{ inches}$$

$$W = 16.15 \text{ lbs.}$$

$$S_r = \frac{3(16.15)}{2\pi(.05)^2}\left[1 - \frac{2(3.125)^2}{\left((3.125)^2 - (2.5)^2\right)^2}\left(\log\frac{3.125}{2.5}\right)\right]$$

$$= \frac{48.4}{.0157}\left[1 - \frac{19.6}{3.55}(.097)\right]$$

$$= 3080\left[1 - .535\right] = 1430 \text{ psi}$$

$$F_{tu} = 63{,}000\,(.12) = 7550 \text{ psi @ } 700^{\circ}\text{F}$$

$$\text{M.S.} = \frac{7550}{1430} - 1 = \text{HIGH}$$

The stiffening beam loads are transferred to the aft cover attachment bolts by clips as shown in Figure 42. A portion of the load is carried by the clips and the remaining load is carried by the fiberglass aft cover. The percent of the load carried by each is based on the stiffnesses of the parts. The critical loading occurs during the re-entry phase of flight.

The stiffness of the .050 steel (301 1/2 hard) angle assuming a 2 inch width effective is:

$$EI = \frac{30 \times 10^6\,(2)\,(.05)^3}{12} = 625 \text{ lb-in}^2$$

The stiffness of the .10 inch thick fiberglass assuming a 2 inch width effective is:

$$EI = \frac{1.53 \times 10^6\,(2)\,(.10)^3}{12} = 255 \text{ lb-in}^2$$

From the ratio of the stiffnesses the fiberglass carries a portion of the load equal to:

$$P_{glass} = \frac{255P}{880} = .290\,P$$

$$P_{st} = \frac{625P}{880} = .710\,P$$

Assuming a beam with one end fixed and the other end guided with the load applied to the guided end, the maximum moments in the fiberglass and steel are:

$$M_{glass} = \frac{.290P\ell}{2} = \frac{.290(1.1)P}{2} = .160\,P$$

$$M_{st} = \frac{.710P\ell}{2} = \frac{.710(1.1)P}{2} = .390\,P$$

For launch conditions the stiffening beam is located as shown below:

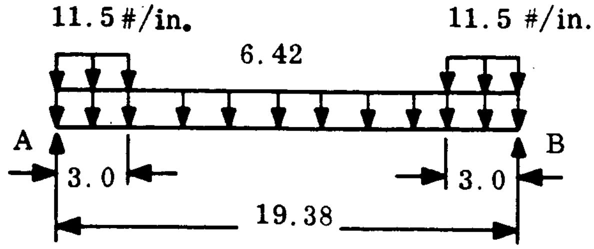

$$R_A = R_B = P = \frac{11.5(6.0) + 6.42(19.38)}{2} = 96.5 \text{ lbs, ult.}$$

$$\therefore M_{glass} = .1975(96.5) = 19.1 \text{ in-lbs}$$

$$f_{glass} = \frac{6(19.1)}{2(.01)} = 5{,}720 \text{ psi, ult.}$$

$$F_{tu} = 25{,}000 \text{ psi}$$

$$M.S. = \frac{25{,}000}{5720} - 1 = \text{HIGH}$$

$$M_{st} = .352(96.5) = 34.0 \text{ in-lbs.}$$

$$f_{st} = \frac{6(34.0)}{2(.0025)} = 40{,}800 \text{ psi, ult}$$

$$M.S. = \frac{150{,}000}{40{,}800} - 1 = \text{HIGH}$$

6. THERMAL STRESSES

If the aft cover is assumed to be fully restrained the resulting compression stress is:

$$\sigma = \frac{\Delta T \alpha E}{1 - v}$$

where:

$\Delta T = 750 - 80 = 670^{\circ}F$

$\alpha = 8.0 \times 10^{-6}$ in/in$^{\circ}$F

$E = 1 \times 10^{6}$ psi

$v = .10$

$$\sigma = \frac{670(8 \times 10^{-6})(1 \times 10^{6})}{1 - .10}$$

$$= \frac{5350}{.9} = 5950 \text{ psi}$$

The above stress does not take into account the expansion of the closure ring to which the aft cover is attached. The coefficient of thermal expansion for the aluminum ring is approximately 12 x 10^6, therefore it is assumed that the ring will expand at a greater rate than the cover, therefore, relieving the stresses calculated above. When the ring temperature during re-entry is determined then, the actual stresses may be calculated in the plate.

G. EQUIPMENT PACKAGE

1. GENERAL

The equipment package assembly consists of a 28 inch beam supported by bulkheads at stations 60.38 and 90.00 and enclosed by a non structural conical shell dust cover. Two bathtub type fittings attached to the aft bulkhead support two batteries mounted "piggy back". The entire assembly is made of 2024-T4 aluminum alloy. The assembly is supported laterally at the forward and aft bulkheads and axially at the aft bulkhead.

2. LOADS

The component and structure weights considered acting on the 28 inch beam are listed below:

Unit	C.G.	Weight
Power Controller	76.0	0.65 lbs.
Transmitter	66.5	2.25
Transmitter	71.5	2.25
SCO	62.0	1.51
SCO	66.0	1.51
C-Band Transponder	77.5	2.50
C-Band Transponder	81.0	2.50
Signal Data Converter	74.0	2.50
Signal Data Converter	76.0	2.50
High Level Commutator	69.0	0.81
5 Volt Power Supply	66.0	0.89
Low Level Commutator	79.0	2.70
Low Level Commutator	87.0	2.70
Reflectometer	85.0	0.24
Accelerometers	84.0	2.68
		28.19 lbs.

In addition to the concentrated loads on the beam there is also assumed a uniformly distributed load due to wiring, miscellaneous attaching hardware and structure weights.

Item	Weight	Distributed Load
Wire	5.50 lbs.	0.197 lb/in
Attaching Hardware	0.42	0.015
Structure	6.28	0.224
	12.20 lbs.	0.436 lb/in

Other components of the equipment package assembly and their weights are listed below:

Item	Weight
Batteries	2 @ 10.0 lbs each
Battery Support Brackets	2 @ 1.0 lb each
Aft Bulkhead	3.73 lbs
Fwd. Bulkhead	1.65 lbs
Rate Gyros	2 @ 2.20 lbs each
Dust Cover	3.0 lbs
	34.78 lbs

The total equipment package assembly weight is therefore equal to 75.17 lbs.

3. ANALYSIS OF BEAM

The support beam to which the components are attached has a varying cross-section. The basic beam is a channel, 28 inches in length, with a width varying from 8.00 inches at station 62.00 to 9.82 inches at station 90.00. The channel flanges are 1.00 inch tall. Mounted to the center of the channel web is a tee extending from station 70.38 to station 90.00. The composite beam is made of 2024-T4 aluminum, 0.18 inch thick. The beam is analyzed assuming it is simply supported at station 62.00 and fixed at station 90.00. Using indeterminate beam analysis methods the unit load factor shear and moment diagrams are obtained and are shown in Figure 43. The maximum beam bending stresses occur for load condition J where the limit load factors G_X and G_N are +23.0 and ±7 respectively.

The maximum beam stress occurs at station 90.00 where from Figure 43 the moment is 428 in-lbs. The axial load is based on the weights of the beam, components and fwd bulkhead and is equal to 42.04 lbs. The beam section properties at Station 90 are

9?

$A = 2.678 \text{ in}^2$

$c = 3.29$ inches

$I = 2.64 \text{ in}^4$

The beam stress is:

$$f_b = \frac{Mc}{I} + \frac{P}{A}$$

$$= \frac{428 \times 7.0 \times 3.29}{2.64} + \frac{42.04 \times 23}{2.678}$$

$$= 3,740 + 360 = 4100 \text{ lbs, limit}$$

$$F_{TU} = 62,000 \text{ psi}$$

$$M.S. = \frac{62000}{4100 \times 1.5} -1 = \text{HIGH}$$

The tee section of the beam is also checked for lateral loads that cause bending about the weaker axis of the section. The maximum loads and stresses occur in the area where the low level commutator is attached to the tee (approximately station 78.90). The loads are applied and reacted as shown below and a unit width beam is conservatively assumed. The maximum moment is equal to:

$$M = 2.5\ (1.65)\ (7.0) = 28.9 \text{ in-lbs.}$$

$$f_b = \frac{6M}{bt^2} = \frac{6(28.9)}{(1)(0.18)^2} = 53.50 \text{ psi}$$

$$F_{TU} = 62,000 \text{ psi}$$

$$M.S. = \frac{62,000}{5350(1.5)} -1 = \text{HIGH}$$

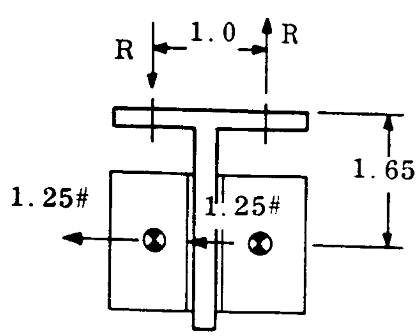

41

The maximum rivet load, R, is:

$$R = \frac{M}{d} = \frac{28.9}{1} = 28.9 \text{ lbs.}$$

This load is very small and a high margin of safety exists in the rivets.

The moment at station 90.00 is transferred to the aft bulkhead via 17 BJ-6 rivets as shown below:

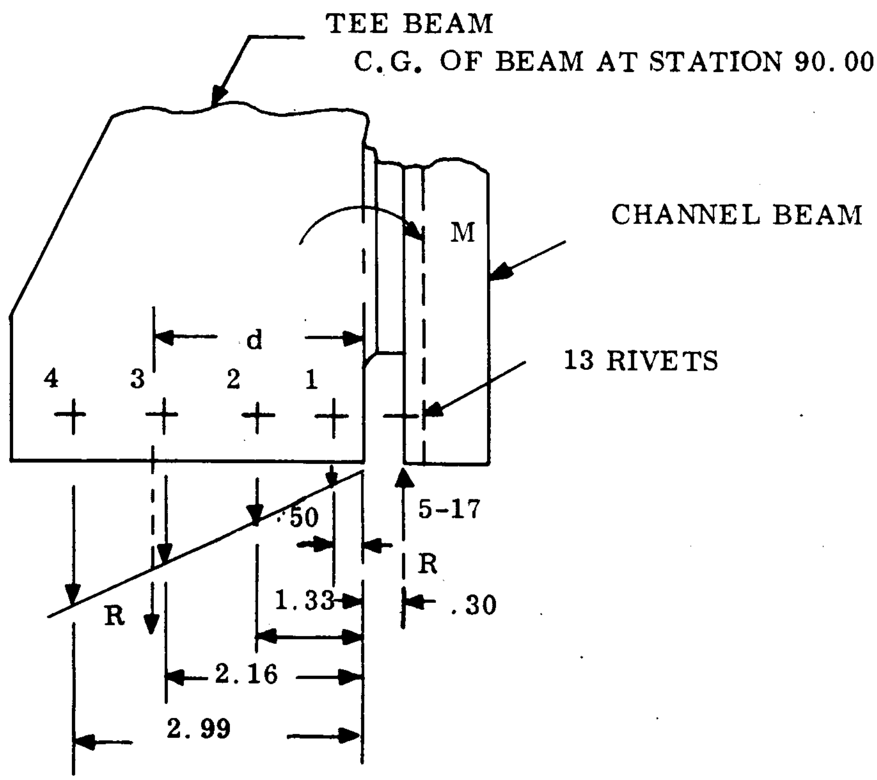

The portion of the load taken by rivets 1 thru 4 is calculated below.

$$\Sigma_y = 0.50 + 1.33 + 2.16 + 2.99 = 6.98$$

$$P_1 = \frac{R \times 0.5}{6.98} = 0.0715\ R$$

$$P_2 = \frac{R \times 1.33}{6.98} = 0.191\ R$$

$$P_3 = \frac{R \times 2.16}{6.98} = 0.309\ R$$

$$P_4 = \frac{R \times 2.99}{6.98} = 0.428\ R$$

$$d = 0.50(0.0715) + 1.33(0.191) + 2.16(0.309) + 2.99(0.428) = 0.0357 + 0.254 + 0.667 + 1.28 = 2.237$$

$$R = \frac{M}{d + 0.30} = \frac{428}{2.237 + 0.30} = 169 \text{ lbs.}$$

The maximum rivet load is P_4 and for $G_N = 7.0$

$$P_4 = 0.428\ (169)(7.0) = 505 \text{ lbs.}$$

The rivet load due to G_x must be added to the above load. For axial loads each rivet is assumed to carry an equal load.

$$P_n = \frac{42.04\ (23)}{17} = 57 \text{ lbs.}$$

The total limit rivet load P_4 is:

$$P_4 = 505 + 57 = 562 \text{ lbs.}$$

The shear allowable for a 3/16 inch diameter BJ rivet is 862 lbs.

$$M.S. = \frac{862}{562 \times 1.5} - 1 = +0.02$$

4. BATTERY MOUNTING BRACKETS

The battery mounting brackets shown in Figure 44 support two 10 lb batteries. The bathtub type brackets have 0.18 inch thick end pads and walls, and are made of 2024-T351 aluminum alloy. The end pad of each bracket is attached to the aft side of the equipment package bulkhead at station 90.87 by 4 #10 bolts. The analysis assumes that only the two outside bolts (nearest the walls) are effective in reacting the battery loads. Also conservatively neglected are the shear panels tying the two mounting brackets together.

The critical load condition is J Re-entry, where G_x and G_y are +23.0 and 7.0 respectively. The battery loads are applied to the bracket at two locations as shown below. Each of the two end pad bolts carry loads as calculated below.

$$P_1 = \frac{10}{4}\ (7.0)(1.5) = 26.2 \text{ lbs, ult.}$$

$$P_2 = \frac{5}{2}\ (23.0)(1.5) = 86.5 \text{ lbs, ult.}$$

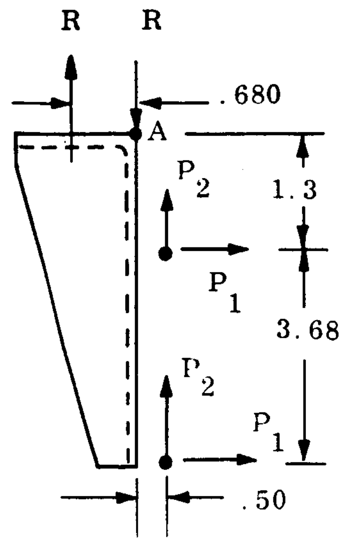

The maximum bolt load is found by summing moments about point A.

$$\Sigma M_A = 0 = 2(86.5)(0.50) + 26.2(1.3 + 4.98) - 0.68\ R$$

$$R = \frac{86.5 + 165}{0.68} = 370 \text{ lbs.}$$

The stresses in the bracket are calculated using the standard bathtub type analysis. The geometry shown below is conservatively assumed.

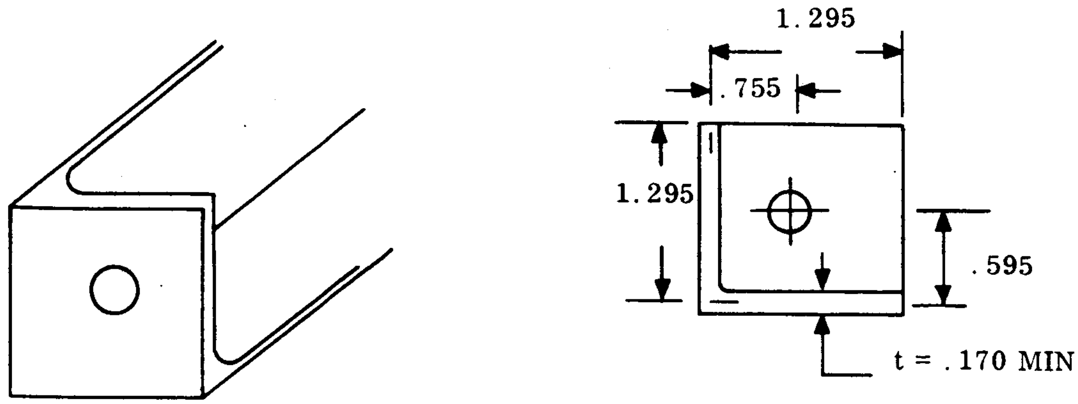

$$a = \frac{A + B}{\pi} = \frac{2(1.295)}{\pi} = 0.825 \text{ inch}$$

$$d = a - \frac{C + D}{2} = 0.825 - \frac{0.595 + 0.755}{2} = 0.15 \text{ inch}$$

$$r_o = 0.20 \text{ inch}$$

$$r_i = 0.10 \text{ inch}$$

$$t_e = t_w = 0.170 \text{ inch}$$

For end pad bending

$$\frac{r_i}{a} = \frac{0.10}{0.825} = 0.121$$

$$\frac{a-d}{r_o} = \frac{0.825 - 0.15}{0.20} = 3.38$$

$$\frac{te}{t_w} = 1.0$$

$$K_1 = 3.6$$

$$K_2 = 0.39$$

$$f_{bu_e} = \frac{Pu}{t_e^2} K_1 K_2 = \frac{370}{0.029} [3.6] [0.39] = 17,950 \text{ psi}$$

$$F_{TU} = 61,000 \text{ psi}$$

$$M.S. = \frac{61,000}{17,950} -1 = \text{HIGH}$$

The plug shear in the end pad is:

$$f_{su_e} = \frac{Pu}{2\pi r_o t_e} = \frac{370}{6.28 (0.20)(0.17)} = 1730 \text{ psi}$$

$$F_{su} = 38,000 \text{ psi}$$

$$M.S. = \frac{38000}{1730} -1 = \text{HIGH}$$

The wall tensile stress is

$$f_{tu_w} = \frac{P_u}{A_g}$$

Where: $A_g = \pi a t_w = \pi (0.825)(0.170) = 0.44 \text{ in}^2$

$$f_{tu_w} = \frac{370}{0.44} = 840 \text{ psi}$$

$$F_{tu} = 61,000 \text{ psi}$$

$$M.S. = \frac{61,000}{840} -1 = \text{HIGH}$$

The wall bending stress is

$$f_{bu_w} = \frac{Mc}{I}$$

Where: $c = 0.637a = 0.637(0.825) = 0.525$ inch

$I = 0.298\, a^3 tw = 0.298(0.562)(0.170) = 0.0284 \text{ in}^4$

$M = P_o (c - d) = 370\ (0.525 - 0.15) = 139$ in-lbs

$f_{bu_w} = \frac{Mc}{I} = \frac{139\ (0.525)}{0.0284} = 2570$ psi

$F_{tu} = 61,000$ psi

$M.S. = \frac{61,000}{2570} - 1 = \text{HIGH}$

The maximum compressive stresses in the tapered flanges of the bracket occur for limit load condition C, Max Q. α. The maximum stress occurs at the intersection of the flanges and end pad of the bracket. The bending moment at this section is calculated below.

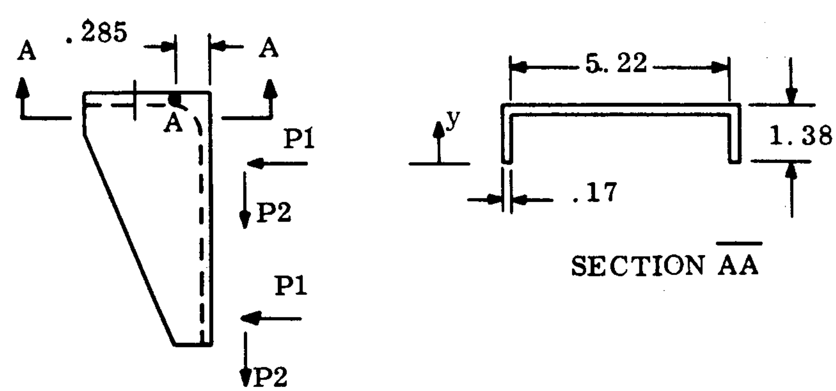

$A = 1.355 \text{ in}^2$

$\bar{y} = 1.095$ inches

$I = 0.161 \text{ in}^4$

$P_1 = \frac{10}{4}(1.6)(1.5) = 6.0$ lbs

$P_2 = \frac{10}{4}(24)(1.5) = 90.0$ lbs.

$\Sigma M_A = 6.0(1.3 + 4.98) + 2(90)(0.785) = 37.7 + 141 = 178.7$ in-lbs.

$f_b = \frac{Mc}{I} = \frac{178.7(1.095)}{0.161} = 12,200$ psi

The crippling strength of the flange is:

$$\left[\frac{F_{cy}}{E}\right]^{\frac{1}{2}} \frac{b}{t} = \left[\frac{38.000}{10.5 \times 10^6}\right]^{\frac{1}{2}} \frac{1.095}{0.17} = 0.387$$

$$\frac{F_{cc}}{F_{cy}} = 1.2$$

Use $F_{cc} = F_{cy} = 38,000$ psi

$$M.S. = \frac{38,000}{12,200} - 1 = \text{HIGH}$$

The angles used to transfer the battery load to the battery mounting brackets are checked. Each angle is 0.094 inches thick. The battery ties to each bracket at 3 places as shown below. The maximum loads occur for limit load condition J where G_X and G_N are +23.0 and +7.0 respectively.

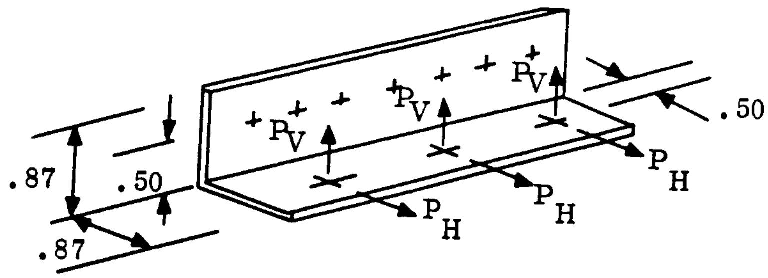

$$P_V = \left(\frac{10}{6}\right)(23)(1.5) = 57.5 \text{ lbs.}$$

$$P_H = \left(\frac{10}{6}\right)(7.0)(1.5) = 17.5 \text{ lbs.}$$

$$M_{max} = (P_V + P_H)(0.5) = 75.0(0.50) = 37.5 \text{ in-lbs.}$$

$$f_{bu} = \frac{6M}{bt^2} = \frac{6(37.5)}{(1)(0.00885)} = 25,400 \text{ psi}$$

$$M.S. = \frac{61,000}{25,000} - 1 = \text{AMPLE}$$

The two battery mounting brackets are connected by shear webs to stiffen the battery assembly. The shear webs are shown in Figure 44. The solid panel is 10.82 x 5.32 inches and 0.032 inch thick. The allowable shear strength of the panel assuming simply supported edges is:

$$F_s = K \frac{E}{1 - v^2} \left(\frac{t}{b}\right)^2$$

For a/b $= 2.04, \quad K = 5.43$

$$F_s = 5.43 \left(\frac{10.5 \times 10^6}{0.91}\right) \left(\frac{0.032}{5.32}\right)^2 = 1870 \text{ psi}$$

Assuming each of the two shear panels carry equal loads

$$P_s = \frac{20 \times 7.0 \times 1.5}{2} = 105 \text{ lbs}$$

$$q = \frac{105}{10.82} = 9.68 \text{ lbs/in}$$

$$f_s = \frac{q}{t} = \frac{9.68}{0.032} = 302 \text{ psi}$$

$$\text{M.S.} = \frac{1870}{302} - 1 = \text{HIGH}$$

The stiffener arrangement on the other side of the battery brackets is also shown in Figure 44. The lateral loads are assumed to be carried by the channel section and brackets as a rigid frame and by the 0.032 plate in shear. Each load path is assumed to carry half the load.

For the rigid frame the approximate moment at the corner is:

$$M = \frac{P_N \times G_N \times h}{\left(4 \ 1.0 + \frac{L}{6h}\right)} = \frac{5.5 \times 7.0 \times 4.98 \times 1.5}{4\left(1 + \frac{9.6}{6(4.98)}\right)} = 55.5 \text{ in-lbs, ult.}$$

The moment of inertia for the 0.050 inch thick 2024-T3 aluminum alloy channel is 0.0546 in^3.

$$f_b = \frac{Mc}{I} = \frac{55.5 \times 0.875}{0.0546} = 890 \text{ psi}$$

The crippling allowable for the section is 28,400 psi.

$$\text{M.S.} = \frac{28,000}{890} - 1 = \text{HIGH}$$

For the 0.032 inch thick shear panel the allowable stress is calculated assuming simply supported edges.

$$F_s = K \frac{E}{1 - v^2} \left(\frac{6}{6}\right)^2$$

For a/b $= \frac{10.82}{2.37} = 4.57$, $K = 4.40$

$$F_s = 4.40 \left(\frac{10.5 \times 10^6}{0.91}\right) \left(\frac{0.032}{2.37}\right)^2 = 4.40\,(11.55 \times 10^6)(1.82 \times 10^{-4})$$

$$= 92.5 \times 10^2 = 9250 \text{ psi}$$

The shear load is:

$$P_s = 5.5 \times 2.0 \times 1.5 = 57.2 \text{ lbs, ult.}$$

$$q = \frac{57.2}{10.82} = 5.28 \text{ lbs/in.}$$

$$f_s = \frac{q}{t} = \frac{5.28}{0.032} = 165 \text{ psi}$$

$$M.S. = \frac{9250}{165} - 1 = \text{HIGH}$$

5. FORWARD BULKHEAD ANALYSIS

The forward bulkhead is basically a 0.25 inch thick 2024-T4 aluminum alloy circular plate with a 0.125 inch wide and 1.25 inch deep integral ring on the periphery of the plate. The bulkhead serves two structural purposes. In addition to supporting the forward end of the non-structural dust cover is also transmits the lateral loads in the panel beam to the ring at station 60.80 via 4 shear pins mounted to the 0.125 inch thick portion of the bulkhead. The bulkhead is critical for limit load condition J, Re-entry, where $G_n = 7.0$. The bulkhead is critical in bearing around the 0.219 inch diameter shear pins made of CRES 17-4 PH Steel (Cond. H1025). Assuming only two pins effective the maximum load per pin is:

$$P_{br} = \frac{5.08 \times 7.0 \times 1.5}{2} = \frac{53.3}{2} = 26.7 \text{ lbs}$$

$$A_{br} = 0.219(0.25) = 0.0548 \text{ in}^2$$

$$f_{br} = \frac{26.7}{0.0548} = 488 \text{ psi}$$

$$M.S. = \frac{53{,}000}{488} - 1 = \text{HIGH}$$

The portion of the shear pin that is in contact with the ring at station 60.80 is 0.247 inch in diameter. The shear stress in the pin is calculated below.

$$P_s = 26.7 \text{ lbs}$$

$$A_s = \pi R^2 = \pi (0.1235)^2 = 0.048 \text{ in}^2$$

$$f_s = \frac{26.7}{0.048} = 557 \text{ psi}$$

$$M.S. = \frac{100,000}{557} - 1 = \text{HIGH}$$

6. AFT BULKHEAD ANALYSIS

The aft bulkhead of the equipment package is basically a beam and reinforced plate as shown in Figure 45. The plate is 0.250 inch thick (±0.010) and the reinforcing members are 0.180 inch thick (±0.010) and is made of 2024-T3 aluminum alloy.

The bulkhead is critical for limit load condition G, Third Stage Ignition,where $G_X = -25.2$. The bulkhead supports the following weights:

Panel Beam	40.39 lbs.
Forward Bulkhead	1.65
Aft Bulkhead	3.73
Dust Cover	3.00
Rate Gyros	4.40
Batteries	22.00
	75.17 lbs.

The panel beams are assumed to uniformly distribute their loads to the reinforcing beams integral with the bulkhead.

$$W = \frac{40.39 \times 25.2}{13.5} = 75.5 \text{ lbs/in.}$$

This load is assumed to be reacted by bolts 2, 3, 4, and 5 as shown in Figure 45. The load per attachment is therefore:

$$P_{2,3,4,5} = \frac{75.5 \times 13.5}{4} = 255 \text{ lbs.}$$

The dust cover, forward and aft bulkheads are assumed to distribute loads evenly to all attachment bolts.

$$P_{1 \rightarrow 6} = \frac{[1.65 + 3.73 + 3.00]\,[25.2]}{6} = 35.2 \text{ lbs.}$$

The rate gyros are assumed to be reacted by bolts 1, 2, 5, and 6. The load per bolt is

$$P_{1,2,5,6} = \frac{4.40 \times 25.2}{4} = 27.8 \text{ lbs.}$$

The battery loads are assumed to be carried by bolts 2 and 5.

$$P_{2,5} = \frac{22 \times 25.2}{2} = 278 \text{ lbs.}$$

The highest loaded bolt is number 5.

$$P_5 = 255 + 35.2 + 27.8 + 278 = 596.0 \text{ lbs.}$$

Since the beam panel is very stiff the bulkhead will have a deflected shape as shown below:

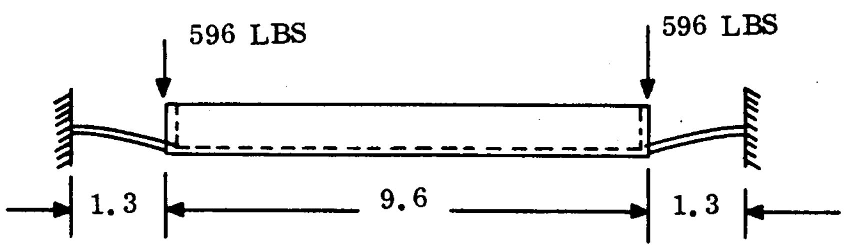

The loads are transferred to the bulkhead - calorimeter attachments assuming beam action with the beam fixed but free to deflect at the ring (no rotation) and fixed at the attachment. The load is applied at the deflected end.

$$M_{max} = \frac{P\ell}{2} = \frac{596 \times 1.3}{2} = 387 \text{ in-lbs.}$$

$$f_b = \frac{6M}{bt^2} = \frac{6(387)}{(1)(0.0625)} = 37,200 \text{ psi}$$

$$F_{TU} = 62,000 \text{ psi}$$

$$M.S. = \frac{62,000}{37,200 \times 1.5} = +0.11$$

The aft bulkhead is attached to the ring at station 90.62 by 6 high strength M.S. 20004 steel bolts. The allowable tensile strength of the 1/4 inch diameter bolt is 160,000 psi. From previous calculations the maximum bolt load occurs for limit load condition G, and is equal to 596 lbs, limit.

$$f_{tu} = \frac{596 \times 1.5}{0.049} = 18,250 \text{ psi}$$

$$M.S. = \frac{160,000}{18,250} - 1 = \text{HIGH}$$

7. EQUIPMENT PACKAGE GUIDE

a. General

Two guides are fastened to the substructure assembly to ease installation of the equipment package. The longitudinal guides are fastened to rings at stations 60.8 and 70.1 and are located at 90° and 270°. The guide is made of 0.063 inch thick 2024-T42 aluminum alloy and is shown in Figure 46.

b. Loads

The guides are critical for limit load condition A, Ground Handling, where G_X and G_N are ±3.0.

c. Analysis

The allowable load on the guide is calculated assuming a load is applied at its center. The guide section properties at that point are:

$$\bar{y} = 0.213 \text{ inch}$$

$$A = 0.0653 \text{ in}^2$$

$$I_{c.g.} = 0.00262 \text{ in}^4$$

The maximum moment is:

$$M = \frac{P\ell}{4} = \frac{8.91\ P}{4} = 2.23\ P$$

$$F_{tu} = 62,000 \text{ psi}$$

$$P_{allow} = \frac{62,000(0.00262)}{2.23\ (0.427)} = 171 \text{ lbs, ult.}$$

Assume that 30% of the equipment package weight is reacted by the guide. The equipment package weight is 75.17 lbs.

$$P_{allow} = 75.17\,(0.30)(3.0)(1.5) = 101.5 \text{ lbs.}$$

$$M.S. = \frac{171}{101.5} - 1 = +0.68$$

VI. NOSE-TIP ANALYSIS

A. DISCUSSION

The nose tip assembly, shown on drawing ER47E190439, extends from stations 1.047 to 8.500 and consists of an ATJ graphite conical shell, a porous carbon insulator inner shell, and a tungsten alloy insert. The bond between the ATJ graphite skirt and the porous carbon is C-10 and the bond between the porous carbon and the tungsten alloy insert is PD162A. In addition to the above parts, a graphite plug is placed between the tungsten alloy insert and the ATJ nose tip. It has the configuration shown in Figure 47. The plug is composed of 0.480 inch of ATJ and 0.173 inch of PG graphite. On its forward end, the plug is surrounded by graphite felt, originally 0.060 ± 0.020 thick but compressed to 0.20 inch. To preload the nose tip assembly to the beryllium calorimeter, a belleville spring arrangement is used. Twenty springs are compressed an amount 0.100 ± 0.030 to create a 0.890 inch total spring height and a resultant preload of 470 ± 175 pounds.

The bonded composite structure scheme of the Re-entry F nose is a follow-on to similar designs in previous programs having these common design features:

1. The heat shield is free from cut-outs or stress raisers
2. Upon bond failure (stress-relief), the ATJ is a free-standing shell without mechanical constraint
3. The tungsten ballast extends the length of the skirt section to provide a lateral load transfer surface

The Re-entry F nose not only has these three advantages, but also adds a more predictable load path by providing low strength porous graphite in addition to the C-10 bond. The details of this design are discussed in the following paragraphs.

In order to minimize thermal stresses in the ATJ shield it was designed in such a manner that upon application of high heating the ATJ is free to expand. This was accomplished by utilizing a .100 thickness of porous carbon between the ATJ and the tungsten ballast. Upon expansion of the ATJ, the porous carbon will either yield or fracture thus allowing the shield to act as a free-standing shell. A bond with good material properties at elevated temperatures (C-10) is required to transfer the load from the ATJ thru the porous carbon to the tungsten ballast. C-10 has another advantage in that it minimizes out-gassing at elevated temperatures. The porous carbon and the hard bond produce structural continuity during boost flight loads. During re-entry, after failure of the porous carbon due to thermal strains, the aerodynamic forces will maintain the nose tip in place. This is shown by Figure 48, where it is seen that a net axial compressive load of 113 + 19 = 132 pounds is developed on the nose.

Bonding the shield to the tungsten ballast has the distinct advantage of eliminating stress concentrations inherent in a mechanically attached shield. Since ATJ can be classified as a brittle material, stress concentrations due to notching, cutting holes, etc., will have a detrimental effect on the load carrying capacity of the shell. The magnitude of this effect is dependent on notch geometry, material sensitivity and loading. The inner surface of the ATJ shell has an ogive transition curve between the cavity radius and the conical shell. This smooth transition prevents any sharp temperature changes in the longitudinal direction thus preventing any severe thermal stress concentration in the nose area.

1. MATERIAL PROPERTIES

Material properties were obtained from the following references

Material	Reference
ATJ for F_{cu} & F_{su}	2
ATJ other properties	3
PG	8
C-10 bond	9
PC (porous carbon)	11
PD-162A bond	16
Tungsten W-2	Vendor data
Graphite Felt	32

The lack of specific property data in most of the above references for the temperatures involved, made a clearly defined analysis of the problem areas very difficult.

2. PROBLEM AREAS

The problem areas for the nose-tip assembly are listed below and then analyzed in the following text.

1. Assembly Problems. Differential thermal expansion stresses which exist during the bond curing cycles at assembly may cause failure of the porous carbon or the C-10 bond.

2. Powered Flight Loads. The design must be shown to have the integrity to resist the vibratory and static loads of powered flight.

3. Re-entry Loads Differential Thermal Expansion. The axial differential thermal expansion load combined with the net inertial and aerodynamic axial load acting between the ATJ shell and the graphite plug may cause high axial compressive stress. When combined with the tensile radial thermal stress, the result may show failure.

4. ATJ Shell Thermal Stress. The geometry of the nose must be controlled to show positive margins for the combination of thermal stresses and aerodynamic stresses in the ATJ shell during re-entry.

5. ATJ Shell Gaps and Concentricity. After the predicted failure of the porous carbon or one of the two bonds during re-entry, the behavior of the free ATJ shell must be shown not to produce any problems related to its non-concentricity with the centerline.

B. ASSEMBLY PROBLEMS

1. SUMMARY

For the C-10 bond, the analysis shows some risk of bond or porous carbon failure when bonding with the low temperature cure. Margins range from -0.26 using worst mechanical properties and min. strengths to +1.90 using average mechanical properties and min. strengths.

For the C-10 bonding at high temperature cure higher risk of scrappage is involved since even use of average mechanical properties and minimum strengths gives negative margins.

Bonding of the PD-162A presents no problem.

2. LOW TEMPERATURE C-10 CURE

Without the use of the high temperature outgassing cycle, the bonding of the porous carbon to the ATJ shell with C-10 bond reaches temperatures limited to 482°F. Differential thermal expansion stresses which exist during the bonding procedure depend primarily upon the properties of C-10 as a function of the specific times and temperature cycles used during the curing operation.

Since the required properties of C-10 are not available for the above conditions, it is not possible to take into account the flexibility of the bond when calculating stresses. However, by assuming the C-10 is completely rigid for shear and radial loads, the resulting stress distributions will be conservative.

The stresses in the hoop and radial directions are approximated by combining Cases 33 and 34 from Table XIII of Reference 5 (page 308). The following maximum stresses result at any specific section:

$f_3 = -pK$ (max radial stress in ATJ, C-10 and porous carbon, at bond line)

$f_2 = pK_A$ (max hoop stress on inner surface of ATJ)

$f_2 = -pK_B$ (hoop stress on outer surface of porous carbon)

$f_2 = -pK'_B$ (max hoop stress on inner surface of porous carbon)

where

$$p = \frac{(\alpha_B - \alpha_A)(T_2 - T_1)}{\frac{1}{E_B}(K_B - \nu_B) + \frac{1}{E_A}(K_A + \nu_A)} + p_o$$

$$K = \frac{2\pi r_2}{2\pi r_2 - N_x} \qquad K'_B = \frac{2 r_2^2}{r_2^2 - r_1^2}$$

$$K_B = \frac{r_2^2 + r_1^2}{r_2^2 - r_1^2} \qquad K_A = \frac{r_3^2 + r_2^2}{r_3^2 - r_2^2}$$

r_1 = radius to inner surface of porous carbon

r_2 = radius to C-10 bond line

r_3 = radius to outer surface of ATJ

N = number of grooves in porous carbon

x = groove width in porous carbon

p_o = initial radial bond pressure

E = Young's modulus

ν = Poisson's ratio

α = thermal expansion coefficient

T_2 = final temperature

T_1 = initial temperature

Subscript B applies to porous carbon

Subscript A applies to ATJ (with grain)

The meridional stresses are not calculated due to the lack of sufficient materials data for C-10. In addition, due to the relatively complex geometry, it would be difficult to obtain reliable results.

At the time the C-10 is bonded, the following geometric conditions exist:

Station (inches)	4.18	4.85	6.31	8.50
r_1 (inches)	0	0	0	0
r_2 (inches)	0.264	0.329	0.465	0.649
r_3 (inches)	0.513	0.578	0.714	0.918
N	4	8	16	16
x (inches)	0.050	0.050	0.050	0.050

K	1.137	1.240	1.378	1.242
K_B	1.000	1.000	1.000	1.000
K'_B	2.000	2.000	2.000	2.000
K_A	1.720	1.955	2.495	3.000

The following material properties are used:

$E_B = 0.6 \times 10^6$ psi (max) $\quad E_A = 1.65 \times 10^6$ psi (max)

$\nu_B = 0.15$ (max) $\quad \nu_A = 0.05$ (min)

$\alpha_B = 1.4 \times 10^{-6}/^\circ F$ (min) $\quad \alpha_A = 2.40 \times 10^{-6}/^\circ F$ (max)

The worst case for analysis is based on the condition that the C-10 bond completely hardens during the 212°F soak temperature condition. Thus when heated to the maximum temperature of 482°F, differential thermal expansion stresses will exist. The initial bond pressure applied during the curing procedure is conservatively neglected. The factor K used in calculating the radial stress at the bond takes into account the reduced bond area due to the grooves cut into the porous carbon. However, it is assumed that the C-10 bond on the net bond area is 100% effective which may not be conservative.

Station (inches)	4.18	4.85	6.31	8.50
p (psi)	-108	-103	-91	-83
$-pK$ (psi)	123	128	125	103
$-pK_A$ (psi)	-186	-202	-227	-249
$-pK_B$ (psi)	108	103	91	83
$-pK'_B$ (psi)	216	206	182	166

The maximum flatwise tensile stress acting on the C-10 occurs at station 4.85 where $f_3 = -pK = 128$ psi, limit (100% bond). Since it has been shown (Reference 9) that the ultimate tensile strength of C-10 may be as low as $F_{tu} = 150$ psi, the minimum margin of safety will be about equal to:

$$M.S. = \frac{150}{1.5\,(128)} - 1 = -0.22 \text{ (conservative)}$$

The maximum tensile stress in the porous carbon is at station 4.18 where $f_2 = -pK'_B =$ 216 psi, limit. Taking the allowable tensile strength to be $F_{tu} = 0.8\ (300) = 240$ psi, the minimum margin of safety will be approximately:

$$M.S. = \frac{240}{1.5\ (216)} - 1 = -0.26 \text{ (conservative)}$$

The minimum margin of safety for the ATJ will be high.

It should be noted that if nominal material properties are used, the margins of safety will be positive. For example, the maximum tensile stress in the porous carbon will be

$$f_2 = -\frac{(1.6 - 2.2)\ (482 - 212)}{\dfrac{1 - 0.10}{0.5} + \dfrac{1.72 + 0.10}{1.55}} (K'_B) = 27.5\ (2.00)$$

$$= 55 \text{ psi, limit (nominal)}$$

$$M.S. = \frac{240}{1.5\ (55)} - 1 = +1.9 \text{ (nominal)}$$

Assuming the parts do not fail during the bonding operation, the temperature will gradually be reduced to room temperature at the end of the 482^{o}F soak condition. Another worst case could exist if the C-10 bond does not completely harden until the 482^{o}F condition. Then, when cooled to room temperature, residual stresses would exist. These stresses can be found by multiplying the previous results by the following factor

$$K_o = \frac{70^{o} - 482^{o}}{482^{o} - 212^{o}} = -\frac{412}{270} = -1.53$$

Thus the C-10 bond flatwise maximum stress will be $f_3 = 128\ (-1.53) = -196$ psi, limit (compression).

M.S. = HIGH

For the porous carbon, $f_2 = 216\ (-1.53) = -\ 330$ psi, limit (compression).

$$M.S. = \frac{0.8\ (1000)}{1.5\ (330)} - 1 = +0.62$$

For the ATJ, $f_2 = -249\ (-1.53) = 380$ psi, limit (tension).

$$M.S. = \frac{3000}{1.5\ (380)} - 1 = \text{HIGH}$$

After the C-10 bonding operation is completed, the porous carbon will be finish machined prior to the PD162A bond operation. This removal of material will tend to reduce the residual stresses.

As an additional check, the performance of the nose in storage must be examined, using the procedure just shown above. The minimum storage temperature is $-35^{\circ}F$. Thus,

$$K_o = \frac{-35 - 482}{482 - 212} = -\frac{512}{270} = -\ 1.896$$

and f_2 in the porous carbon will be $216\ (-1.896) = -\ 410$ psi, limit compression

$$\text{Min. } M.S. = \frac{0.8 \times 1000}{1.5 \times 410} - 1 = +\ 0.30$$

3. HIGH TEMPERATURE (OUTGASSING) CURE

An alternate (and presently planned for use) assembly procedure during the C-10 bonding operation is to gradually increase the temperature after the $482^{\circ}F$ cure cycle up to $1560^{\circ}F$. As previously stated, reliable material properties are not available for C-10 and the available properties for porous carbon are very limited. In view of the above, it is conservatively assumed that the C-10 bond is infinitely rigid in shear and in flatwise tension and compression. A worst case analysis is based on the assumption that the C-10 bond is completely hardened during the first temperature cycle ($212^{\circ}F$). Using the parameters and conservative properties given in section VI. B. 1, the margins of safety would be highly negative for the C-10 bond and the porous carbon. Even using nominal material properties the margins of safety would be negative. The maximum tensile stress in the C-10 bond using nominal properties will be about

$$f_3 = -pK = 128 \left(\frac{1560 - 212}{482 - 212}\right) \left(\frac{27.5}{108}\right) = 128\ (1.273)$$

$$= 163 \text{ psi, limit (nominal)}$$

$$\text{M.S.} = \frac{150}{1.5\ (163)} - 1 = -0.39$$

For the porous carbon

$$f_2 = -pK'_B = 216\ (1.273) = 275 \text{ psi, limit (nominal)}$$

$$\text{M.S.} = \frac{240}{1.5\ (275)} - 1 = -0.42$$

4. PD162A BOND CURE

After the C-10 bond operation, the tungsten alloy insert is bonded to the porous carbon with PD162A. The bond thickness is 0.020 ± 0.010 inch and the maximum curing temperature is 190°F. The "residual" stresses which may exist after the C-10 bond operation are neglected in this analysis.

It is assumed that the PD162A bond does not harden until the 190°F soak temperature is in progress. Then, when the assembly is reduced in temperature to room temperature (70°F), differential thermal expansion stresses will exist.

The radial and hoop stresses are approximated using the same method described in section VI. B. 1. The following two stresses are most critical.

$f_3 = -p_1$ (max radial stress in the porous carbon and in the PD162A bond)

$f_2 = p_1 K_B - pK'_B$ (max hoop stress in porous carbon)

$f_3 = -pK$ (max radial stress in C-10 bond)

where

$$p = \frac{(\alpha_B - \alpha_A)(T_2 - T_1) + P_1 K''_B / E_B}{K_{AB}}$$

$$p_1 = \frac{(\alpha_c - \alpha_{AB})(T_2 - T_1)}{\frac{1}{E_c}(K_c - \nu_c) + X_{AB}}$$

$$\alpha_{AB} = \alpha_B \left(1 - \frac{K'_B}{K_{AB} E_B}\right) + \alpha_A \frac{K'_B}{K_{AB} E_B}$$

$$K_{AB} = \frac{1}{E_B}(K_B - \nu_B) + \frac{1}{E_A}(K_A + \nu_A)$$

$$X_{AB} = \frac{1}{E_B}\left[K_B + \nu_B - \frac{K'_B K''_B}{K_{AB} E_B}\right]$$

$$K''_B = \frac{2 r_1^2}{r_2^2 - r_1^2}$$

$$K_c = 1$$

Subscript A applies to ATJ (with grain)

Subscript B applies to porous carbon

Subscript C applies to tungsten

All other terms not defined are the same as those given in section VI. B. 1. The following conservative material properties are used:

$E_A = 1.65 \times 10^6$ psi (max)

$\nu_A = 0.05$ (min)

$\alpha_A = 2.00 \times 10^{-6}$ in/in/°F (min)

$E_B = 0.6 \times 10^6$ psi (max)

$\nu_B = 0.15$ (max)

$\alpha_B = 1.40 \times 10^{-6}$ in/in/°F (min)

$E_c = 54 \times 10^6$ psi (max)

$\nu_c = 0.3$ (max)

$\alpha_c = 2.35 \times 10^{-6}$ in/in/°F (max)

The bond stiffnesses are neglected and radii are taken to be on the inside of the bond surfaces at any lateral section.

The following values show the geometry and parameters which exist:

Station (inches)	4.18	4.85	8.50
r_1 (in.)	0.136	0.199	0.509
r_2 (in.)	0.264	0.329	0.649
r_3 (in.)	0.513	0.578	0.918
K	1.137	1.240	1.242
K_A	1.720	1.955	3.000
K_B	1.722	2.154	4.20
K'_B	2.724	3.160	5.20
K''_B	0.722	1.155	3.20
K_c	1.000	1.000	1.000
$K_{AB}(psi)^{-1}$	3.690×10^{-6}	4.615×10^{-6}	8.600×10^{-6}
X_{AB} $(psi)^{-1}$	1.638×10^{-6}	1.644×10^{-6}	1.875×10^{-6}
α_{AB} (in/in/°F)	2.14×10^{-6}	2.08×10^{-6}	2.01×10^{-6}
p_1 (psi)	-15.3	-19.6	-21.6
p (psi)	14.6	7.4	5.0

Thus the maximum radial stress in the PD162A bond is at station 8.5 where $f_3 = - p_1 = 21.6$ psi, limit (tension).

The maximum hoop stress in the porous carbon is at station 4.18 where $f_2 = p_1 K_B - p K'_B = -66.2$ psi, limit (compression).

As indicated by the two stresses shown above, the radial and hoop stresses are not critical in any of the parts or bonds. Thus, for all parts:

M.S. = HIGH

C. POWERED FLIGHT LOADS

1. LOAD CONDITION L (Axial Sinusoidal Test)

This condition, $G_x = \pm 32.4$, results in the maximum inertial axial tensile loads on the bonds at room temperature.

The maximum load on the C-10 bond is approximately:

$$P_1 = (0.131 + 0.007)(32.4) = 4.46 \text{ pounds, limit}$$

Assuming the C-10 bond extends from station 4.32 to station 8.5 and taking into account the sixteen slots in the porous carbon, the area is approximately:

$$A = 7.8 \text{ sq. in.}$$

Assuming only 25% bond efficiency, the shear stress in the C-10 bond is approximately:

$$F_s = \frac{4.46}{0.25\ (7.8)} = 2.3 \text{ psi, limit}$$

The minimum allowable ultimate shear strength of C-10 at room temperature is conservatively taken to be $F_{su} = 150$ psi

$$M.S. = \frac{150}{1.5\ (2.4)} - 1 = \text{HIGH}$$

The maximum load on the PD162A bond is approximately:

$$P_2 = (0.131 + 0.007 + 0.031)\ 32.4 = 5.47 \text{ pounds, limit}$$

Assuming the bond extends from station 4.32 to station 8.5, the bond area is approximately:

$$A = 8.1 \text{ sq. in.}$$

Using 50% efficiency for the bond, the shear stress is approximately:

$$f_s = \frac{5.47}{0.5\ (8.1)} = 1.35$$

$$F_{su} = 320 \text{ psi} \quad \text{(min)}$$

$$M.S. = \frac{320}{1.5\ (1.35)} - 1 = \text{HIGH}$$

Check the nose assembly for separation at station 8.6 using a total effective weight of 1.5 pounds:

$$P \cong 1.5\ (32.4) = 48.6 \text{ pounds, limit}$$

The spring load is about 470 ± 175 pounds. Thus, the minimum margin of safety is:

$$M.S. = \frac{295}{1.5\ (48.6)} - 1 = \text{HIGH}$$

2. LOAD CONDITION C (Lateral - Max Q α)

This condition, $G_n = 9.2$, results in the maximum inertial bending loads on the nose assembly at room temperature.

The maximum bending moment at station 8.6 is about

$$M_1 = WG_n \bar{X} = 1.1535\ (9.2)(8.6 - 7.24)$$

$$= 14.5 \text{ in-lb., limit}$$

The maximum allowable bending moment with respect to separation of the nose from the washer at station 8.6 is calculated.

$$M_{allow} = \frac{P_o}{A}\left(\frac{I}{C}\right)$$

where P_o = 470 ± 175 pounds spring preload

$$A = \pi\ (r_1^2 - r_2^2)$$

$$I/c = \frac{\pi}{4r_1}\ (r_1^4 - r_2^4)$$

$$\left.\begin{aligned} r_1 &= \frac{1.000}{2} = 0.500 \text{ inch radius} \\ r_2 &= \frac{0.525}{2} = 0.2625 \text{ inch radius} \end{aligned}\right\} \text{washer dimensions}$$

$$M_{allow} = P_o\ \frac{r_1^2 + r_2^2}{4r_1} = 295\ \left[\frac{0.25 + 0.069}{4\ (0.50)}\right]$$

$$= 47.0 \text{ in-lbs}$$

The minimum margin of safety for nose bending separation is given by

$$M.S. = \frac{47.0}{1.5\ (14.5)} - 1 = \text{Ample}$$

The maximum compressive stress in the pyrolytic graphite washer at station 8.6 is given by:

$$F_c = -\frac{P_o}{A} - \frac{Mc}{I}$$

$$= -\frac{470 + 175}{\pi\ (0.25 - 0.069)} - \frac{14.5\ (0.5)\ 4}{\pi\ (0.0625 - 0.0048)} = \frac{645}{0.569} - 160$$

$$= -1135 - 160 = -1295 \text{ psi, limit}$$

$$F_{cu} = 20,000 \text{ psi}$$

$$M.S. = \frac{20000}{1.5(1295)} - 1 = \text{HIGH}$$

The maximum stress in the shaft due to preload at room temperature is about

$$f_t = \frac{470 + 175}{A}$$

$$A = \frac{\pi}{4}\left[(0.200)^2 - (0.130)^2\right] = 0.026 \text{ in}^2$$

$$f_t = \frac{645}{0.026} = 24,800 \text{ psi, limit}$$

$$F_{tu} \cong 140,000 \text{ psi for 17 - 4 PH (H1025)}$$

$$M.S. = \frac{140,000}{1.5\ (24800)} - 1 = \text{HIGH } (+2.8)$$

D. RE-ENTRY LOADS DIFFERENTIAL THERMAL EXPANSION

1. DISCUSSION (Old Design)

The old all-PG plug design is discussed in the following paragraphs. The latest ATJ-plus-PG plug analysis appears in Section VI. D. 3. During re-entry the nose assembly will experience thermal conditions which cause thermal stresses. Since the assembly consists of parts of different materials, stresses due to differential thermal expansion will exist and must be combined with the thermal stresses.

The PG insert is surrounded by a "blanket" of graphite felt. The felt "free" thickness is 0.040 inch (nominal) and at assembly is supposed to be compressed to a thickness of 0.020 ± 0.010 inch. Thus, the combined thicknesses of the felt on the forward and aft ends of the PG insert is to be 0.040 ± 0.020 inch. It is highly likely that the forward felt region will be compressed much more than the aft felt pad due to the geometry of the parts. As calculated below, this geometry could result in comparatively high compressive stresses. One reason for having the felt "blanket" is to provide for the relatively high axial thermal expansion of the PG insert with very little load "build-up". This will insure that high axial tensile stresses due to axial differential thermal expansion will not occur in the ATJ shell at about station 3.9. Another reason for using the graphite felt is to provide a bearing surface between the ATJ and the PG insert at staion 3.547 such that possible point contact between parts is eliminated.

Because material properties data is not always available or reliable for the materials used for the nose assembly, analyses are not always conclusive or exact. Wherever possible or applicable, maximum or minimum (whichever is more conservative) property values are used to reduce the possibility of failure due to the lack of specific material properties.

The sequence of events which occur during re-entry are as follows. As the temperature and pressure distributions on the nose increase, the nose stagnation point area begins to ablate. At the same time, the heat transfer to the PG insert causes it to expand axially at a higher rate than the ATJ shell. Thus, the PG insert exerts an axial load (in addition to the preload induced at assembly by compressing the graphite felt) through the graphite felt pads to the tungsten insert and to the ATJ stagnation point back face area. As the altitude is reduced and assuming no parts have failed structurally, the load caused by the PG expansion will increase, causing the ATJ shell to move forward with respect to the rest of the spacecraft (provided the aerodynamic axial load is less than the ATJ inertial load combined with the PG expansion load). The above events will cause the C-10 bond, the porous carbon, and the PD162A bond all to carry the net axial load in shear (and a small radial tension component) into the tungsten insert. In addition to the above loads and resulting stresses, thermal stresses exist in the axial, radial and hoop directions in all parts. The combined stress distribution is very complex when nonlinear temperature distributions, complex geometry and unknown material properties are considered. Still, assuming no structural failures have occurred, the PD162A bond axial deflection produced by bond shear will cause the porous carbon to move forward with the ATJ shell. As long as the porous carbon forward surface does not move as far forward as the tungsten insert, the porous carbon will not be loaded by the PG insert in compression (at about station 4.05). If, however, the porous carbon forward annular surface contacts the PG insert, a serious problem could exist since most of any increase in load due to thermal expansion of the PG insert will be transferred to the porous carbon (which is relatively stiff compared with the shear rigidity of the PD162A bond) and put the ATJ shell between stations 3.55 and 4.1 in tension. Thus, to be conservative and eliminate a potential problem it is recommended that the minimum distance at assembly between the forward surfaces of the tungsten insert and the porous carbon be at least equal to the maximum thermal expansion of the PG insert.

Provided the above recommendation is included in the nose design, one of the following acceptable failure modes will probably occur:

a. The porous carbon will fail in tension (stress-relieve) in the radial on hoop direction due to excessive thermal stresses.

b. The C-10 bond will fail in tension or axial shear due to excessive thermal stresses.

c. The PD162A bond will fail in tension or axial shear due to excessive thermal stresses.

After any of the above stress reliefs occurs, the ATJ shell will probably transmit all axial loads through the PG insert to the tungsten insert.

It should be noted that if one of the above failures occurs at a high altitude, the aerodynamic axial load on the ATJ shell must be greater than the inertial load from the ATJ shell. Otherwise the nose could possibly fly off of the vehicle.

2. ANALYSIS (Old Design)

Due to the lack of load-deflection data for the graphite felt parts as a function of temperature, the following conservative case is analyzed.

Assume the PG insert is incorrectly installed such that it is "fixed" between the ATJ nose cavity at station 3.547 and the tungsten insert at station 4.047. Now, the following modes of failure must be investigated:

a. ATJ tension at about station 3.7

b. C-10 bond shear-tension

c. Porous carbon shear-tension

d. PD162A bond shear-tension

Due to the lack of reliable material properties data, maximum & minimum (whichever is conservative) values are used.

Consider the differential thermal expansion between stations 3.547 & 4.047 between ATJ & PG:

$$\Delta_t = \left[(\alpha \Delta T)_{PG} - (\alpha \Delta T)_{ATJ}\right] L_{PG}$$

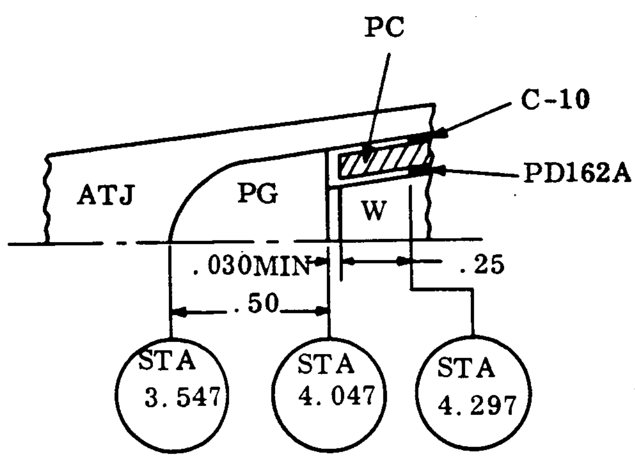

The thermal expansion differential must be equal to the combined deformations in the various parts caused by stress.

$$\Delta_t = \Delta_{PG} + \Delta_{ATJ} + \Delta_{PD162A}$$

$$\cong P_o\left[\left(\frac{L}{AE}\right)_{PG} + \left(\frac{L}{AE}\right)_{ATJ} + \frac{t}{AG}_{PD162A}\right]$$

$$L_{PG} = 0.50 \text{ inch} \quad L_{ATU} = 0.75 \text{ inch} \quad t_{PD162} = 0.020 \text{ inch}$$

$$A_{PG} \cong \pi (0.188)^2 = 0.111 \text{ in}^2$$

$$A_{ATJ} \cong \pi \; (0.350)^2 - (0.208)^2 = \pi (0.0792) = 0.249 \text{ in}^2$$

$$A_{PD162A} \cong 8.0 \text{ in}^2 \text{ (shear area for 100\% bond)}$$

$$P_o = \frac{\Delta_t}{\frac{0.50}{0.111\, E_{PG}} + \frac{0.75}{0.249\, E_{ATJ}} + \frac{0.020}{8.0\, G_{PD162A}}}$$

$$P_o = \frac{\Delta_t}{\frac{4.5}{E_{PG}} + \frac{3.01}{E_{ATJ}} + \frac{0.0025}{G_{PD162A}}}$$

$$P_o = \frac{(\alpha \Delta T)_{PG} - (\alpha \Delta T)_{ATJ}}{\frac{9}{E_{PG}} + \frac{6.02}{E_{ATJ}} + \frac{0.005}{G_{PD162A}}}$$

The max stresses due to differential thermal expansion are given below. These must be combined with thermal and aerodynamic stresses.

For ATJ:

$$f_t = \frac{P_o}{A_{ATJ}} = P_o/0.249 \quad \text{(axial tension, at about station 3.9)}$$

For ATJ & PG:

$$f_c = \frac{P_o}{A_c} \quad \text{(axial compression at sta. 3.547)}$$

$$\text{Say } A_c \cong \pi (0.100)^2 = 0.0314 \text{ in}^2$$

$$f_c = 31.8\, P_o$$

For PD162A:

$$f_s = \frac{P_o}{A_{PD162A}} = 0.125\, P_o \text{ (shear)}$$

For PC &
C-10:

$$f_s = \frac{P_o}{A_{C-10}} = P_o/7.4$$

$$= 0.135\ P_o \text{ (shear with 100\% bond)}$$

At 145,000 feet:

Say $T_{ATJ} \leq T_{PG} = 1300^oR - 840^oF$

$(\alpha \Delta T)_{ATJ} \leq 10.8 \times 10^{-3}$ in/in ("C")

$(\alpha \Delta T)_{ATJ} \leq 1.2 \times 10^{-3}$ in/in (C/G) assumed

$E_{PG} \leq 4.5 \times 10^6$ psi ("C") assumed

$E_{ATJ} \leq 1.24 \times 10^6$ psi (C/G)

$G_{PD162A} \leq$ 210 psi at are temp of $900^oR = 440^oF$

$$P_o = \frac{(0.0108 - 0.0012)\ 10^6}{\frac{9}{4.5} + \frac{6.02}{1.24} + \frac{0.005}{0.000210}} = \frac{9600}{2.0 + 4.85 + 23.8} = \frac{9600}{30.65}$$

$$= 313\#$$

<u>ATJ</u> $f_t = \frac{313}{0.249} = 1260$ psi (tension)

ATJ
&
<u>PG</u> $f_c = 31.8\ (313) = 9,950$ psi (compression)

<u>PD162A</u>
$f_s = 0.125\ (313) = 39$ psi (shear) 100% bond

<u>PC & C-10</u>
$f_s = 0.135\ (313) = 42$ psi (shear) 100% bond

The above stresses show that the compressive contact stress between the ATJ & PG is above the minimum allowable compressive allowables for both materials. Consequently, this case is too conservative and more material data must be obtained for graphite felt before a better analysis can be performed.

For ATJ

$$F_{cu} \cong 6000 \text{ psi (PIR U-8155-1139) at } 840^{\circ}\text{F}$$

$$\text{M.S.} = \frac{6000}{1.5\ (9950)} - 1 = -0.60$$

The simplest method of eliminating the negative margin of safety is to increase the effective compressive capability of the graphite felt such that the above case never occurs or to change the PG insert to a material (such as ATJ) such that the differential thermal expansion problem no longer exists. The latter course was taken for the latest design as shown in the following section.

3. DISCUSSION (Latest Design)

The latest nose design utilizes an ATJ graphite plug in place of the PG plug described in section VI. D. 1 for the old design. Also, a PG disc is installed between the ATJ plug and the tungsten insert. Graphite felt is used between the ATJ plug and the ATJ shell. The maximum temperature of the PG cylinder at 40,000 feet altitude is estimated to be 3000°F based on Figure 4.1.4 and 4.1.5 of Reference 19. The thermal expansion of the PG cylinder (0.178 max axial length, "C" direction) which is much greater than the ATJ skirt, will cause the ATJ plug to move forward. The thickness of the graphite felt must be great enough such that the thermal expansion of the PG will not cause the ATJ plug to have solid contact with the ATJ nose tip.

4. ANALYSIS (Latest Design)

The thermal expansion of the ATJ plug and ATJ skirt are neglected (slightly conservative). The thermal expansion of the PG will be approximately:

$$\Delta_{PG} = (L\,\alpha\,\Delta T)_{PG} \sim 0.178\ (\epsilon_t)_{PG}$$

$$\cong 0.178\ (0.043) = 0.00765 \text{ inch}$$

Thus, it is recommended that the graphite felt be capable of being compressed a minimum of 0.008 inch. The current design felt thickness determined by a tolerance study is $0.020 \pm \frac{0.014}{0.004}$ inch. Assuming the minimum thickness of 0.016 inch exists, the minimum compressed thickness will be 0.016 - 0.008 = 0.008 inch. If the original free height of the felt is 0.080 inch, then the maximum compression will be 0.072/

0.808 = 90%. Preliminary test data at room temperature indicates that 90% compression requires a compressive stress of about 250 psi.

Based on the above analysis, the current design of the nose with respect to differential thermal expansion problems during re-entry is judged to be satisfactory.

5. CONTACT STRESS BETWEEN ATJ NOSE AND PLUG

Assuming that one of the predicted modes of failure occurs (i.e., C-10 bond, porous carbon, or PD162A bond) before the spacecraft reaches 47,000 feet, the maximum axial stress between the ATJ and the spherical tip of the plug will be about

$$f_c \cong \frac{P}{A}$$

where

$$A \cong \pi(0.100)^2 = 0.0314 \text{ sq. in. effective area}$$

$$P = 113 + 19 = 132 \text{ pounds, limit (Figure 48)}$$

$$f_c = \frac{132}{0.0314} = 4200 \text{ psi, limit, compression}$$

The radial thermal stress at the contact area has been calculated to be 1160 psi, limit tension. Combining the stresses, the maximum shear stress is given by

$$f_s = \frac{f_1 - f_2}{2} = \frac{1160 - (-4200)}{2}$$

$$= 2680 \text{ psi, limit, shear}$$

The temperature of the ATJ on the centerline at station 3.55 is about $3560^{\circ}R = 3100^{\circ}F$ (Figure 50) at 47,000 feet. For ATJ at $3100^{\circ}F$,

$$F_{cu} = 8000 \text{ psi (across grain, typical)}$$

$$F_{su} = 3150 \text{ psi (across grain, min.)}$$

For compression,

$$M.S. = \frac{8000}{1.5\ (4200)} - 1 = +0.27$$

For shear,

$$M.S. = \frac{3150}{1.5\ (2680)} - 1 = -0.22$$

To eliminate the negative margin of safety it is recommended that the radius of the ATJ plug be increased from 0.080 to 0.098 inch. This will provide a larger effective bearing area which is approximated by an effective bearing circle radius of 0.120 inch:

$$A' = \pi (0.120)^2 = 0.0452 \text{ sq. in.}$$

Now $$f_c = \frac{P}{A'} = \frac{132}{0.0452} = 2920 \text{ psi, limit, comp.}$$

and $$f_s = \frac{1160 + 2920}{2} = 2040 \text{ psi, limit, shear}$$

For compression,

$$M.S. = \frac{8000}{1.5\,(2920)} - 1 = +0.83$$

For shear,

$$M.S. = \frac{3150}{1.5\,(2040)} - 1 = +0.03$$

If it is desired that the geometry not be changed, then it is recommended that tests be performed to show that the current design will or will not perform properly.

6. STRESSES ON PG WASHER DURING RE-ENTRY

The pyrolytic graphite washer is located at station 8.6. The items to be considered in analyzing stresses during re-entry at 47000 feet are the preload differential thermal expression load and re-entry load.

All three cases must be combined to set max & min stresses.

$$A = \pi \left[(0.500)^2 - (0.2625)^2\right] = \pi\,(0.181) = 0.568 \text{ in}^2$$

$$\frac{I}{c} = \frac{\pi}{4(0.5)} \left[(0.500)^4 - (0.2625)^4\right] = \frac{\pi}{2}\,(0.0625 - 0.00476) = 0.0908$$

a. Preload

$$P_o = -470^{\#} \pm 175^{\#} \text{ (comp.)}$$

$$\sigma_p = \frac{P_o}{A} = \frac{-470 \pm 175}{0.568} = -826 \pm 308 \text{ psi}$$

b. Differential Thermal Expansion

$$\text{Say } \Delta = \alpha \Delta T L \quad 0.01\,(2.5) = 0.025 \text{ (max)}$$

$$\text{Say } \Delta P_o = P_o \frac{\Delta}{\Delta_o} = P_o \frac{0.025}{0.100} = 0.25\, P_o$$

Say Tolerance is $^{+0}_{-0.25}$ P_o $\therefore \Delta P_o = {}^{+0.25}_{-0} P_o$

$$\therefore \sigma_1 = {}^{+0.25}_{-0} (-826 \pm 308) = {}^{+0}_{-284}$$

$$= -142 \pm 142 \text{ psi}$$

c. Re-entry Loads

$$P = -166^{\#} \text{ however, say } P \cong -100 \pm 66^{\#}$$

$$M \cong (10.7 \pm 1.1) + (-6.10 {}^{+0}_{-6.7})$$

$$= 4.6 {}^{+1.1}_{-7.8} = 1.25 \pm 4.45 \text{ in-lb}$$

$$\sigma_R = \frac{P}{A} \pm \frac{Mc}{I}$$

$$\cong - \frac{100 \pm 66}{0.058} \pm \frac{1.25 \pm 4.45}{0.0908}$$

$$= (-1760 \pm 1160) \pm 13.8 \pm 49)$$

$$= -1760 \pm (1160 + 63)$$

$$= -1760 \pm 1225 \text{ psi}$$

d. Combined Stresses

$$\sigma_o = -826 - 142 - 1760 \pm (308 + 142 + 1225)$$

$$= -2728 \pm (1675)$$

$$= -4403 \text{ psi, limit, compression (max)}$$

$$-1053 \text{ psi, limit, compression (min)}$$

$$F_{cu} \cong 15,000 \text{ psi}$$

$$M.S. = \frac{1500}{1.5(4403)} - 1 = \text{Ample}$$

E. ATJ SHELL THERMAL STRESS

1. DISCUSSION

An analysis was performed on the nose overhang and transition sections of the present design which has a 2.50 inch manufactured stagnation depth, showing successful performance during re-entry at all locations. Previous analyses were conducted for nose concepts employing 3.60 inch and 1.40 inch stagnation depths. The former revealed a negative margin for tension at the centerline, while the latter exhibited such high temperatures that the ability of the material to withstand air load stresses was placed in doubt.

2. ANALYSIS

The analysis of the nose overhang (2.5 in stag. depth) was performed at body station 2.95 and 3.55 at 31.5, 33.4, and 35.5 seconds after re-entry. The thermal gradient profiles were obtained from the Thermodynamics Technology Component. These profiles are shown in Figure 50.

Stresses were calculated using the isotropic portion of the thick cylinder computer program Reference 17. This analysis is based on modified plane, strain theory not including shear deformation. A comparison of a three dimensional solution (Ref. 8) and a thick cylinder solution at the transition zone of the 3.6 in. stagnation depth is given in Figure 51. Figure 52 gives the stresses for the previous 3.6 in. stag. depth design. Based on this comparison the plane strain solution was used to investigate the 1.4 and 2.5 in. stag. depth nose configurations.

This analysis indicates satisfactory performance of the ATJ heat shield at the two stations investigated.

Figure 53 shows a comparison of predicted margin-of-safety vs. stagnation depth. This margin is based only on the plane strain analysis of the maximum thickness section at the midpoint of the overhang.

The resulting axial and hoop stresses for the 2.5 stag. depth are shown in Figures 54 thru 57 with their tensile and compressive allowables. All curves show positive margins of safety for both compression and tensile stresses throughout the shell thickness. The resulting margins of safety are:

Station		Allowable		Max Actual		M. S.	
		Ten	Comp.	Ten	Comp	Ten	Comp.
Axial	3.55	> 3800	>-7500	1160	-1200	+2.27	+5.25
	2.95	> 3800	>-7500	920	-900	+3.14	+7.3
Hoop	3.55	> 4000	>-1100	+560	-1250	+6.15	+7.8
	2.95	> 4000	>-1100	480	-850	+7.35	+11.9

F. ATJ SHELL GAP AND CONCENTRICITY

1. GAP BETWEEN CALORIMETER AND NOSE (Old Design)

The following summation gives the resulting minimum gap between the ATJ skirt and the beryllium calorimeter at station 8.6 during re-entry, based on the old all-PG plug. The latest plug is included in Section IV. F. 2.

$$\Delta_F = \Delta_o - \Delta_{ATJ} - \Delta_{GF} + \Delta_{PG} + \Delta_W$$

At 32, 000 feet,

Δ_{ATJ} = $L\alpha\Delta T \cong (8.5 - 3.55)\ (11 \times 10^{-3})$ at $3260^{\circ}F$

= 0.545 inch (ATJ axial expansion)

Δ_{GF} $\cong$ $0.030 \pm 0.020 = 0.050$ inch (maximum compression of both graphite felt pads)

Δ_{PG} = is conservatively taken to be zero (expansion of PG plug)

Δ_W = $L\alpha\Delta T = (8.5 - 4.05)\ (2.4 \times 10^{-6})\ (590^{\circ} - 70^{\circ}) = 0.0055$ inch (expansion of tungsten insert)

Δ_o = $0.100\ ^{+0.005}_{-0.000}$ inch (initial gap)

Now Δ_F = $0.100 - 0.0545 - 0.050 + 0.0055$

= 0.001 inch clearance (minimum)

Note that the PG expansion, if taken into account, would tend to increase the clearance.

2. GAP BETWEEN CALORIMETER AND NOSE (Latest Design)

Using the same method as given above for the old design, the following minimum gap at station 8.6 is calculated.

132

$$\Delta_F = \Delta_o - \Delta_{ATJ} - \Delta_{GF} + \Delta_{PG} + \Delta_W$$

Δ_{ATJ} = 0.0545 inch (ATJ shell expansion)

Δ_{GF} = $0.020 \begin{smallmatrix} +0.014 \\ -0.004 \end{smallmatrix}$ = 0.034 inch (maximum compression of graphite felt pad)

Δ_{PG} = is conservatively taken to be zero (expansion of PG)

Δ_W = 0.055 inch (expansion of tungsten insert)

Δ_o = $0.100 \begin{smallmatrix} +0.005 \\ -0.000 \end{smallmatrix}$ (initial gap)

$$\Delta_F = 0.100 - 0.0545 - 0.034 + 0 + 0.0055$$

$$= 0.017 \text{ inch (minimum gap)}$$

These results are considered satisfactory.

3. CONCENTRICITY OF ATJ AT STATION 8.5

During re-entry, if one of the predicted modes of failure occurs (in the porous carbon or one of the two bonds). the skirt of the ATJ shell at station 8.5 may be slightly eccentric with the centerline of the spacecraft. Since only aft facing steps are acceptable on the outer surface of the spacecraft, the maximum eccentricity and ablation must not produce a forward facing step with the beryllium calorimeter.

The radius of the ATJ shell is 0.8025 ± 0.004 inch. The radius of the beryllium at station 8.6 is 0.7525 ± 0.003 inch. Thus, the minimum aft facing step at assembly will be

$$h_o = (0.8025 - 0.004) - (0.7525 + 0.003)$$

$$= 0.043 \text{ inch}$$

During re-entry the beryllium thermal expansion should not be greater than 0.8% strain or

$$\Delta h_1 = -(0.7525 + 0.003)(0.08)$$

$$= -0.006 \text{ inch}$$

The surface of the ATJ is assumed to ablate a maximum of 0.016 inch (radial) at station 8.5.

$$\Delta h_2 = -0.016 \text{ inch}$$

It is conservative to assume the PD162A bond is very soft and that the bond can be forced to be eccentric by the amount of its thickness:

$$\Delta h_3 = -0.020 \text{ inch}$$

The minimum net aft facing step will be:

$$h = h_o + \Delta h_1 + \Delta h_2 + \Delta h_3$$

$$= 0.043 - 0.006 - 0.016 - 0.020$$

$$= 0.001 \text{ inch}$$

VII. REFERENCES

1. Timoshenko and Goodier, "Theory of Elasticity", Second Edition, McGraw-Hill Book Company.

2. D'Amelio, V. J., "P/A Candidate Materials - Material Properties Data", PIR 8155-1174 of August 1, 1966.

3. D'Amelio, V. J., "Physical Mechanics Laboratory Stage II Release-Penetration Aids Program", PIR 8155-1341 of December 2, 1966.

4. MIL-HDBK-5A, "Metallic Materials and Elements for Aerospace Vehicle Structures", February 8, 1966.

5. Roark, R.J., "Formulas for Stress and Strain", McGraw-Hill Book Company, Fourth Edition, 1965.

6. Peery, D.J., "Aircraft Structures", McGraw-Hill Book Company, 1950.

7. Shigley, J. E., "Machine Design", McGraw-Hill Book Company, 1956.

8. Mehan, R. L., "Experimental Data on HTM BPG", PIR 8155-242 of October 1963.

9. Mehan, R. L., "Properties of National Carbon C-10 Cement", PIR 2243-552 of July 27, 1962.

10. McKendrick, M., "Re-entry F Vehicle Loads and Criteria, Stage III", PIR SM-8156-000-3340 of December 15, 1966.

11. Wesendorf, L. E., "Preliminary Materials Recommendation - Porous Carbon", PIR 8157-785 of October 13, 1966.

12. "Study to Determine the Effects on the Scout Vehicle Structure Due to Uncoventional Vehicle-Spacecraft Configurations", LTV Astronautics Report 23.175 of November 20, 1964.

13. Document L-6345 Exhibit A "Statement of Work, Re-entry F Turbulent Heating Experiment", Langley Research Center, November 29, 1965, with revised preliminary interface, "Vibration, Shock and Acceleration Requirements for Re-entry F Spacecraft", undated from NASA/Langley, handcarried to GE-RSD on January 10, 1967.

14. Bost, R.D., "Scout Flight Vibration and Shock Environment", LTV Astronautics Report 00.766 of March 2, 1966.

15. Hilton, Bracalenta and Hubbard, "In-Flight Aerodynamic Noise Measurements on a Scout Launch Vehicle", NASA TN-D-1818 of July 1963.

VII. REFERENCES (Cont'd)

16. "AMLO Data Source Book", Aeromechanics and Materials Laboratory of GE-RSD.

17. Jeglic, J.M., "Thermal Stresses in Thick Orthotropic, Transversely Isotropic, and Isotropic Cylinders, "G. E. 64SD272, August 28, 1964.

18. Hecht, A.M., "Re-entry F Aft Cover Thermodynamics Analysis", PIR 8151-665 of December 28, 1966.

19. Hecht and Hann, "Thermodynamics Stage II Release - Re-entry F", PIR TTFM 8151-052 of November 22, 1966.

20. Tanzilli, R., Dolan, C. and Strable, E., "Stage 1-Material Support", PIR 8155-970 of January 7, 1966.

21. Crawford, R. F. and Burns, A. B., "Strength, Efficiency, and Design Data for Beryllium Structures", ASD TR 61-692, February, 1962.

22. Bruhn,"Analysis and Design of Flight Vehicle Structures", Tri-State Offset Company, 1965.

23. Timoshenko and Woinowsky-Krieger, "Theory of Plates and Shells", McGraw-Hill Second Edition, 1959.

24. Zlupko, J., "Antenna Window Material, Beryllium Oxide (BeO)", PIR 8157-774 of October 6, 1966.

25. Dubin, P., "Material Properties of Beryllium Oxide", PIR 8155-1365 of December 16, 1966.

26. Johns, R.H. and Orange, T.W., "Theoretical Elastic Stress Distributions Arising from Discontinuities and Edge Loads in Several Shell-Type Structures", NASA TR R-103.

27. "General Electric Structures Manual", First Edition, January 1959, GE-RSD.

28. Faupel, J., "Engineering Design", Wiley Book Co., 1964.

29. Menkes, E.G., "Thermo-Elastic Analysis of Beams, Plates and Shells Including the Effect of Variable Material Properties", SM-TM-8156-11 of August, 1962.

30. McGlincy, J., "Elasto-Plastic Thermal Stress Analysis", PIR SM-8156-000-1759 of November 19, 1965.

31. Menkes, E.G., "Use of Thermal Stress Program (TSP)", PIR SM-TM-8156-1032 of September 11, 1964.

32. Zlupko, J., "High Temperature Insert Material Between ATJ/PG", PIR 8157-844 of December 15, 1966.

VII. REFERENCES (Cont'd)

33. PIR 8155-156 of October 30, 1962.

34. Kachadourian, G., "Re-entry F Vibration Environment and Vibration Test Requirement", PIR SM-8156-VR-3303 of December 10, 1966.

35. Edighoffer, H., "Mechanical Properties of Laminated Phenolic Glass (91LD-181 Cloth)", PIR-SM-8156-1217 of December 11, 1964.

VIII. FIGURES

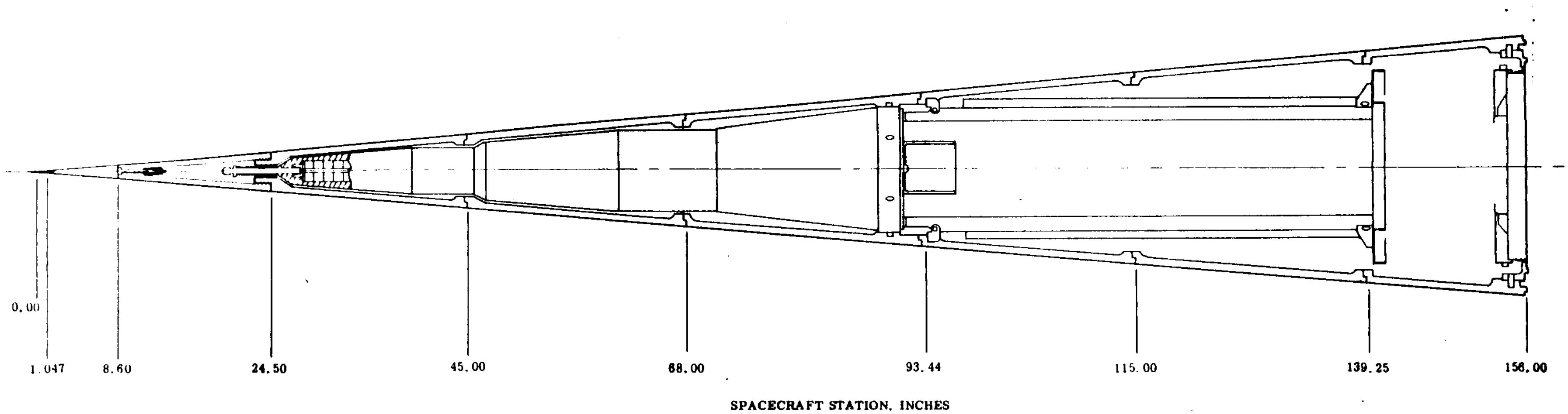

Figure 1. Inboard Profile of the Re-entry F Spacecraft, Feb. 10, 1967.

148

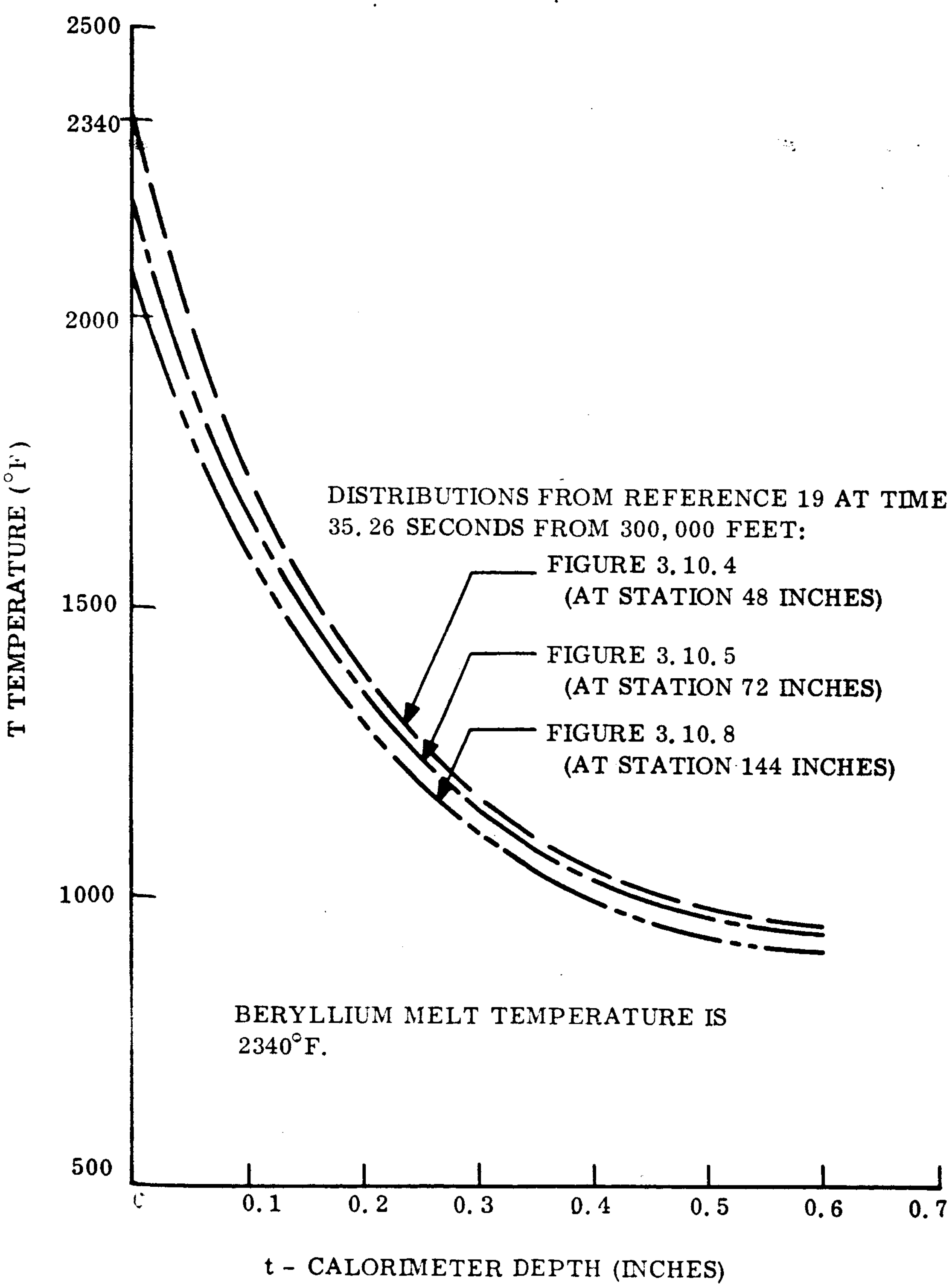

Figure 2. Calorimeter Critical Temperature Distribution During Re-entry

101 1984	102 1924	103 1902	104 1936	105 1972	106 1895	107 1922	108 1990
201 1906	202 1847	203 1826	204 1859	205 1895	206 1818	207 1845	208 1912
301 1634	302 1579	303 1559	304 1590	305 1624	306 1552	307 1577	308 1640
401 1215	402 1156	403 1135	404 1164	405 1209	406 1128	407 1154	408 1220
501 849	502 759	503 731	504 756	505 861	506 722	507 758	508 856
601 768	602 595	603 549	604 528	605 405	606 534	607 597	608 775
	702 492	703 433	704 403	705 363	706 419	707 499	
	802 408	803 348	804 322	805 312	806 340	807 421	
	902 359	903 311	904 288	905 286	906 308	907 378	

151 1995	152 1973	153 1963	154 1970	155 1973	156 1963	157 1971	158 1998
251 1917	252 1895	253 1885	254 1893	255 1895	256 1886	257 1894	258 1920
351 1644	352 1625	353 1615	354 1622	355 1625	356 1615	357 1623	358 1648
451 1225	452 1206	453 1197	454 1203	455 1206	456 1197	457 1204	458 1228
551 863	552 839	553 829	554 834	555 838	556 829	557 838	558 865
651 784	652 756	653 745	654 746	655 743	656 744	657 755	658 787

Figure 3. Calorimeter Temperature Distribution at Scalloped Bolted Joint at Station 72 (inches) at Time 35.3 Seconds

101 1816	102 1753	103 1728	104 1763	105 1797	106 1720	107 1750	108 1823
201 1751	202 1689	203 1665	204 1698	205 1732	206 1657	207 1686	208 1758
301 1521	302 1463	303 1441	304 1472	305 1505	306 1433	307 1461	308 1528
401 1160	402 1099	403 1076	404 1105	405 1147	406 1069	407 1097	408 1166
501 838	502 748	503 718	504 743	505 840	506 709	507 747	508 845
601 765	602 598	603 552	604 533	605 418	606 538	607 601	608 773
	702 503	703 444	704 415	705 378	706 431	707 510	
	802 423	803 364	804 339	805 329	806 357	807 437	
	902 376	903 329	904 307	905 304	906 327	907 395	

151 1829	152 1803	153 1791	154 1799	155 1802	156 1791	157 1801	158 1832
251 1763	252 1738	253 1726	254 1734	255 1737	256 1727	257 1737	258 1767
351 1533	352 1510	353 1499	354 1506	355 1509	356 1499	357 1508	358 1536
451 1172	452 1150	453 1139	454 1145	455 1148	456 1139	457 1148	458 1175
551 852	552 827	553 815	554 820	555 824	556 815	557 825	558 855
651 782	652 752	653 740	654 741	655 738	656 739	657 751	658 785

Figure 4. Calorimeter Temperature Distribution at Scalloped Bolted Joint at Station 144 (inches) at Time 35.3 Seconds

101: 1970	102: 1892	103: 1867	104: 1973	105: 1982	106: 1850	107: 1887	108: 1979
201: 1892	202: 1816	203: 1792	204: 1895	205: 1904	206: 1775	207: 1811	208: 1901
301: 1622	302: 1550	303: 1527	304: 1624	305: 1633	306: 1511	307: 1545	308: 1630
401: 1203	402: 1128	403: 1105	404: 1183	405: 1212	406: 1091	407: 1125	408: 1211
501: 838	502: 730	503: 698	504: 728	505: 854	506: 683	507: 728	508: 847
601: 756	602: 567	603: 519	604: 496	605: 366	606: 499	607: 568	608: 766
	702: 471	703: 411	704: 380	705: 337	706: 394	707: 477	
	802: 391	803: 332	804: 305	805: 294	806: 323	807: 403	
	902: 344	903: 297	904: 274	905: 271	906: 293	907: 362	

Figure 5. Calorimeter Unscalloped Bolted Joint Temperature Distribution at Station 72 (inches) at Time 35.3 Seconds

101: 1800	102: 1716	103: 1688	104: 1787	105: 1800	106: 1670	107: 1711	108: 1810
201: 1735	202: 1653	203: 1625	204: 1723	205: 1735	206: 1607	207: 1648	208: 1745
301: 1507	302: 1430	303: 1404	304: 1496	305: 1507	306: 1387	307: 1425	308: 1516
401: 1147	402: 1063	403: 1042	404: 1116	405: 1146	406: 1027	407: 1064	408: 1155
501: 825	502: 716	503: 861	504: 712	505: 830	506: 666	507: 714	508: 834
601: 752	602: 567	603: 519	604: 499	605: 377	606: 499	607: 569	608: 762
	702: 479	703: 420	704: 390	705: 350	706: 403	707: 485	
	802: 404	803: 347	804: 320	805: 309	806: 337	807: 416	
	902: 360	903: 314	904: 291	905: 288	906: 310	907: 377	

Figure 6. Calorimeter Nonscalloped Bolted Joint Temperature Distribution at Station 144 (inches) at Time 35.3 Seconds

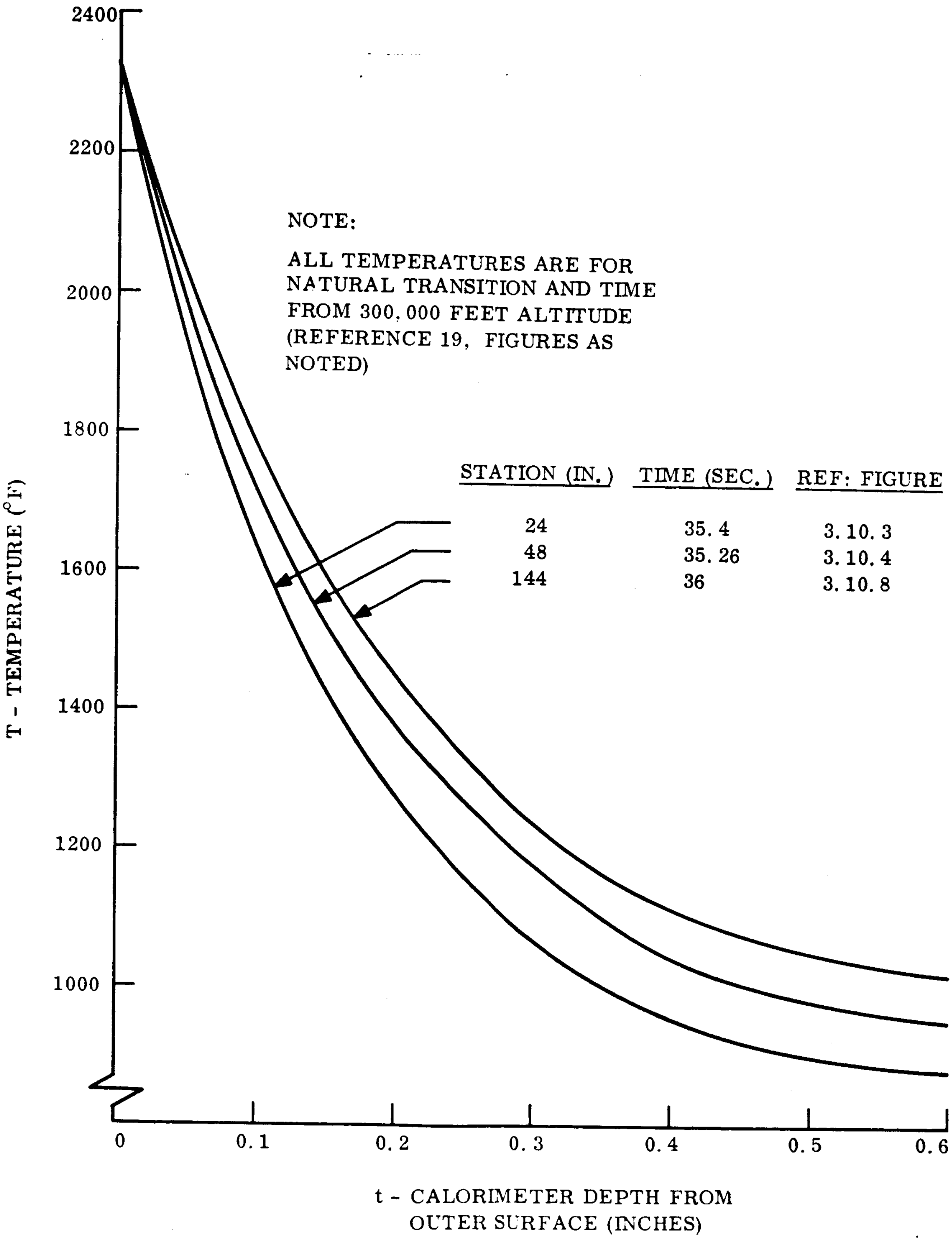

Figure 7. Beryllium Calorimeter Temperature Distributions During Re-entry

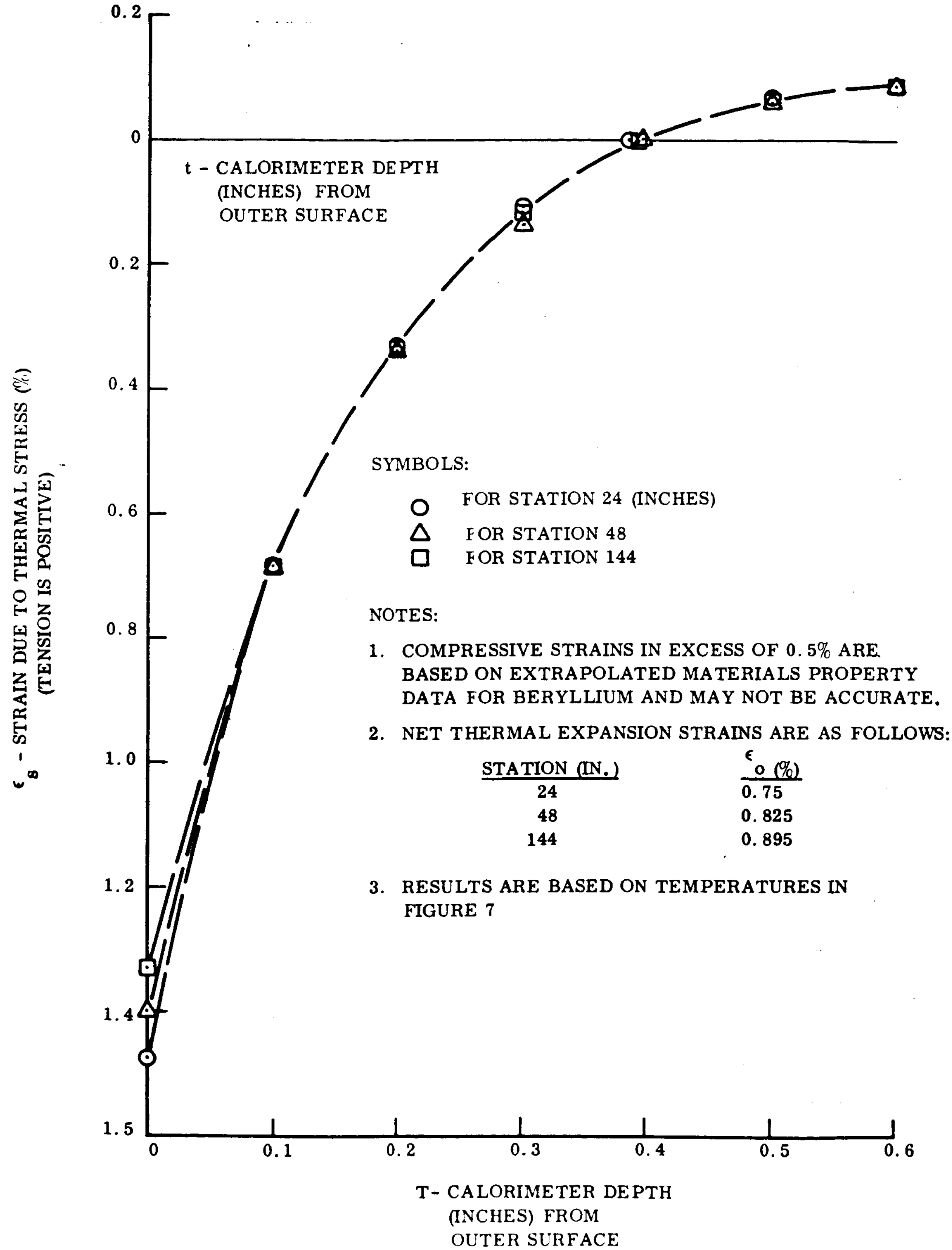

Figure 8. Calorimeter Strain Distributions During Re-entry

1114

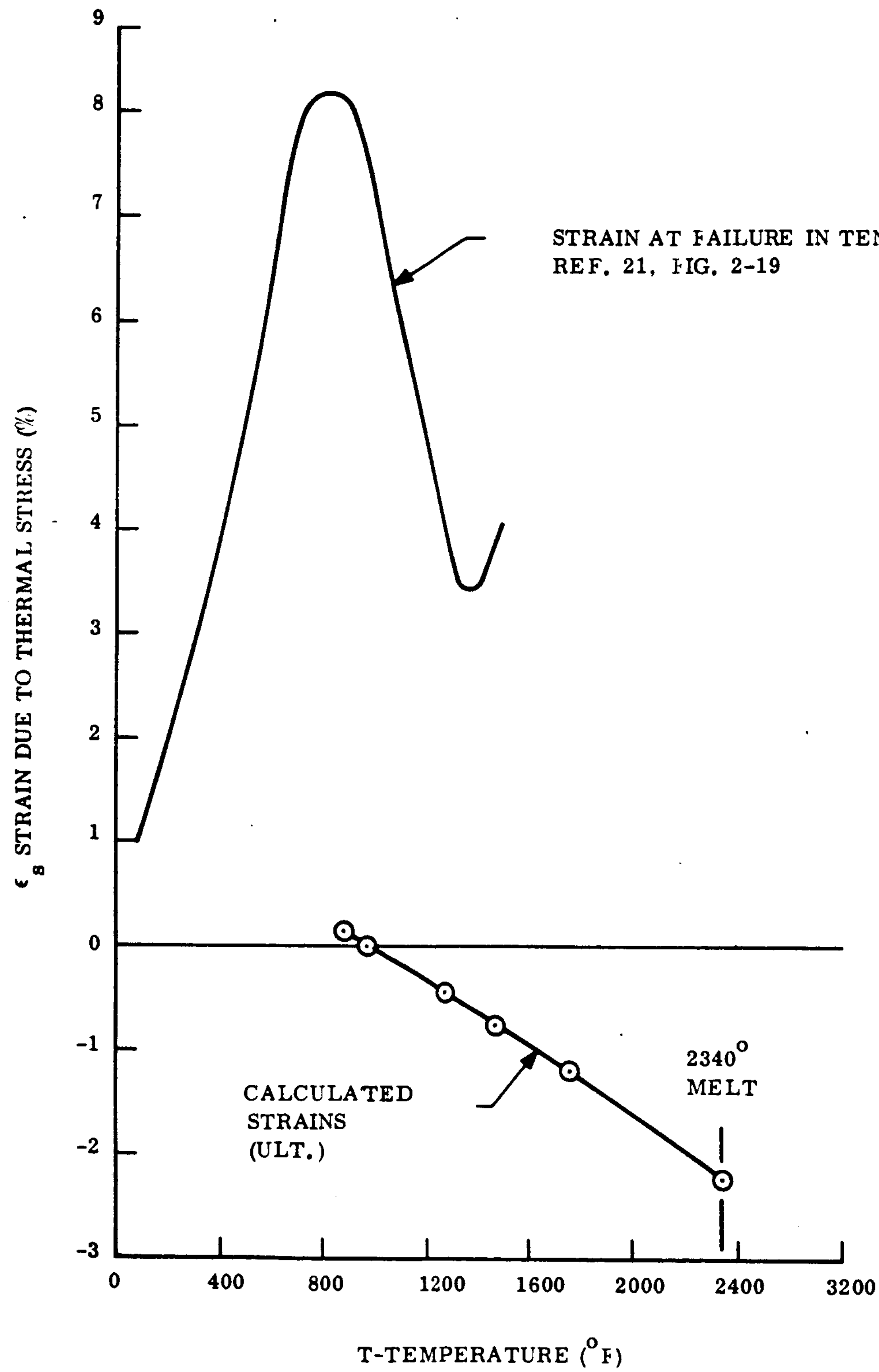

Figure 9. Comparison of Calculated Strains Due to Thermal Stress and Strain at Failure

115

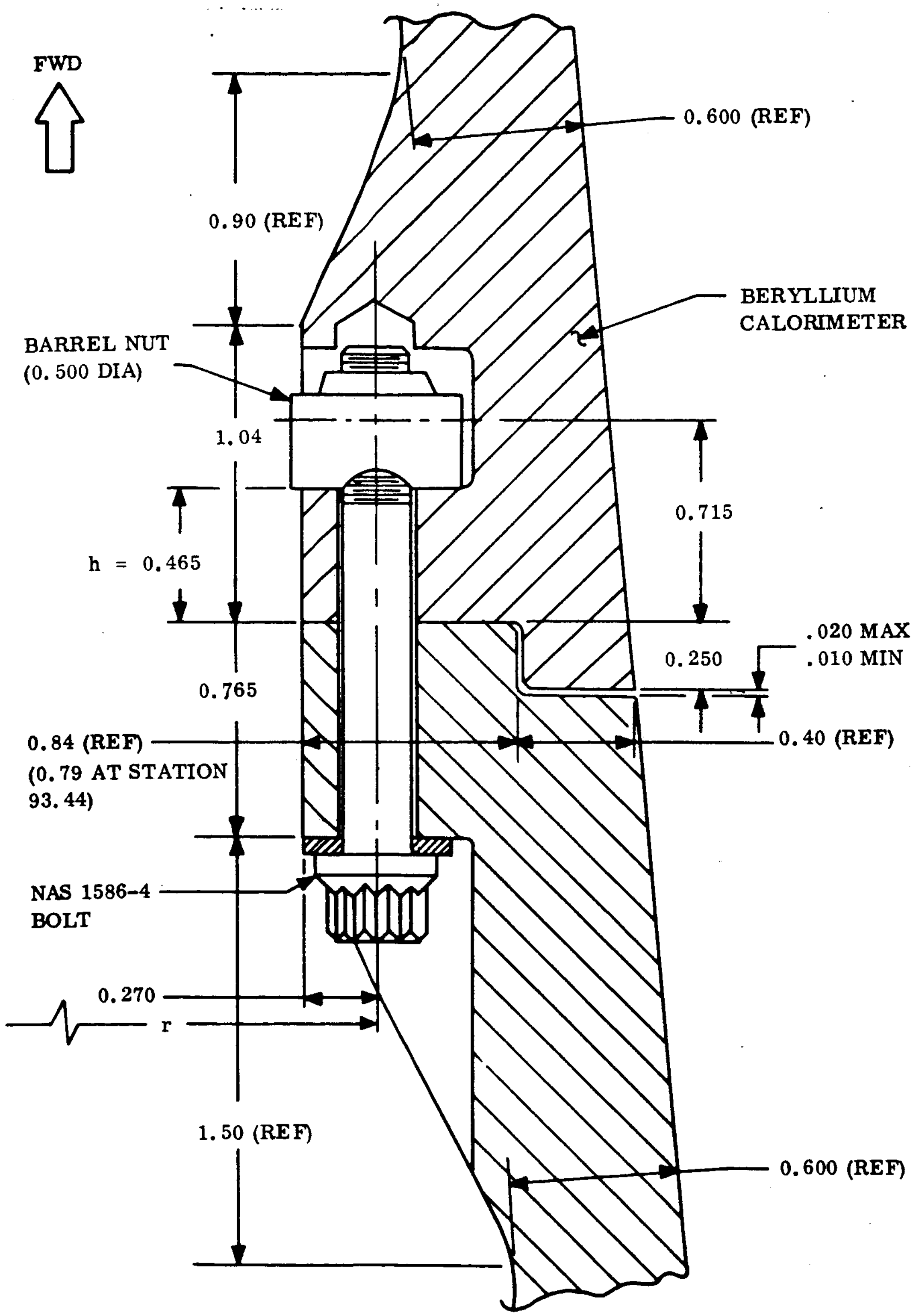

Figure 10. Calorimeter Bolted Joint

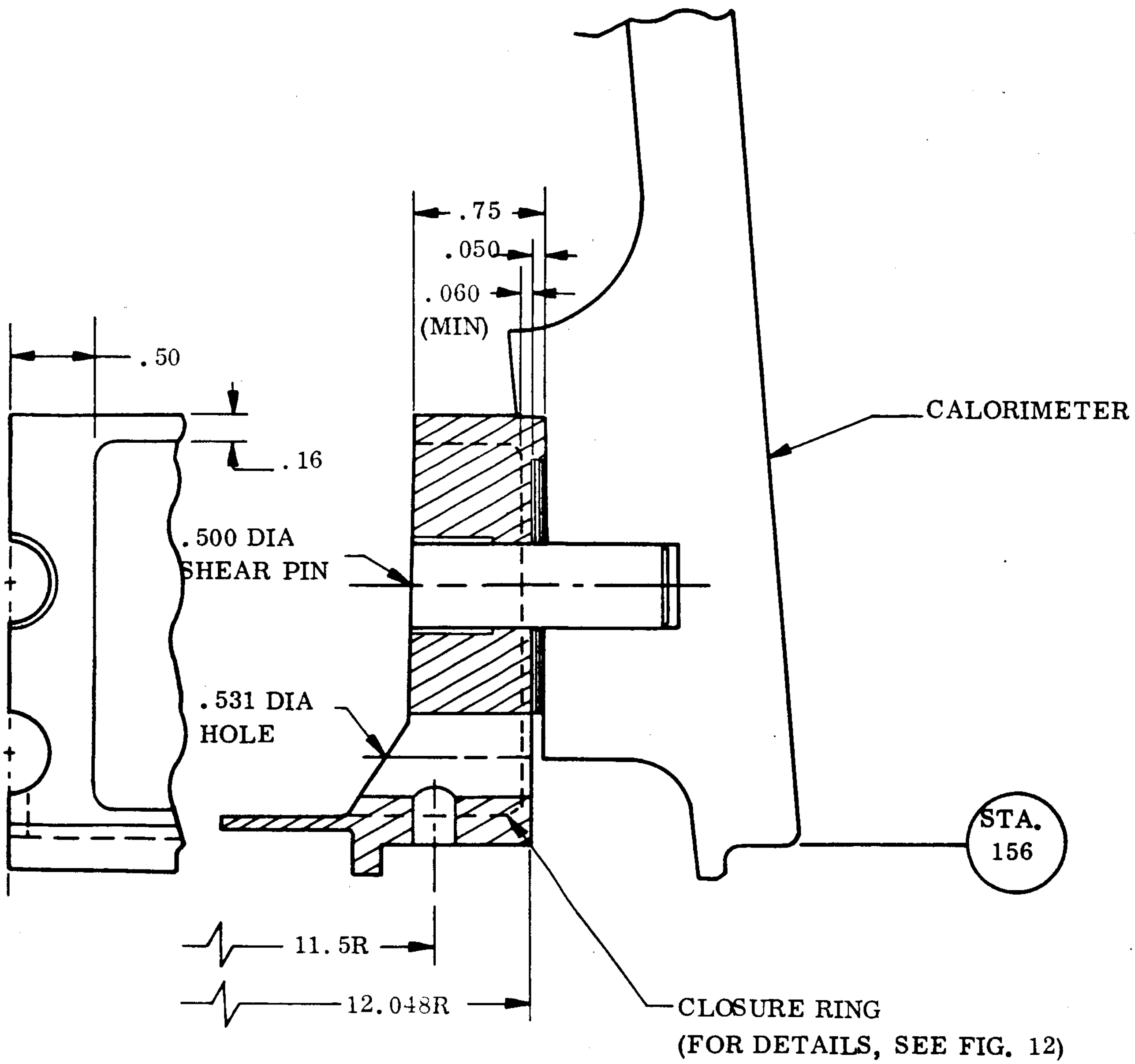

Figure 11. Interface Joint Design

1117

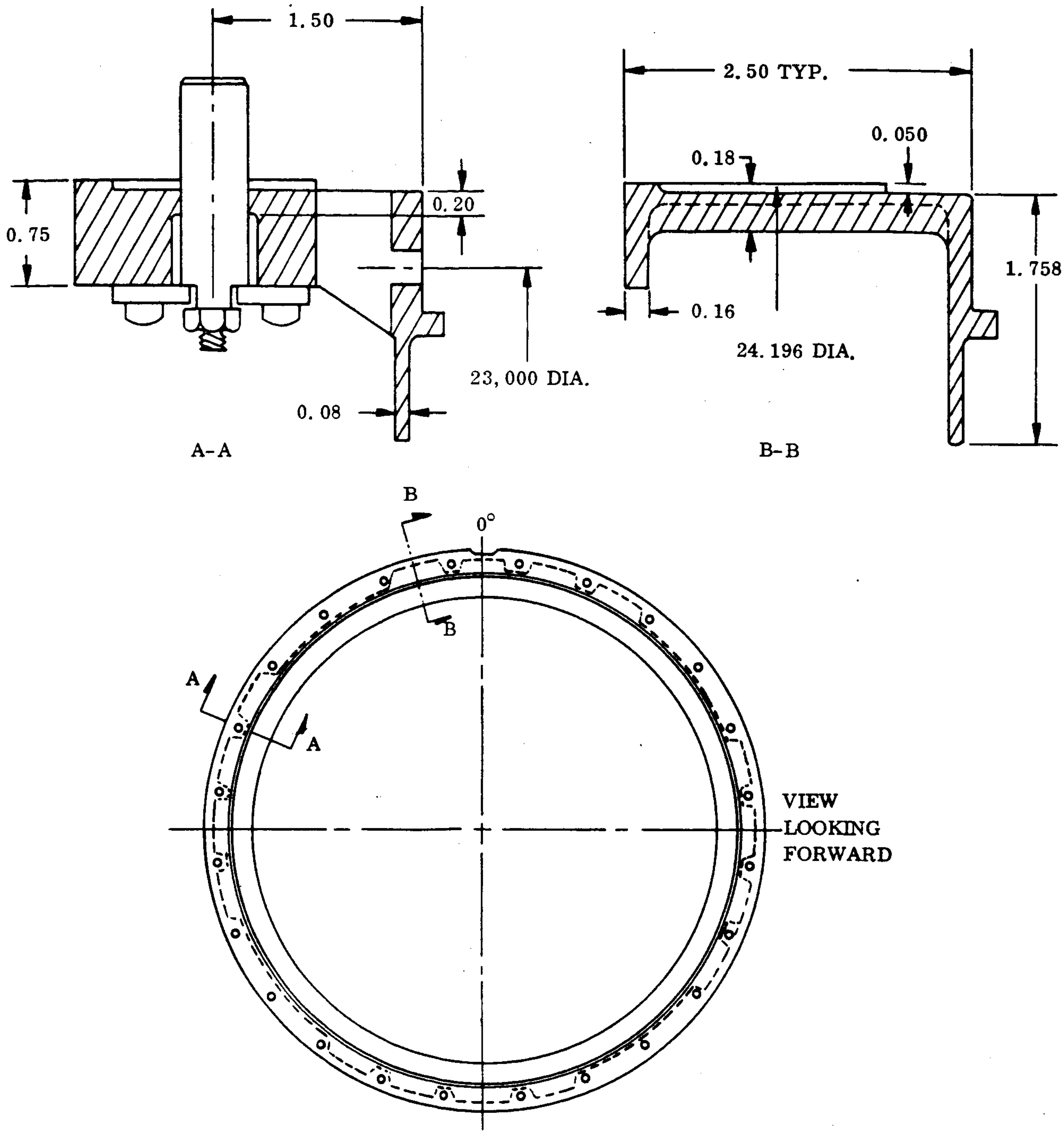

Figure 12. Closure Ring Design

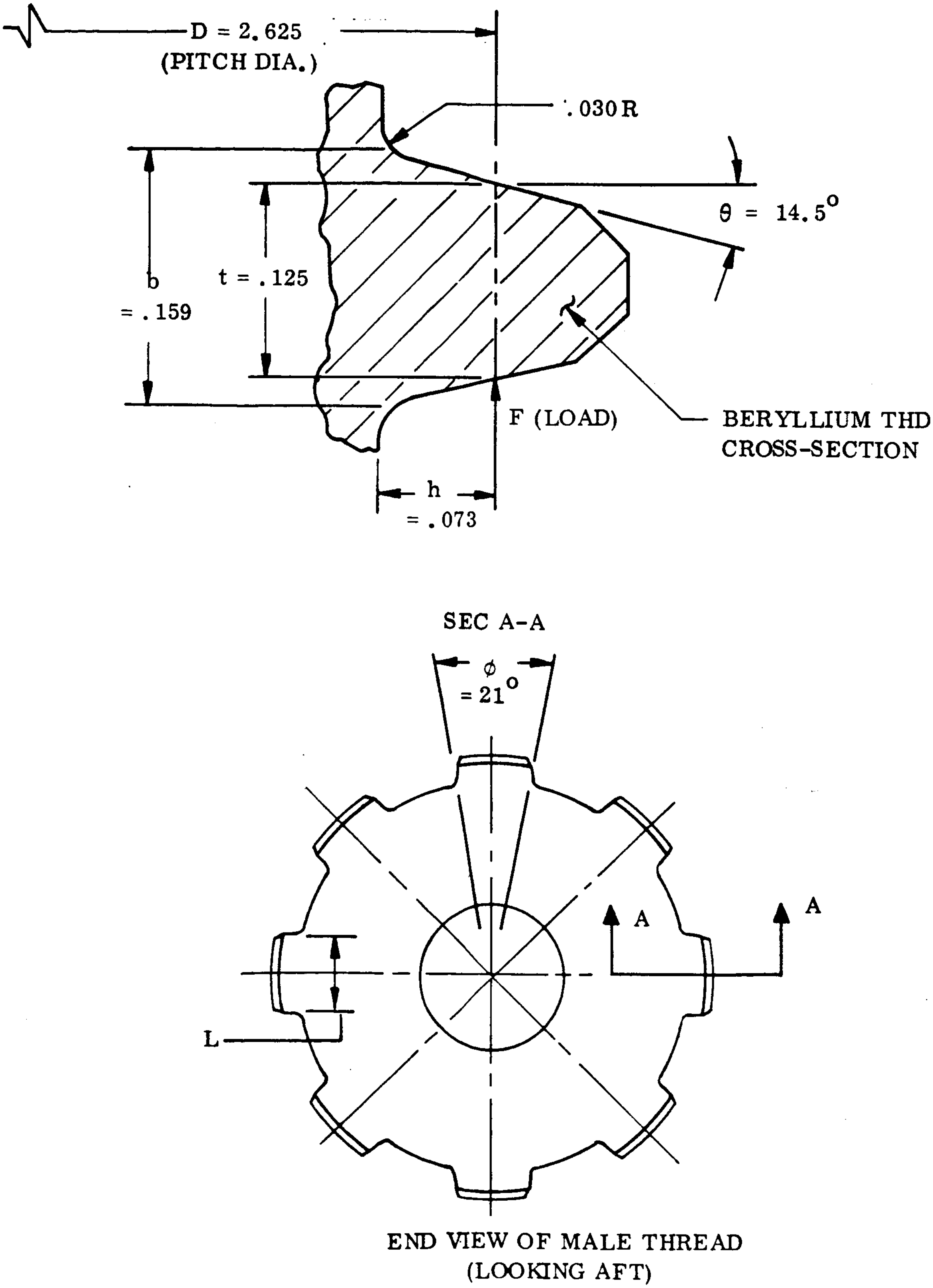

Figure 13. Breech Joint Thread Details

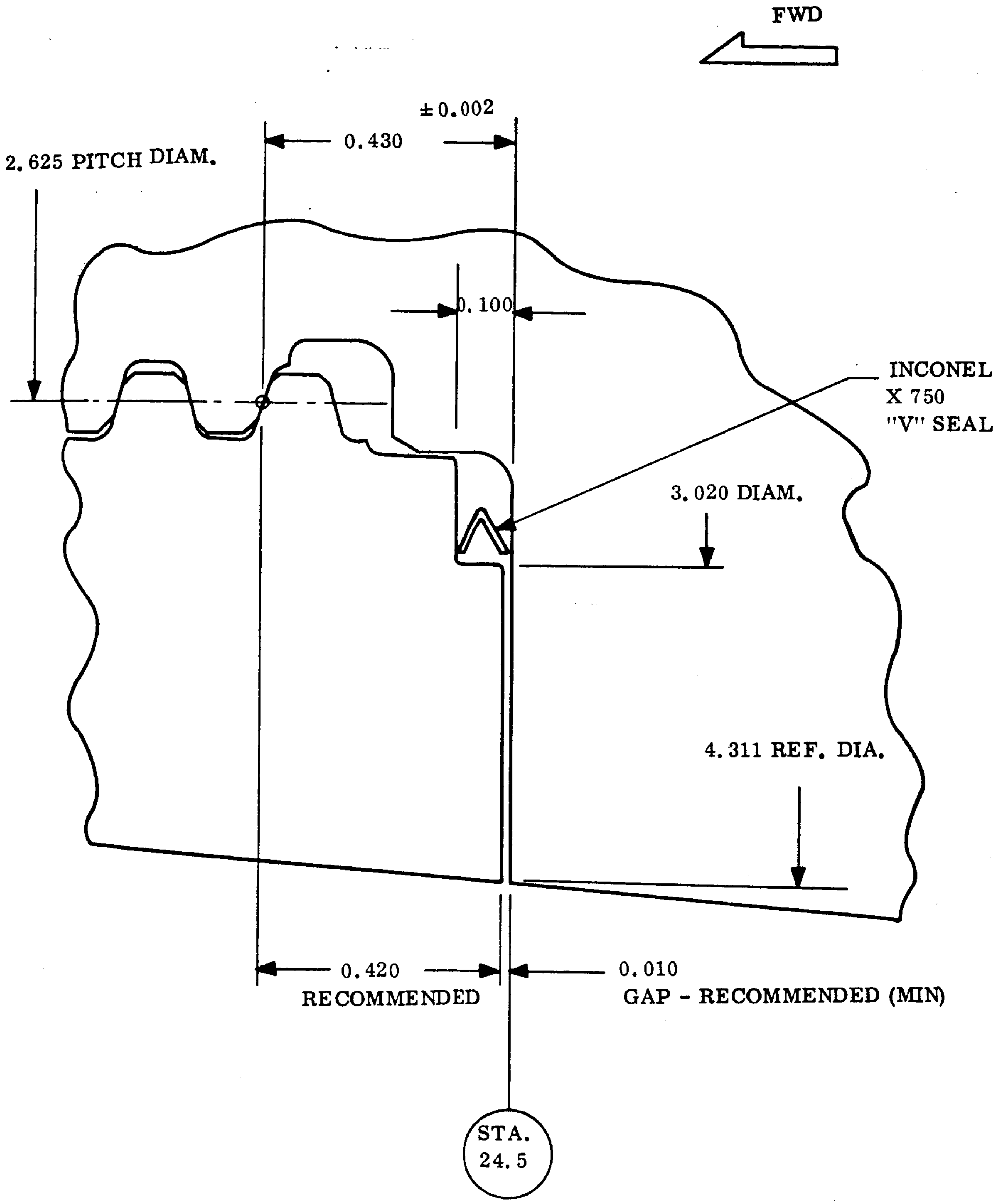

Figure 14. Assembled Breech Joint

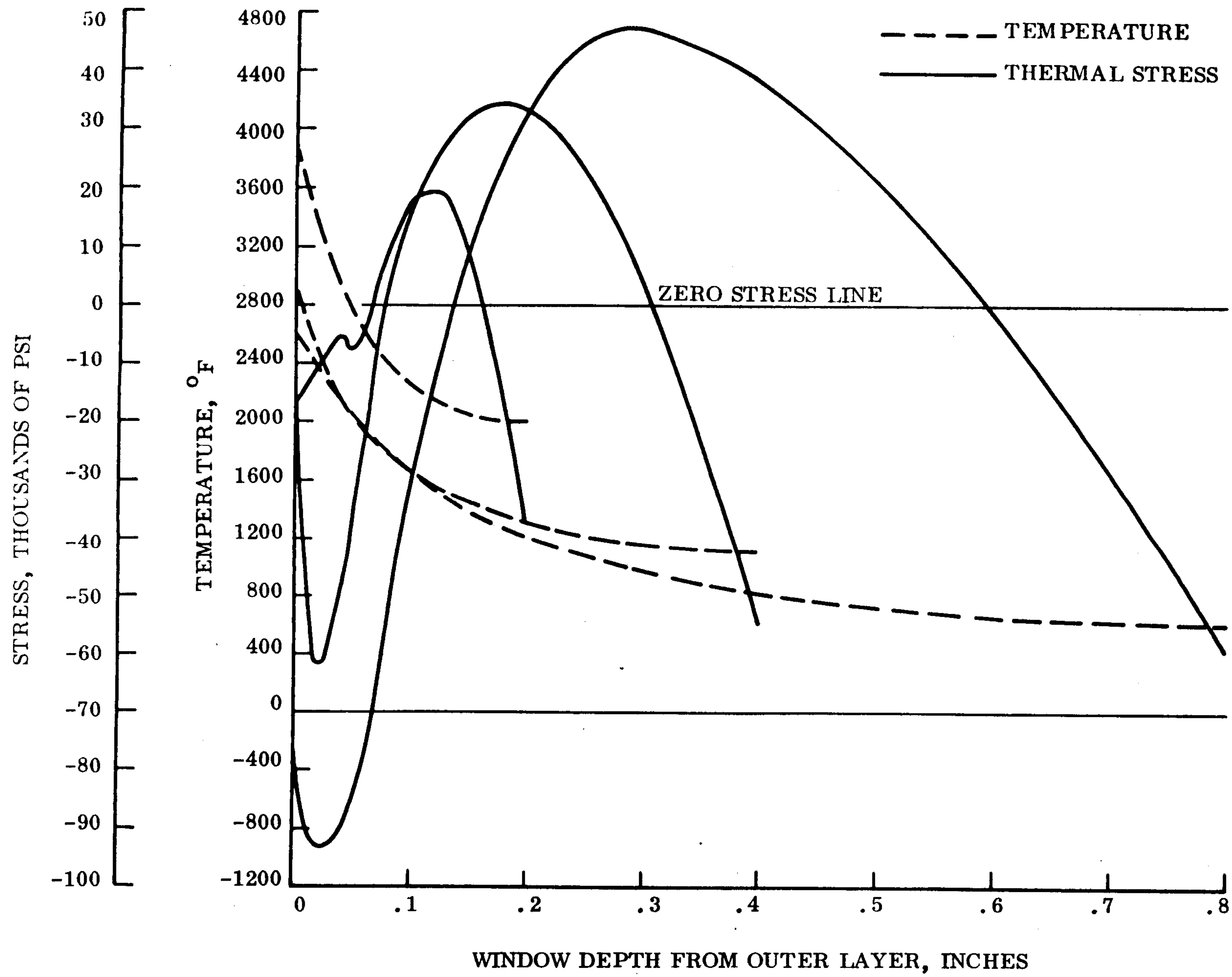

Figure 15. Termperatures and Thermal Stress Distributions in the B_eO Windows.

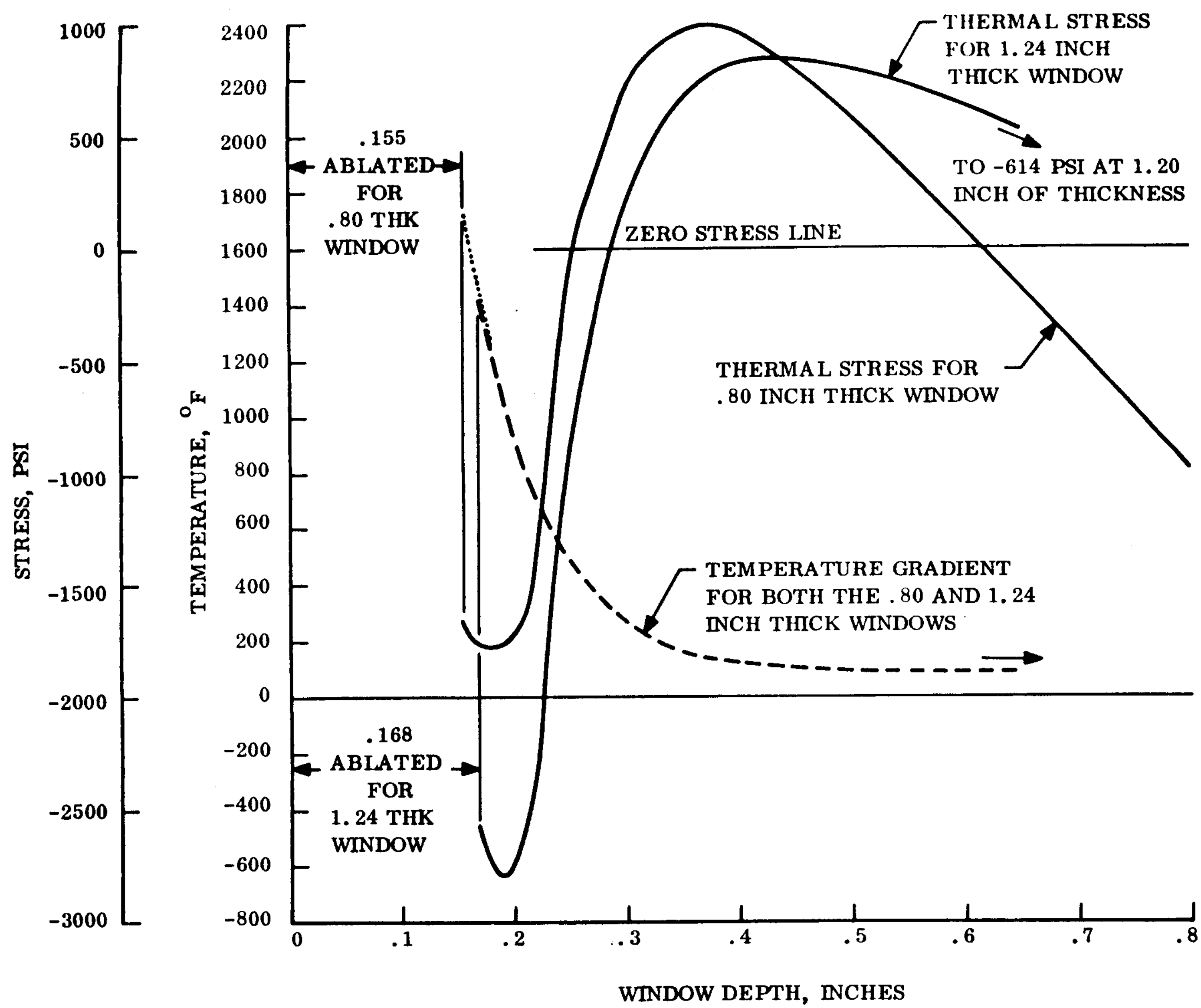

Figure 16. Temperatures and Thermal Stress in the Fuzed Silica Antenna Windows.

152

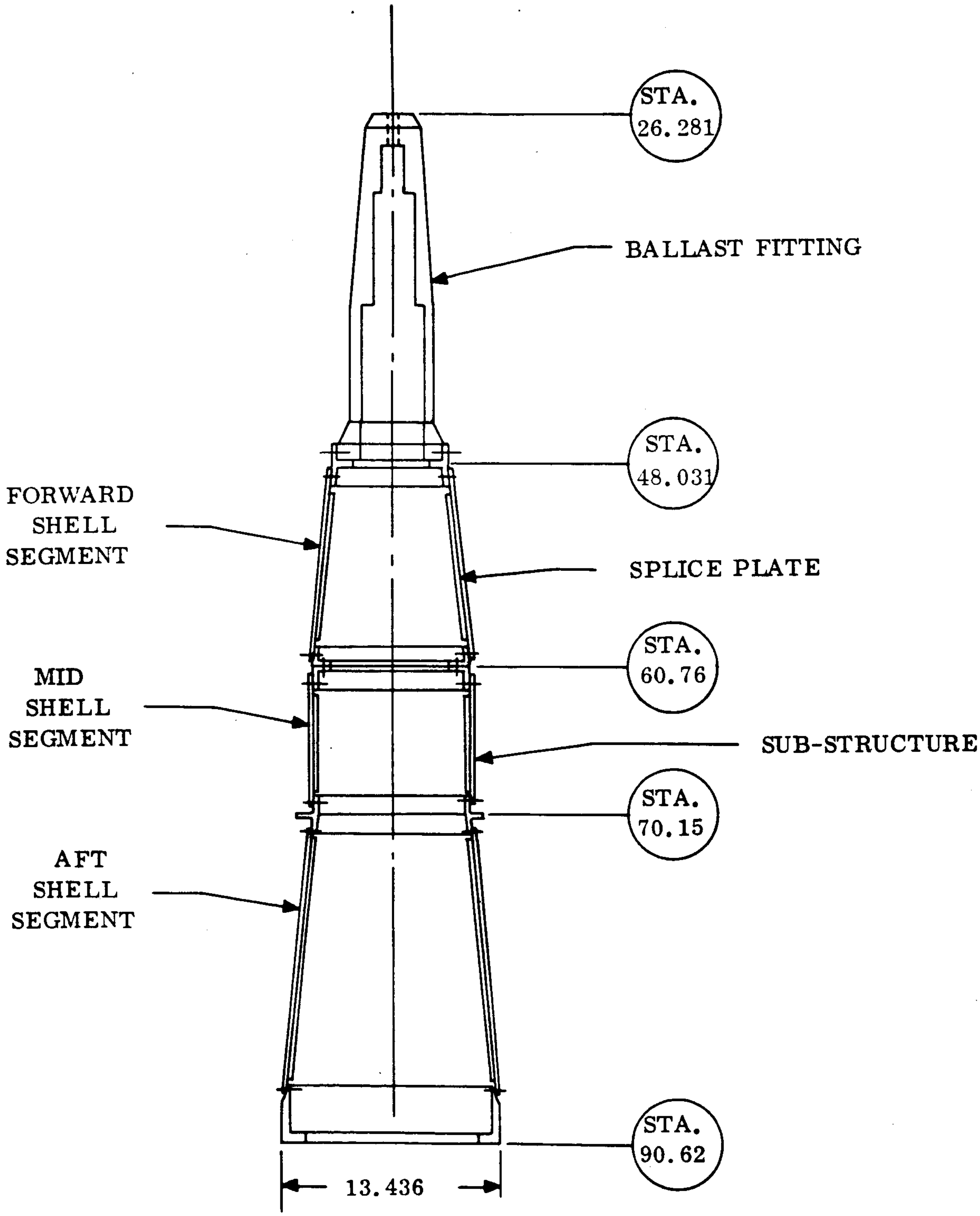

Figure 17. Forward Substructure and Ballast Fitting

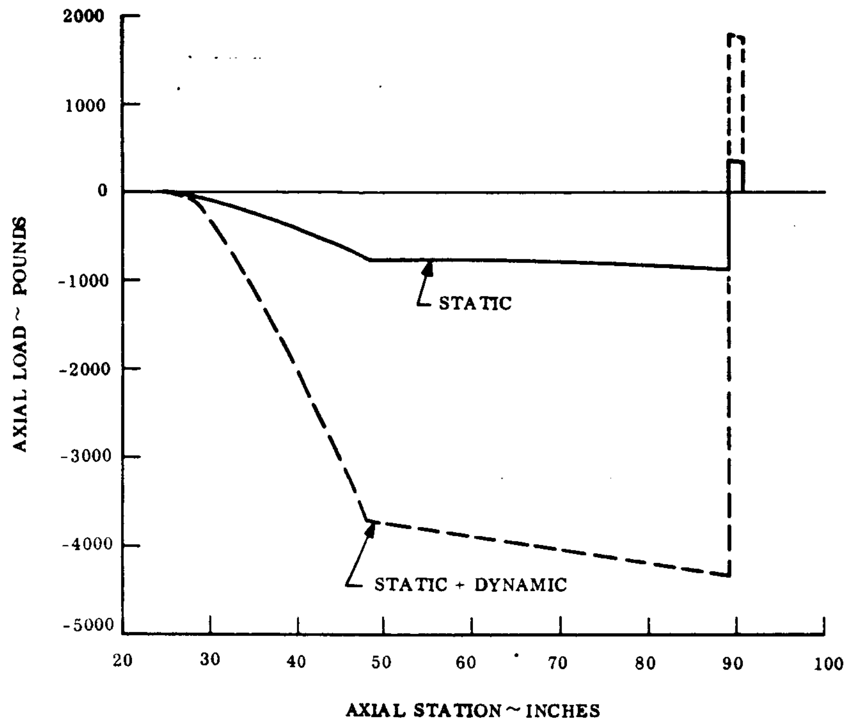

Figure 18. FWD Substructure, Limit Axial Load vs. Axial Station for Load Condition C

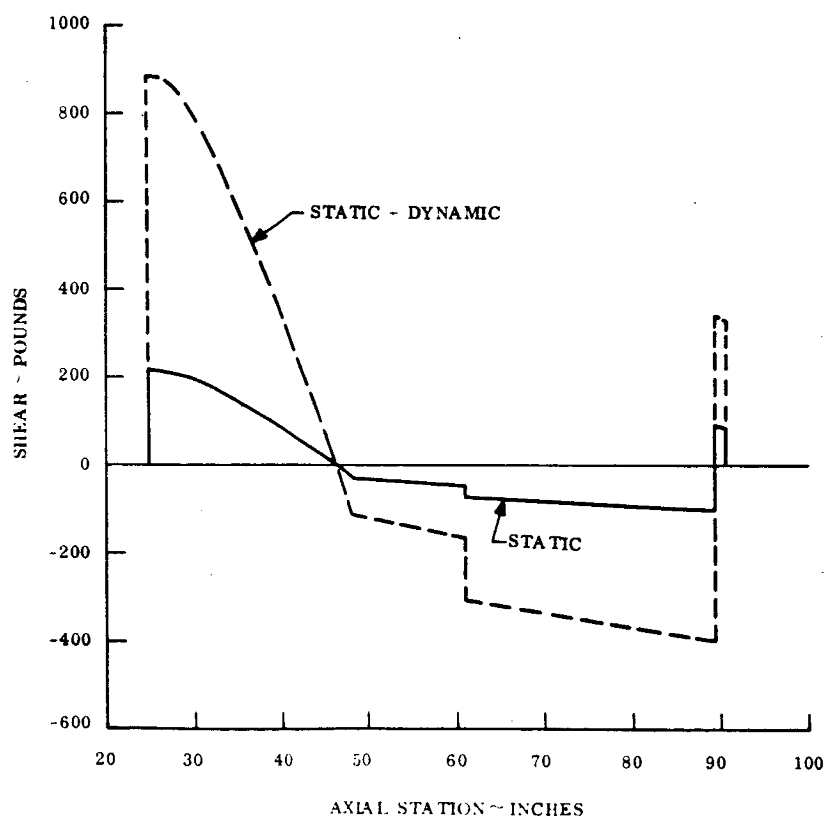

Figure 19. FWD Substructure, Limit Shear vs. Axial Station for Load Condition C

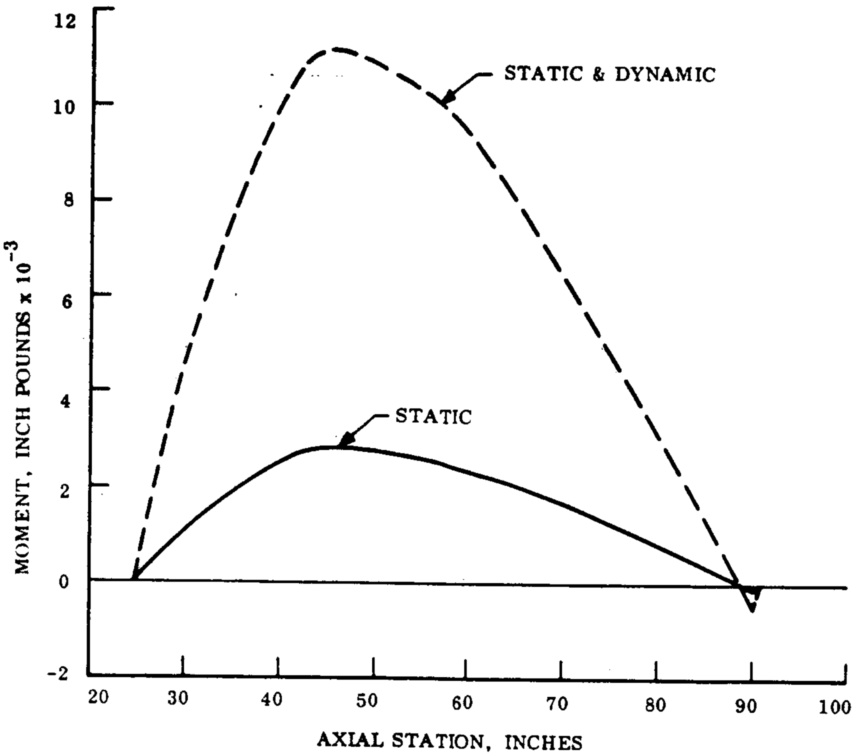

Figure 20. FWD Substructure, Limit Moment vs. Axial Station for Load Condition C

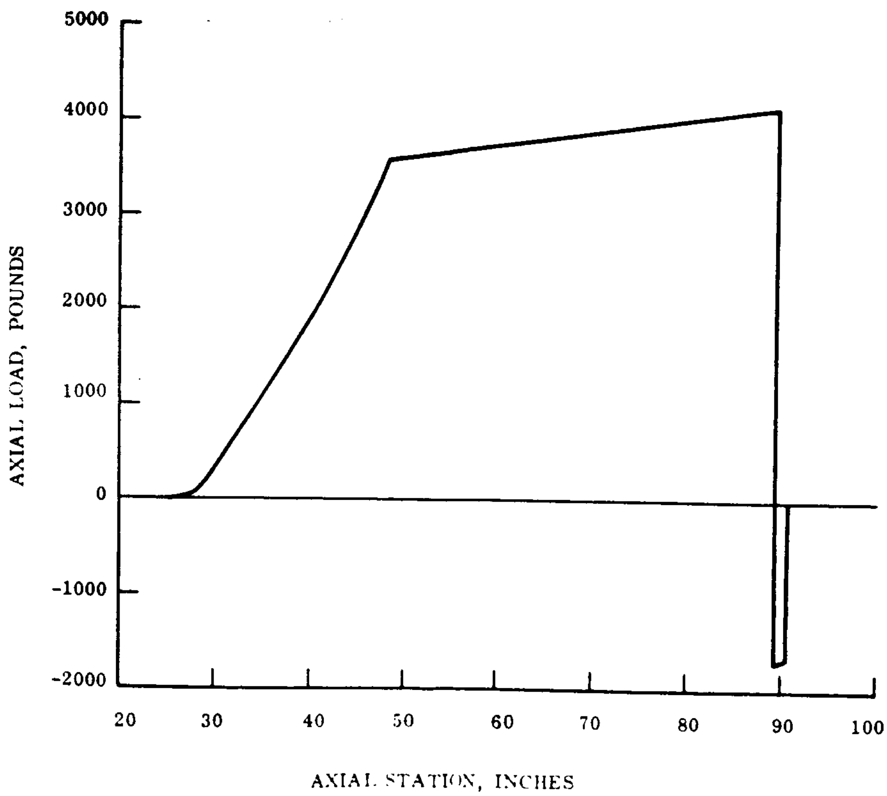

Figure 21. FWD Substructure, Limit Axial Load vs. Axial Station for Load Condition J

--1-

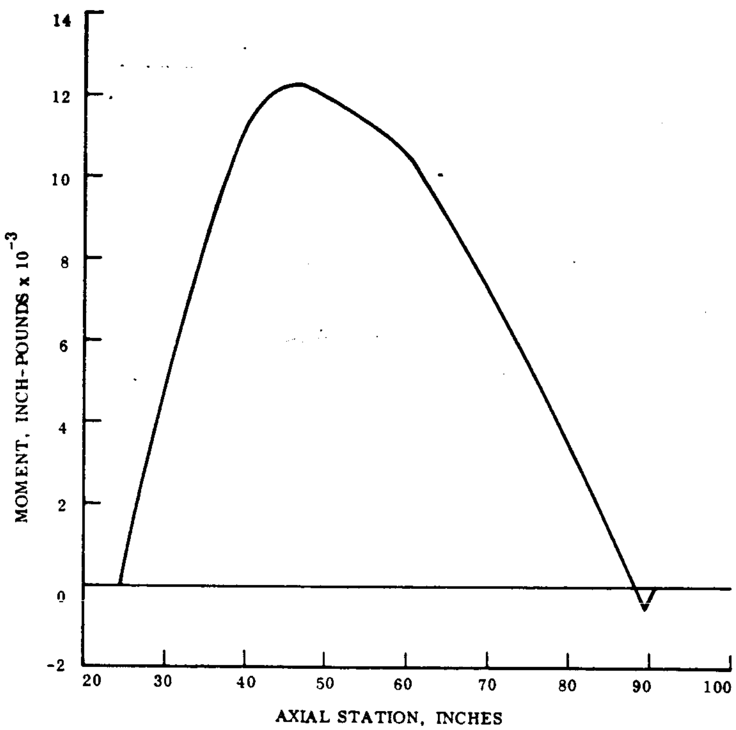

Figure 22. FWD Substructure, Limit Shear vs. Axial Station for Load Condition J

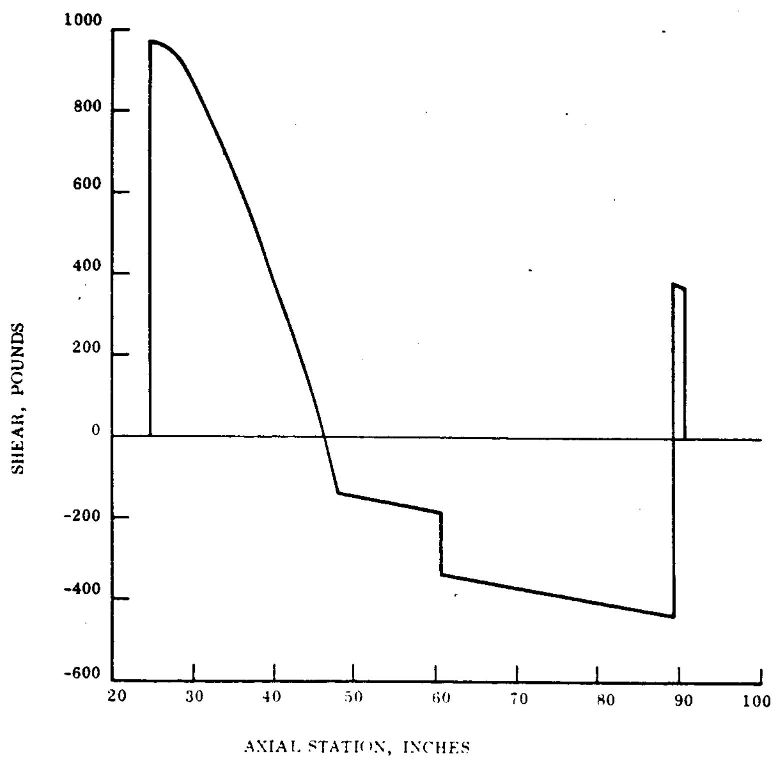

Figure 23. FWD Substructure, Limit Moment vs. Axial Station for Load Condition J

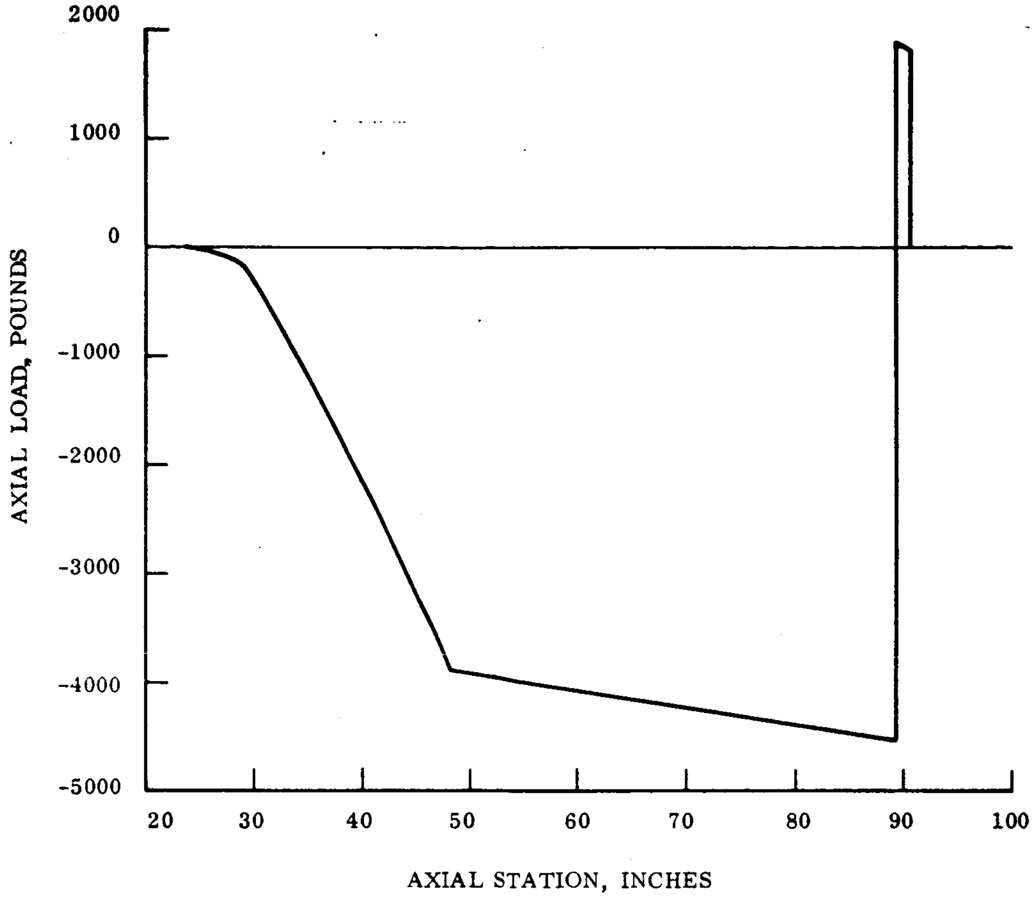

Figure 24. FWD Substructure, Limit Axial Load vs. Axial Station for Load Condition G

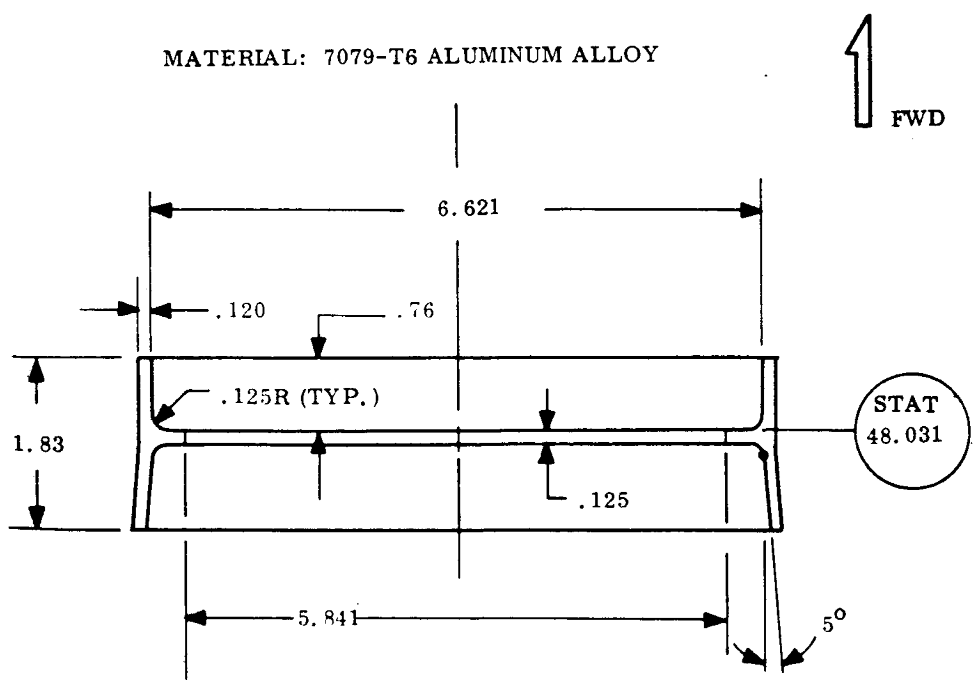

Figure 25. Ring Sta. 48-Internal Structure Mid Section

157

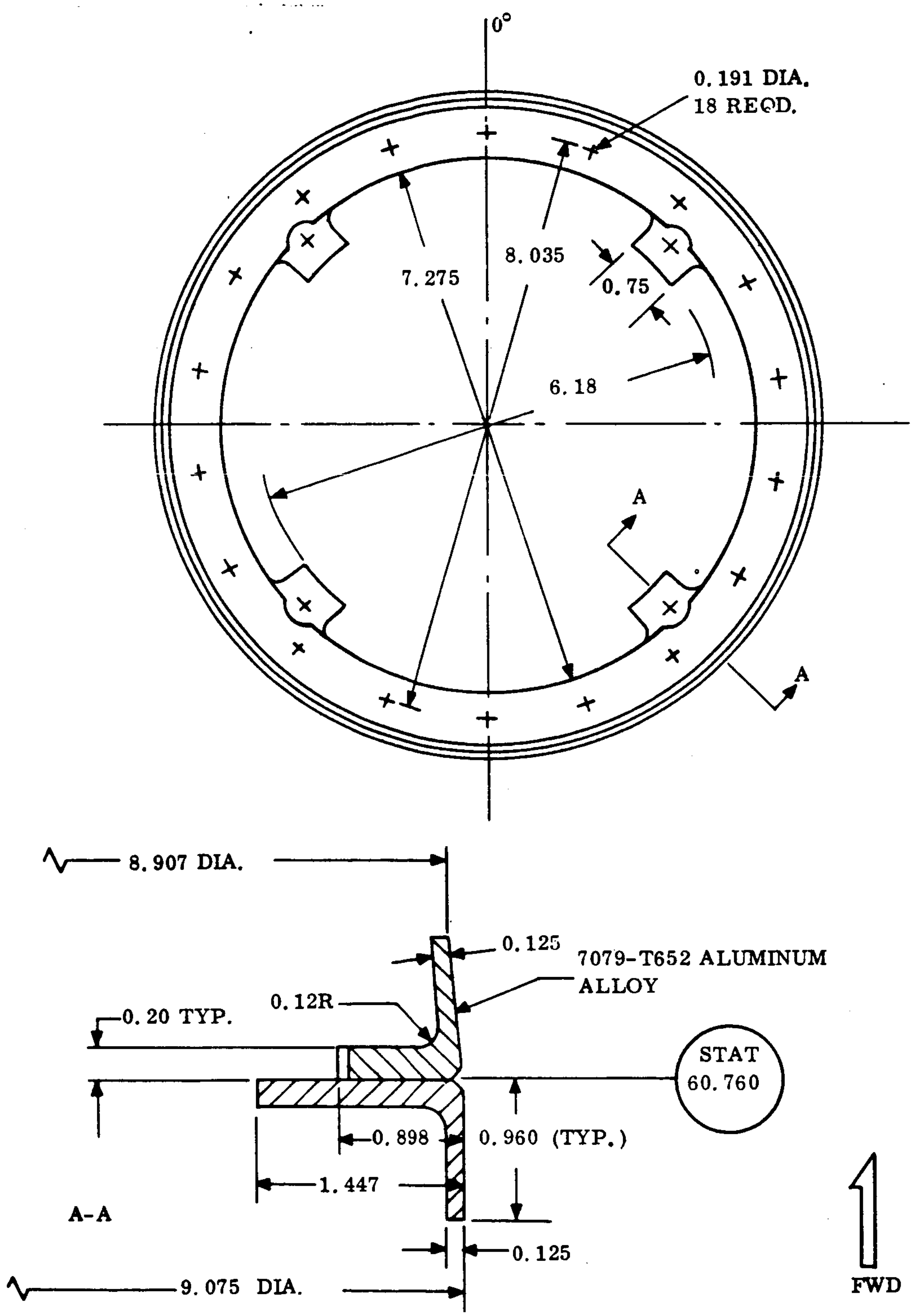

Figure 26. Ring Sta. 60.8 Internal Structure Mid-Section

158

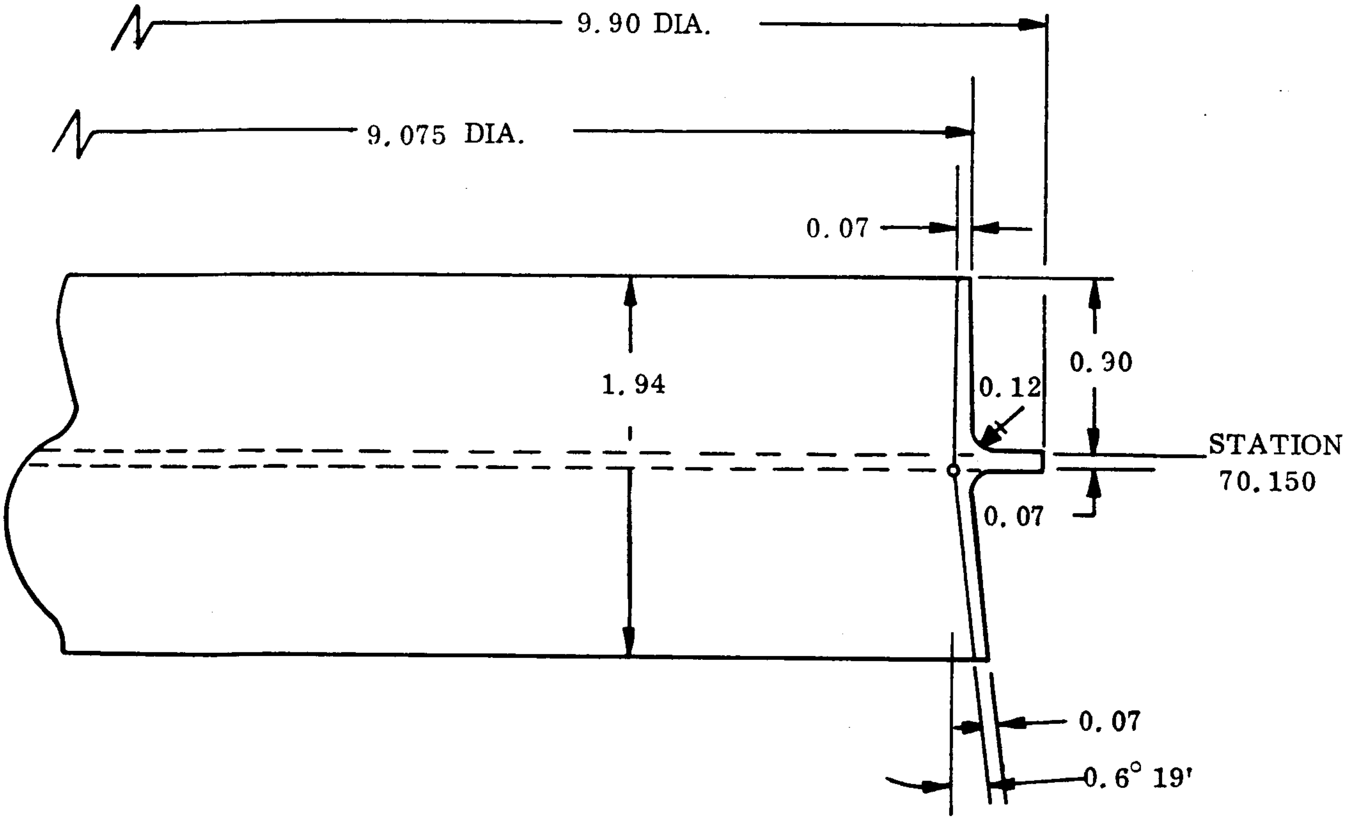

Figure 27. Ring Sta. 70-1, Internal Structure Mid Section

FOR RING CROSS-SECTIONS, SEE FIGURE 29

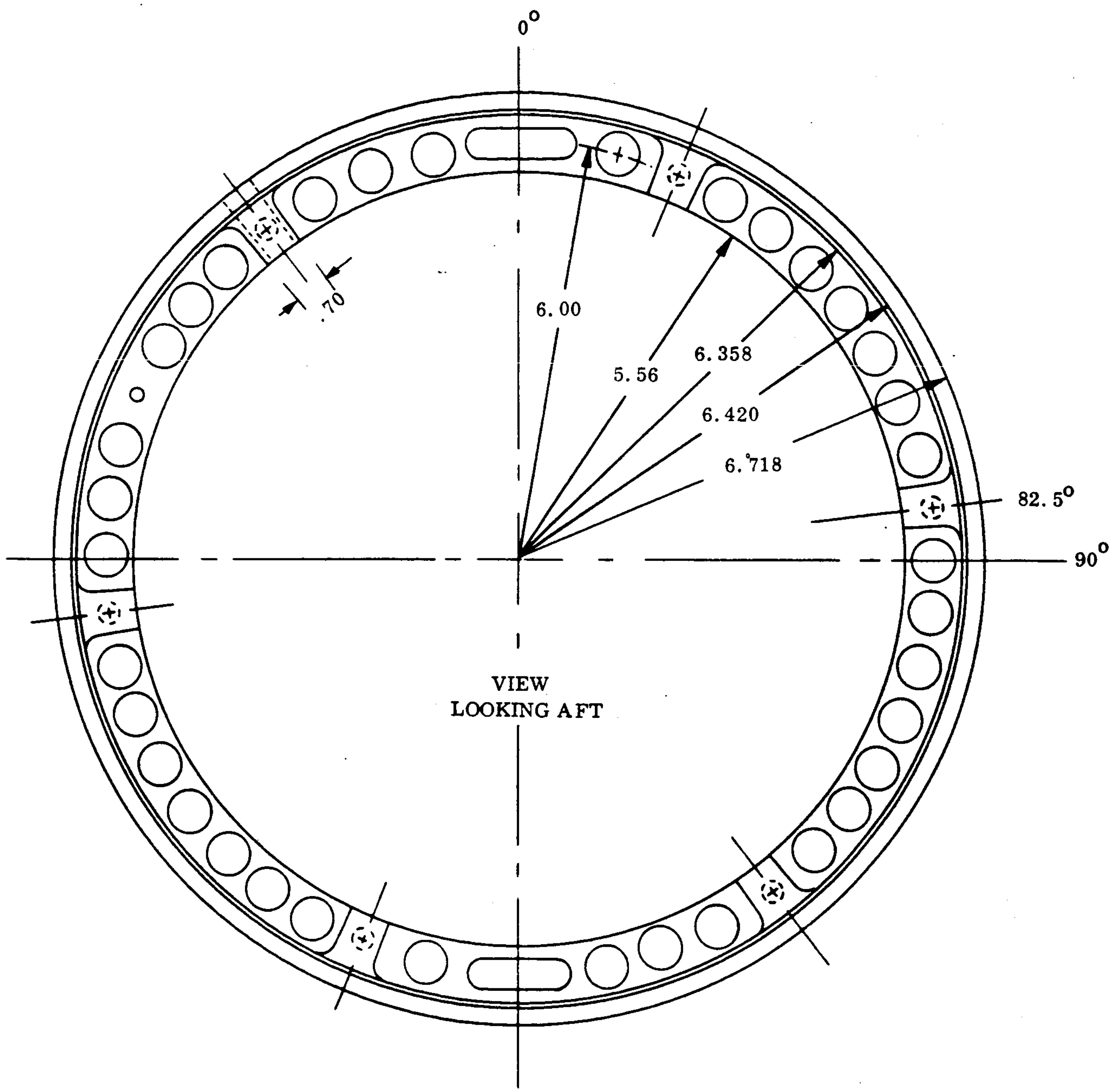

Figure 28. Ring at Station 90

160

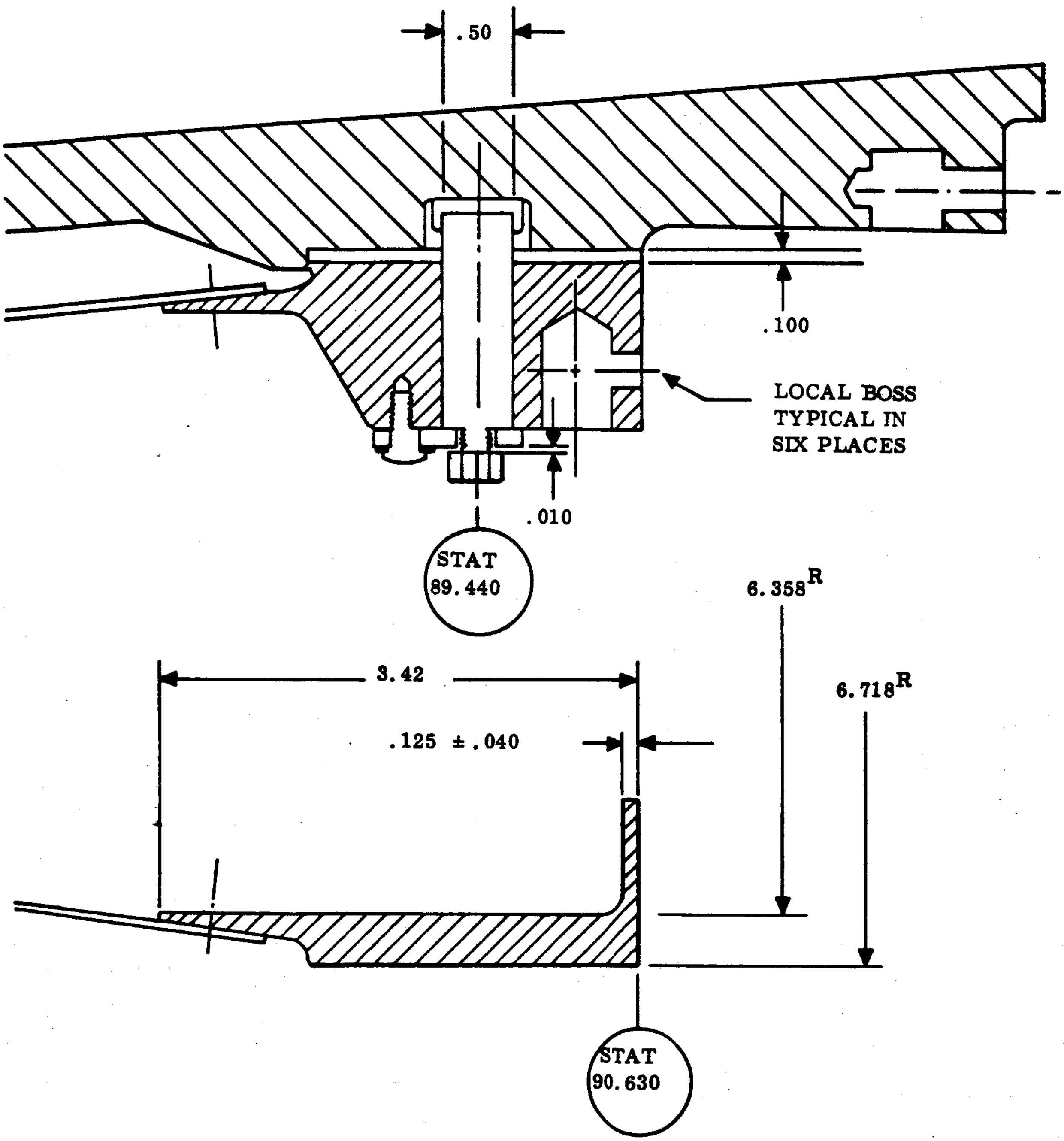

Figure 29. Cross-sections of Ring at Station 90

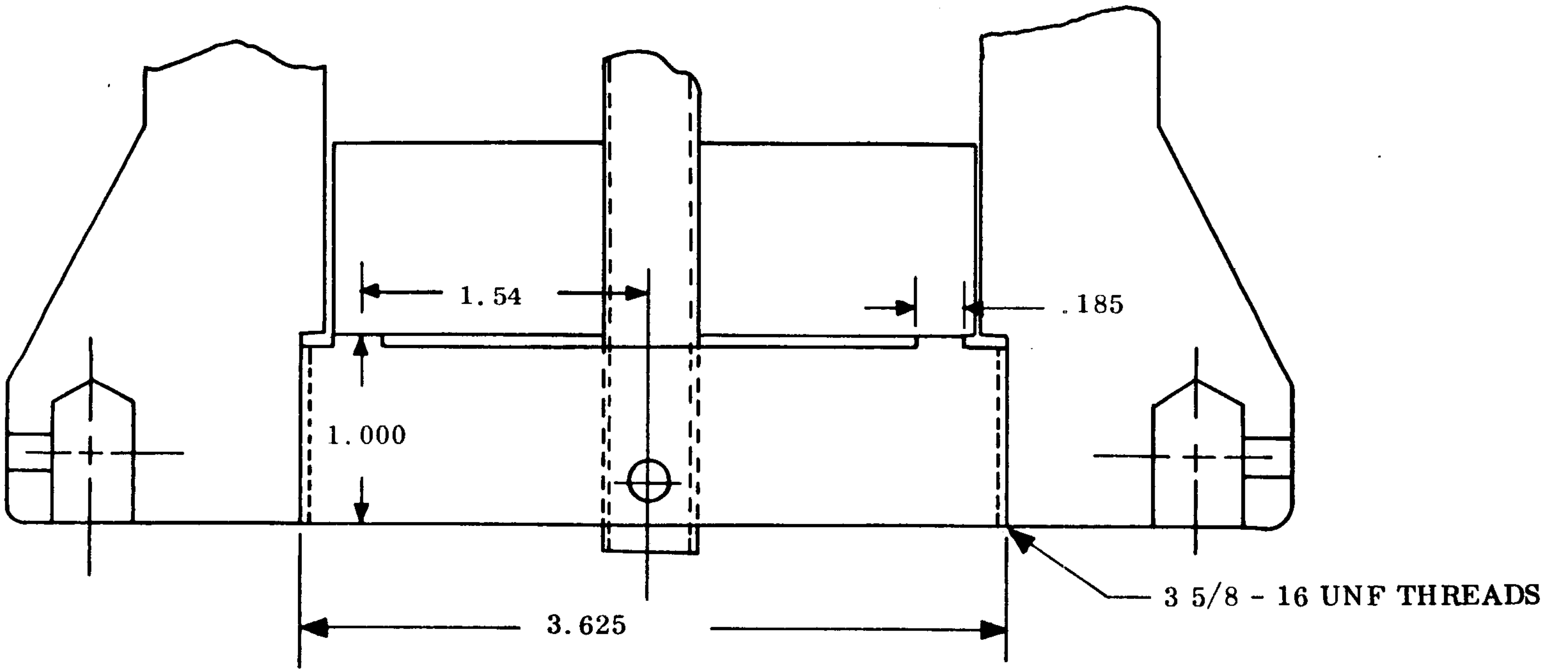

Figure 30. Ballast Retention Plug

1v2

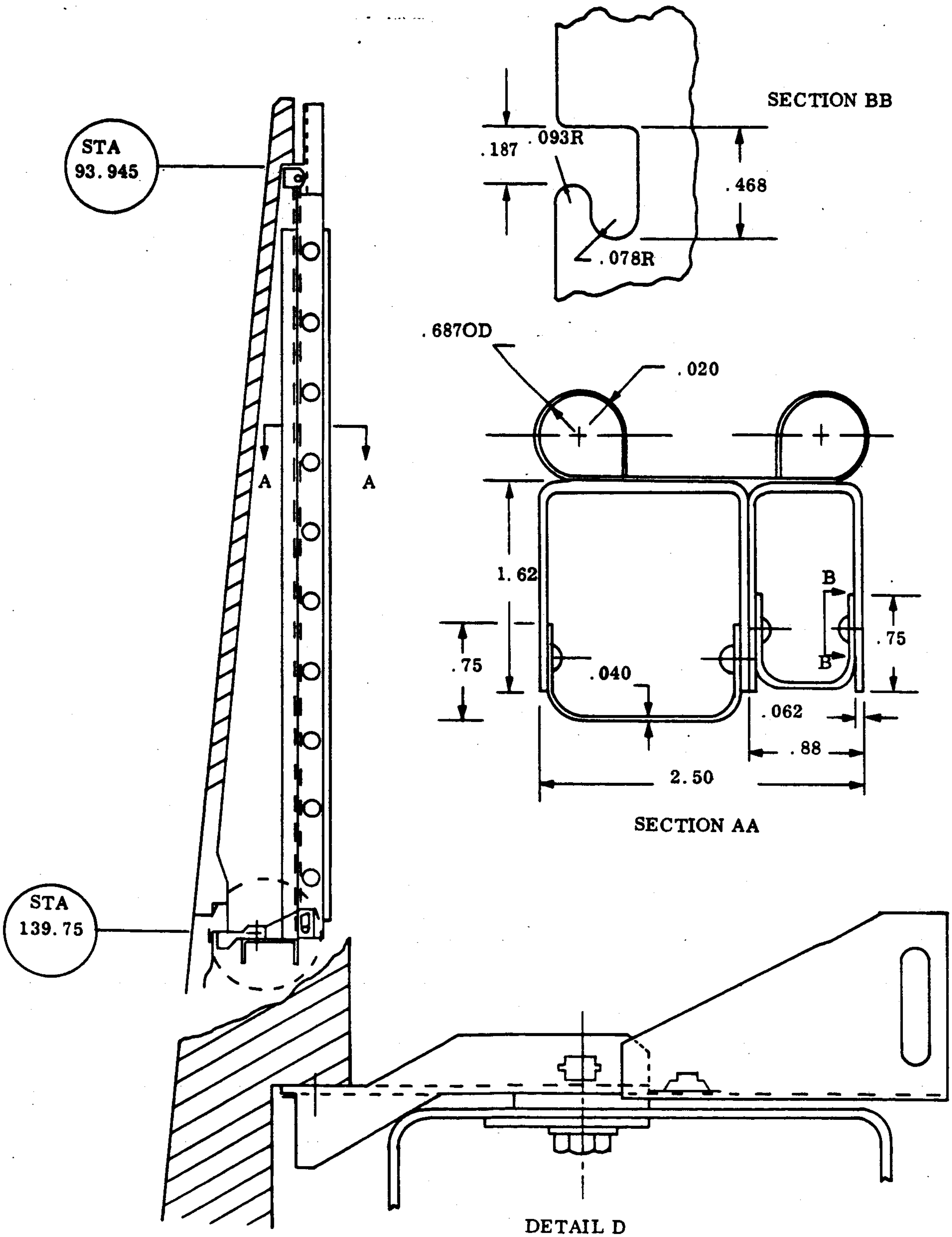

Figure 31. Aft Substructure

163

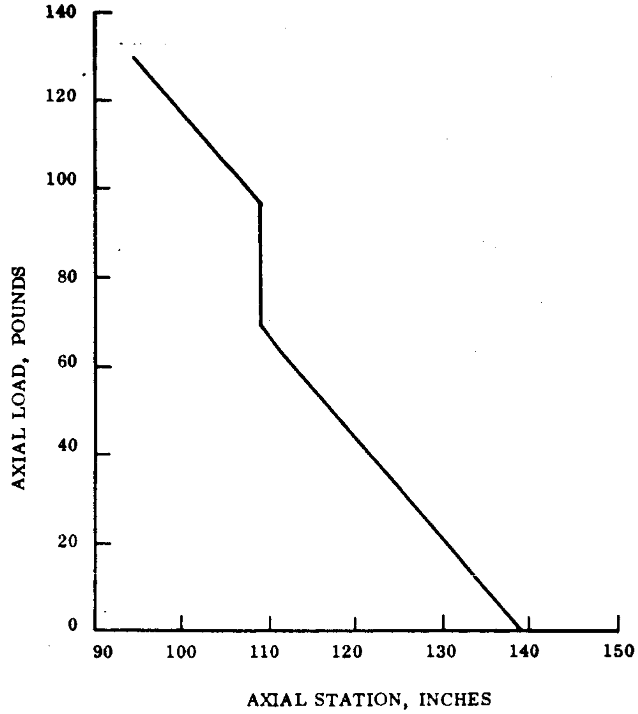

Figure 32. Aft Substructure, Limit Axial Load vs. Axial Station for Load Condition J

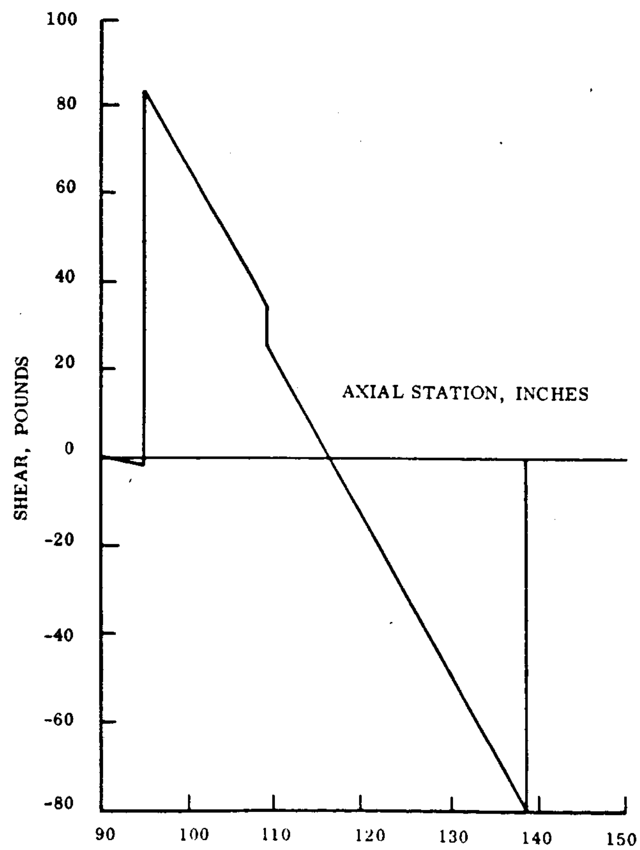

Figure 33. Aft Substructure, Limit Shear vs. Axial Station for Load Condition J

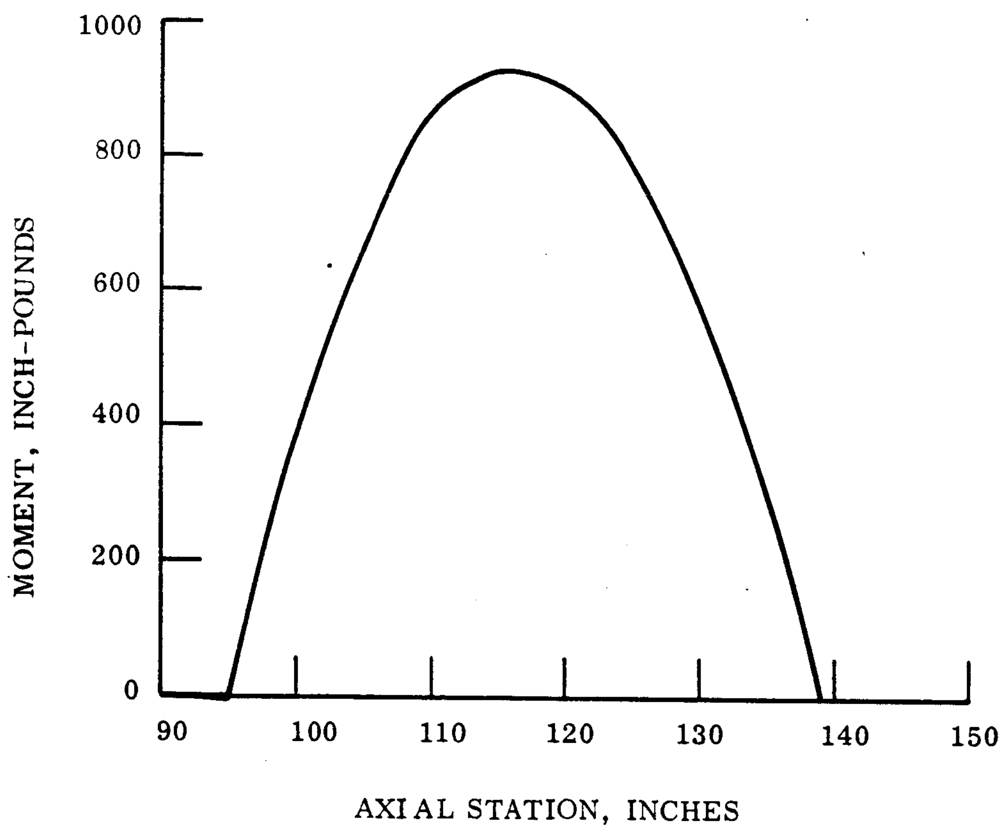

Figure 34. Aft Substructure, Limit Moment vs. Axial Station for Load Condition J

FORWARD SUPPORT BRACKET

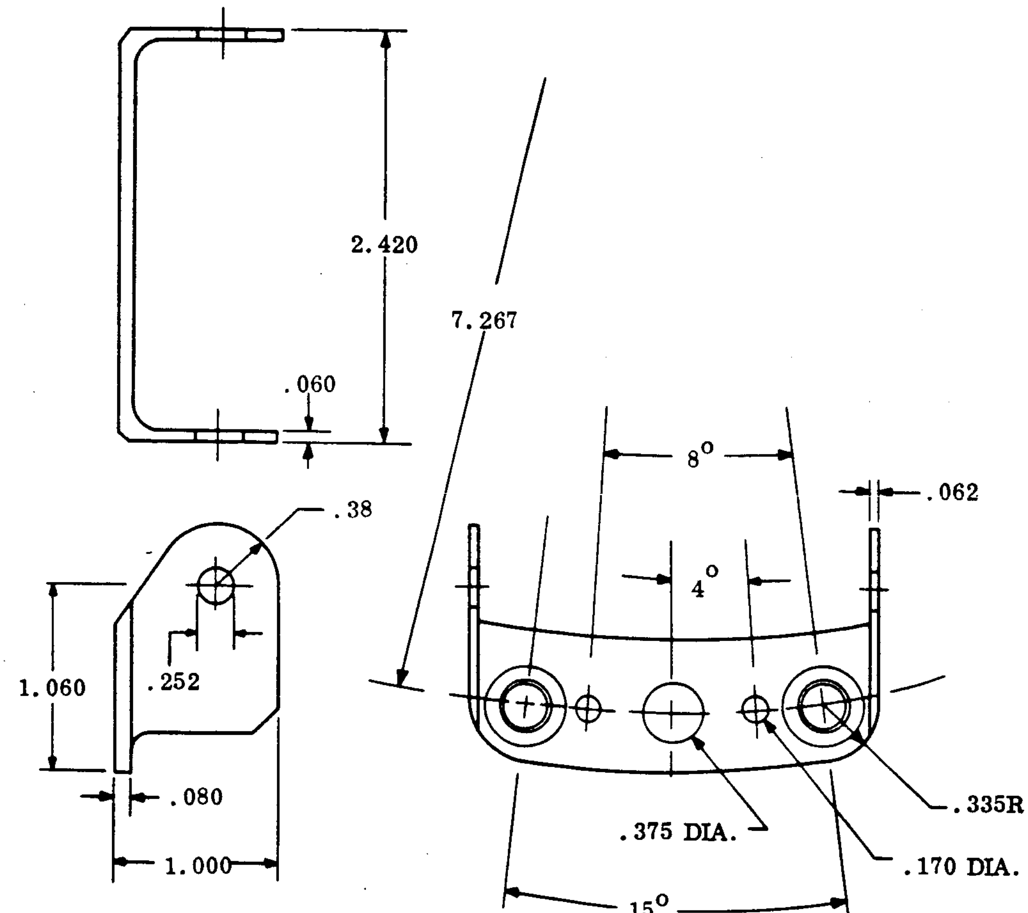

SUPPORT CLIPS

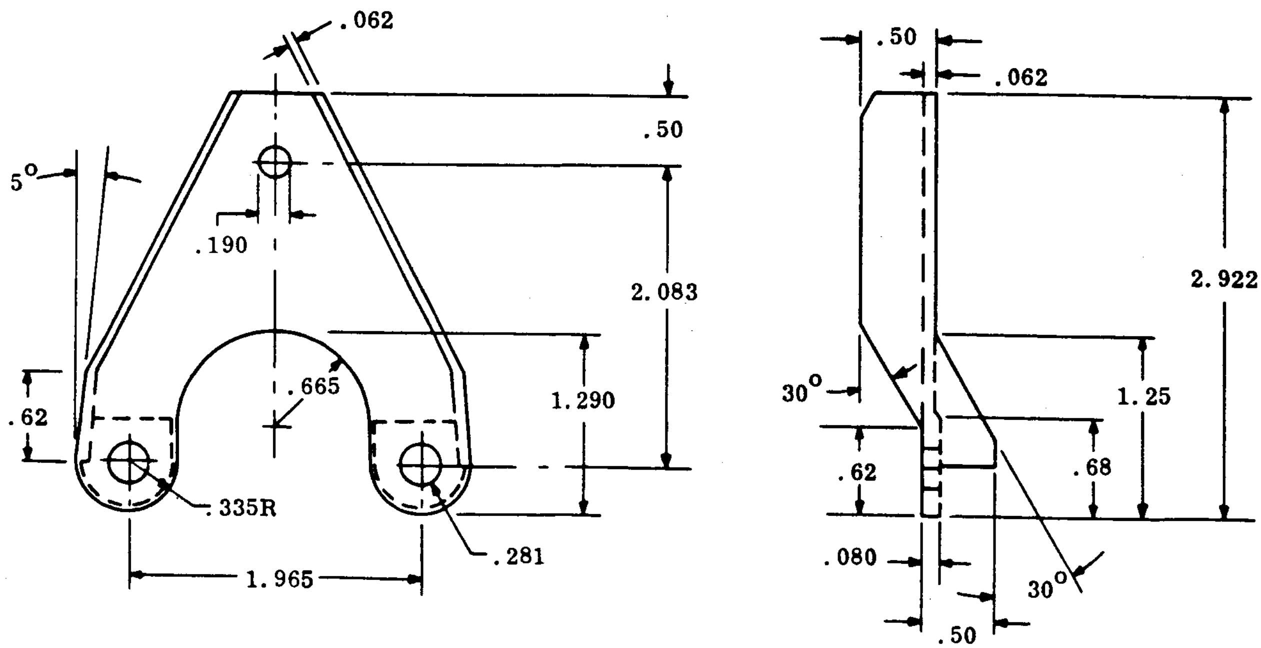

Figure 35. Brackets, Aft Section

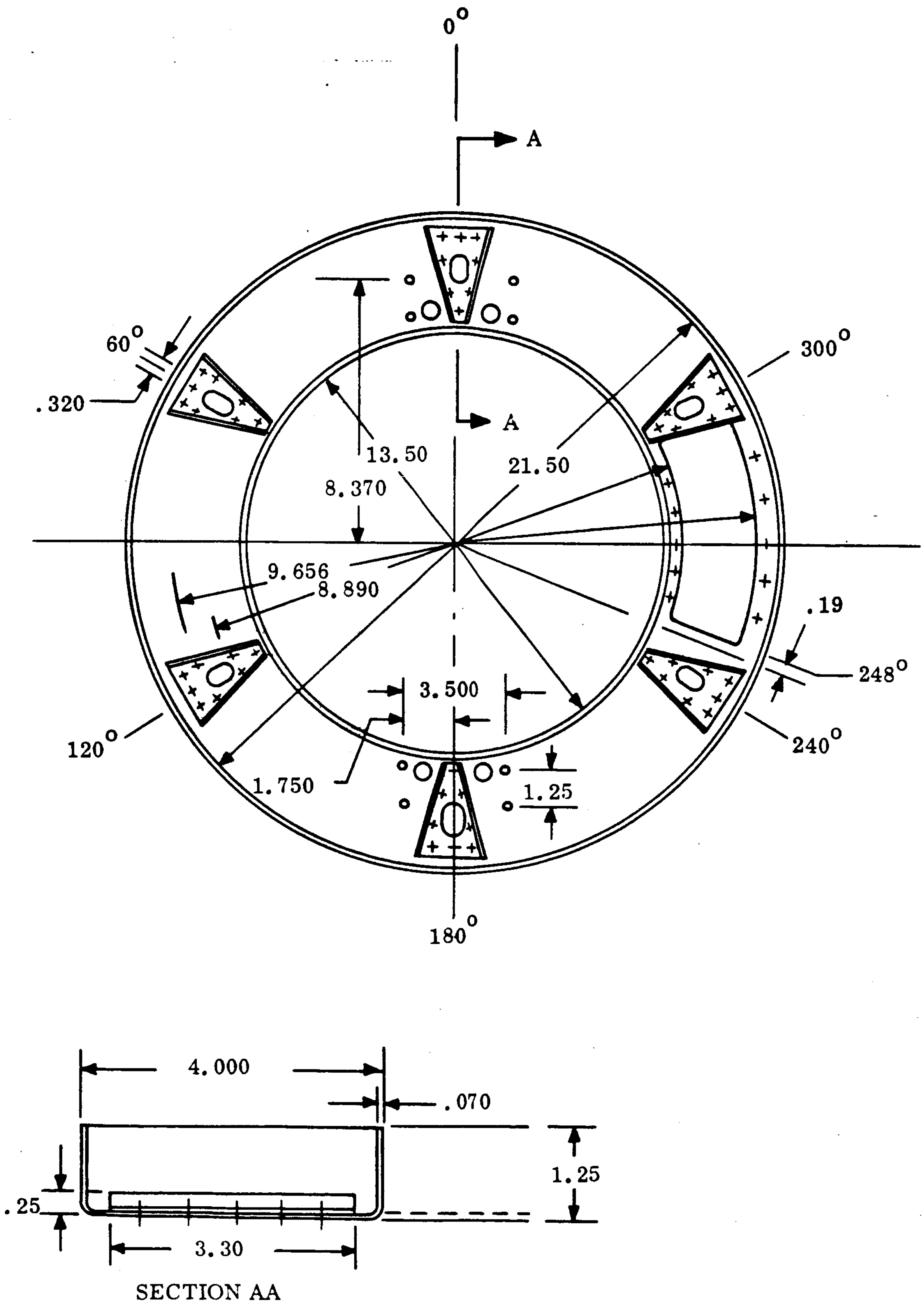

Figure 36. Bulkhead Assembly, Aft Section

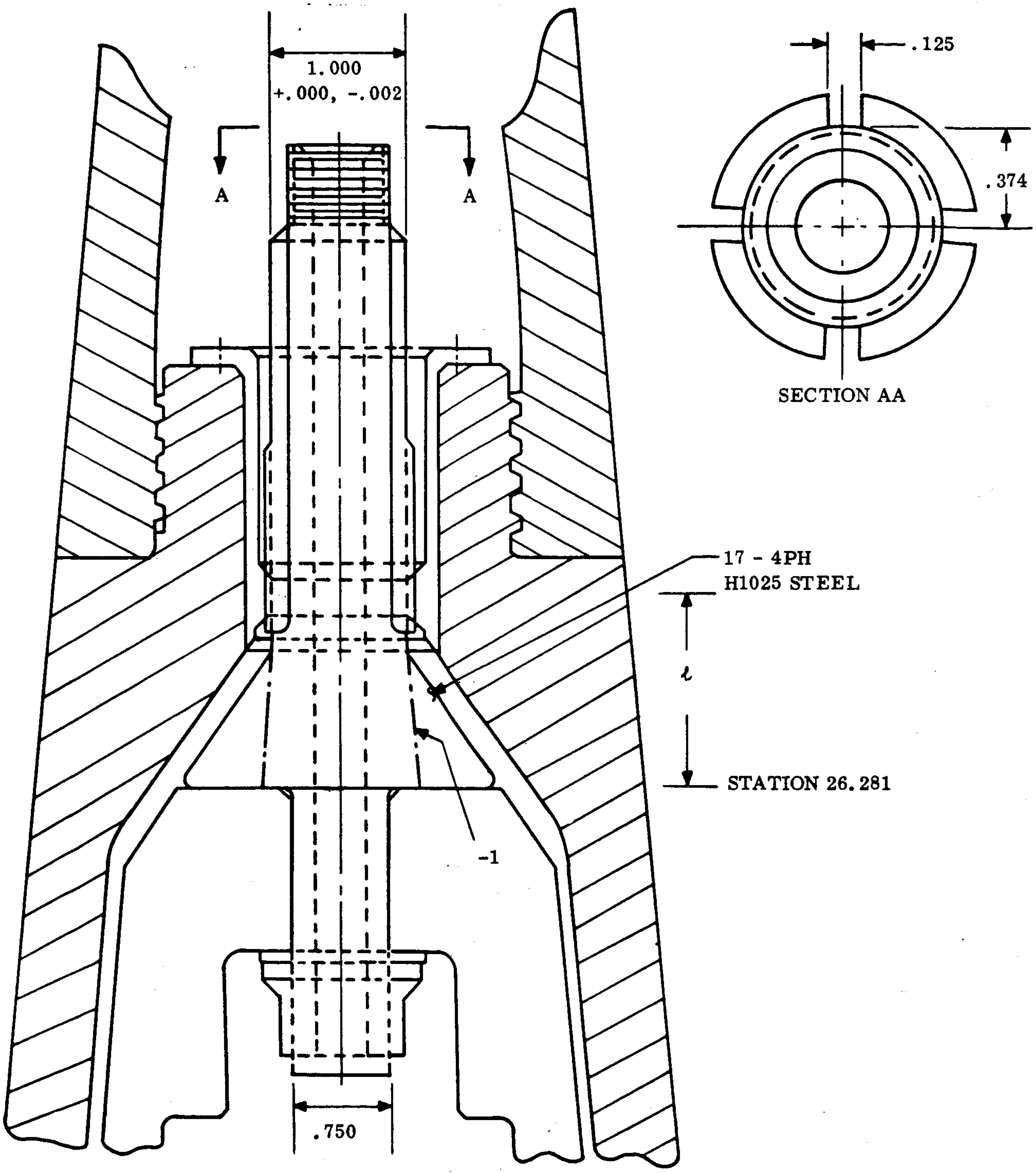

Figure 37. Payload Retention Scheme

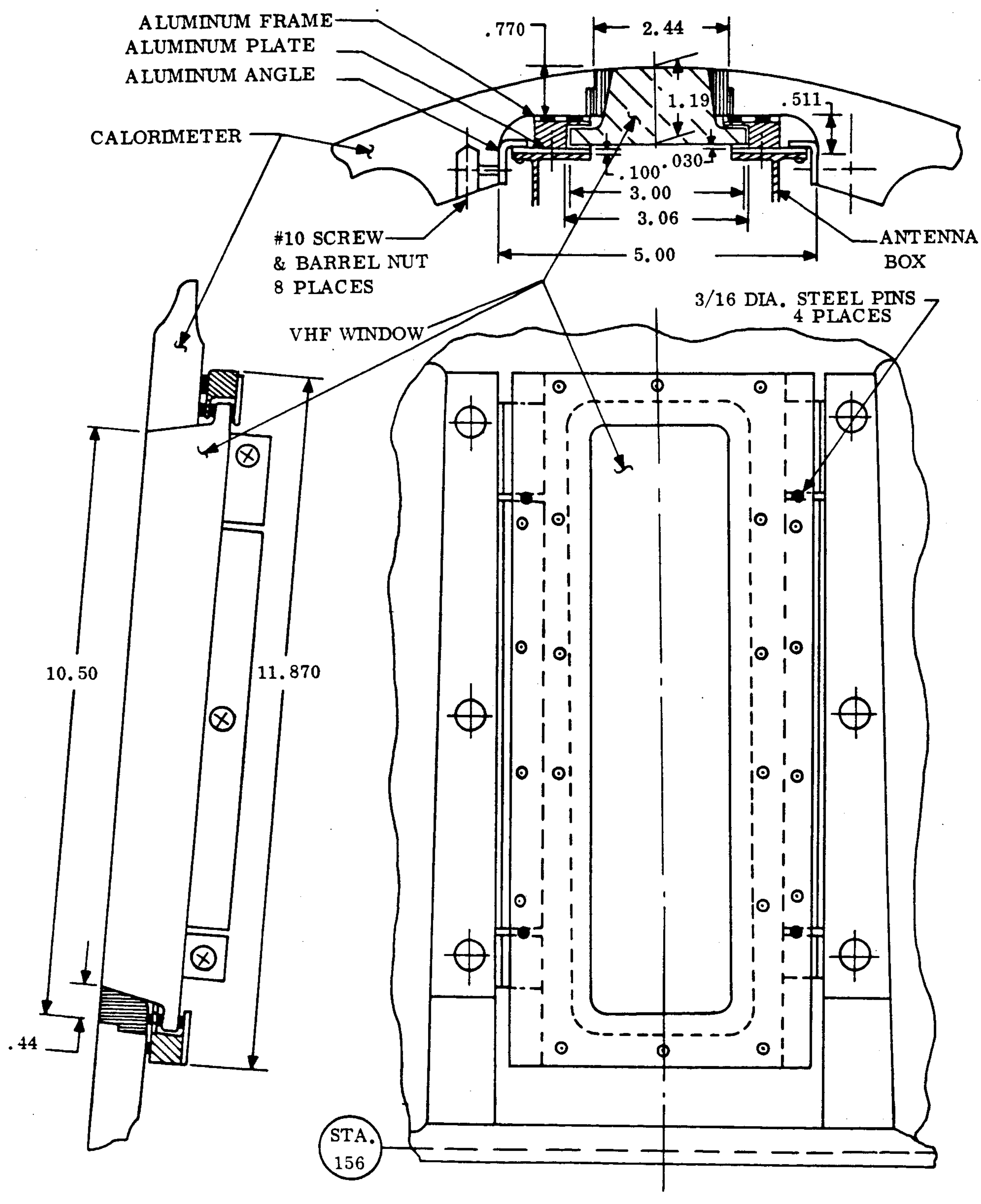

Figure 38. VHF Window Design

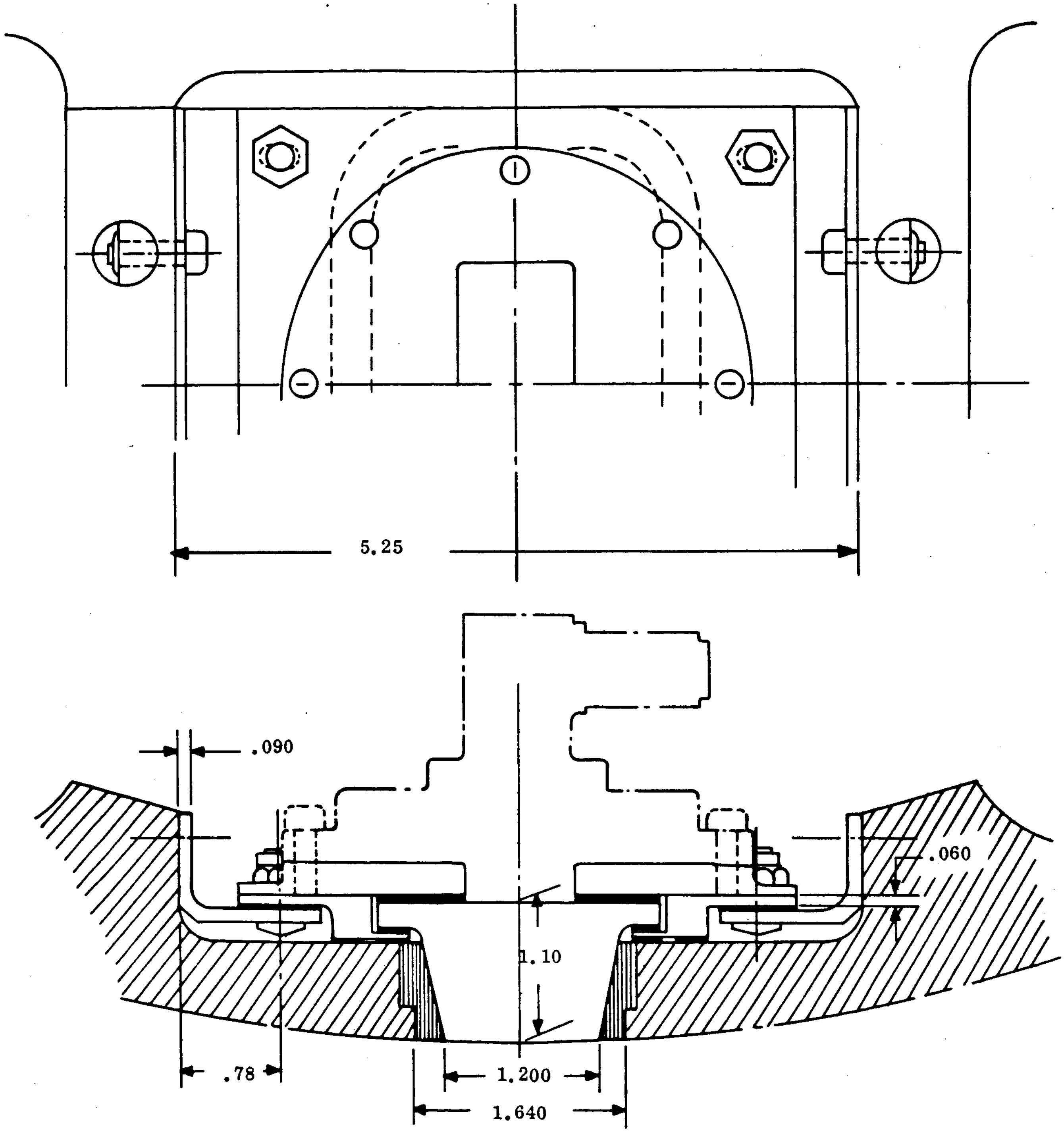

Figure 39. C-Band Window Assembly

170

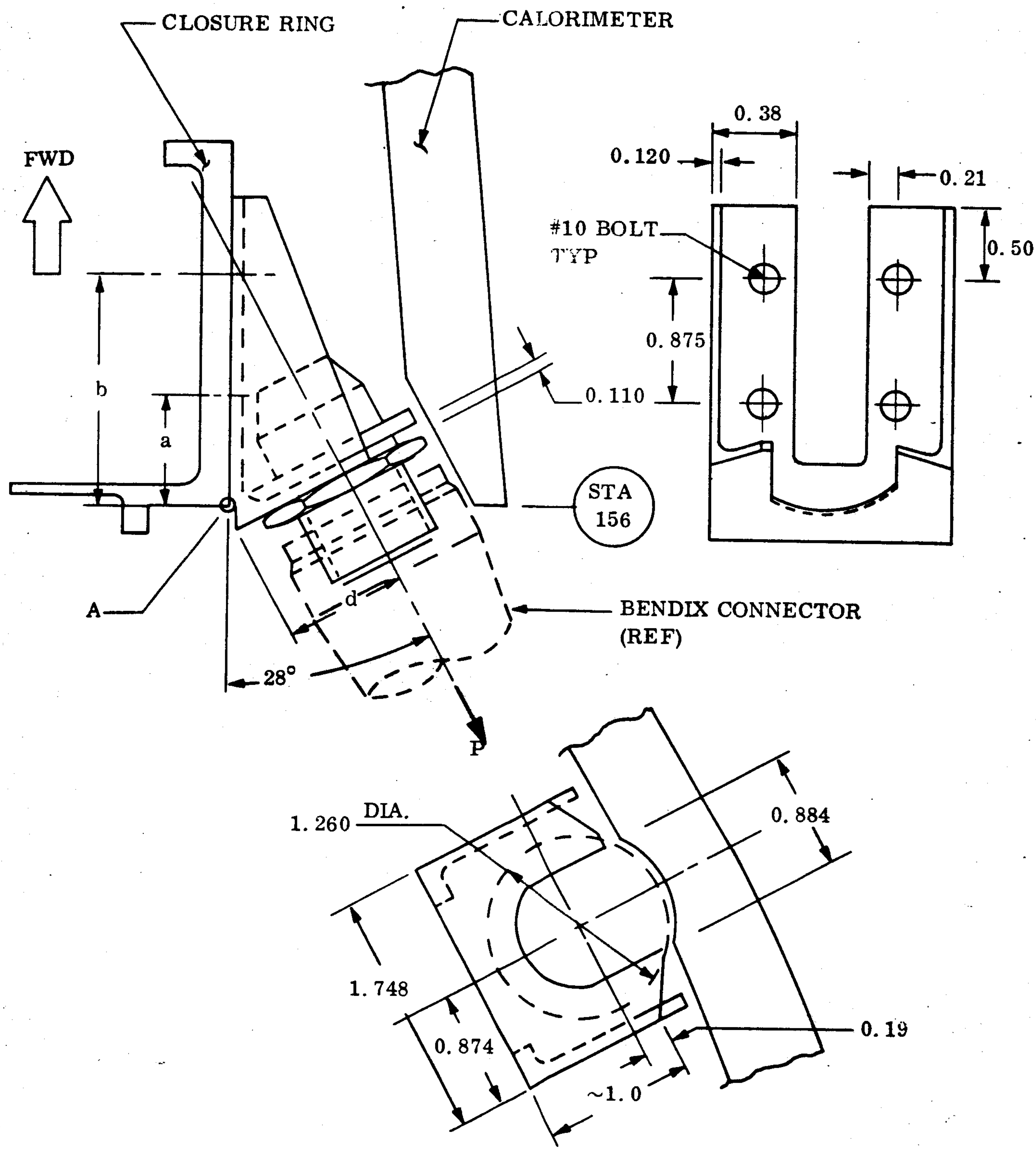

Figure 40. Umbilical Bracket Details

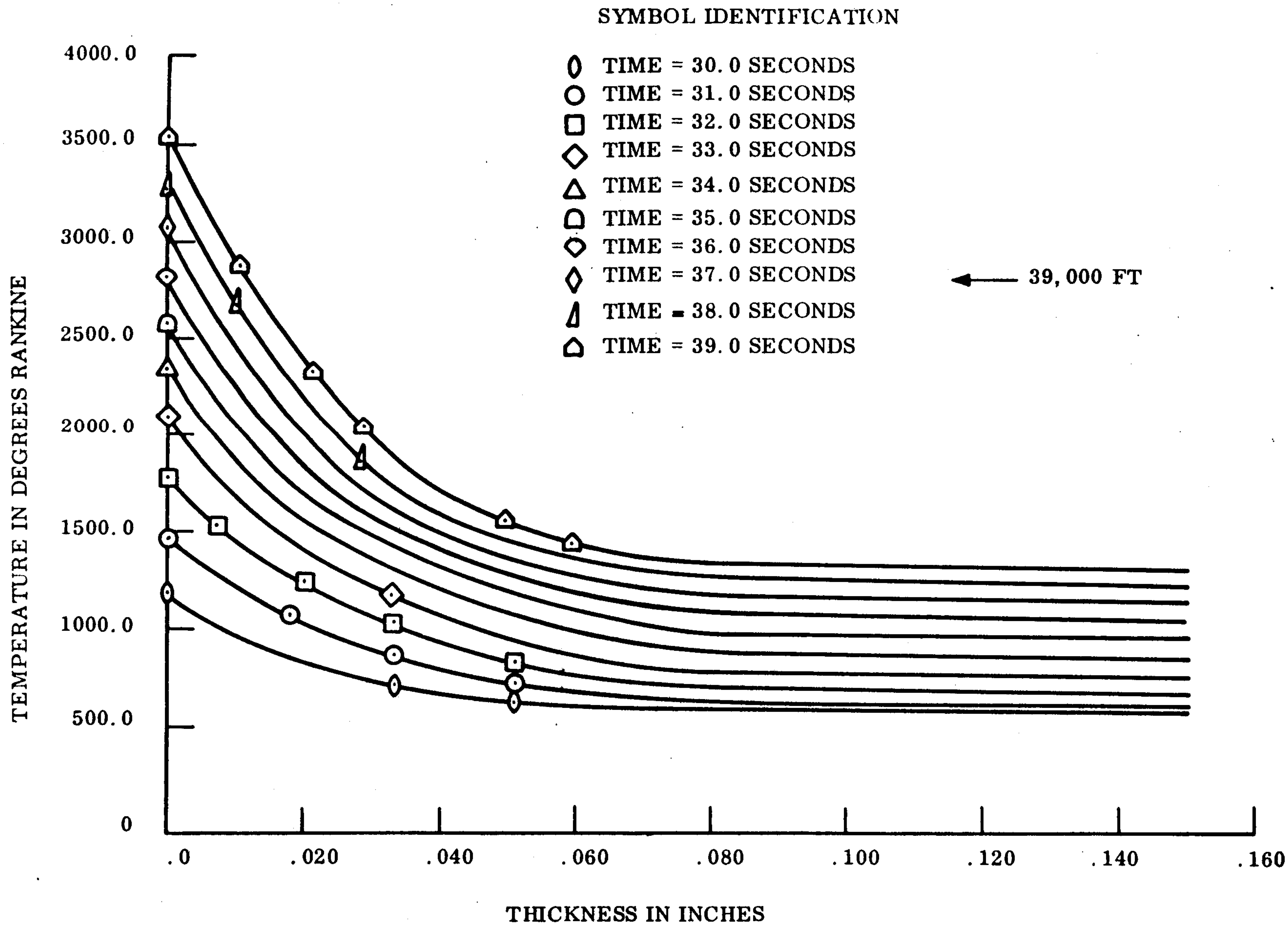

Figure 41. Re-entry-F Aft Cover Analysis . 15 Inch Temperature Profiles

172

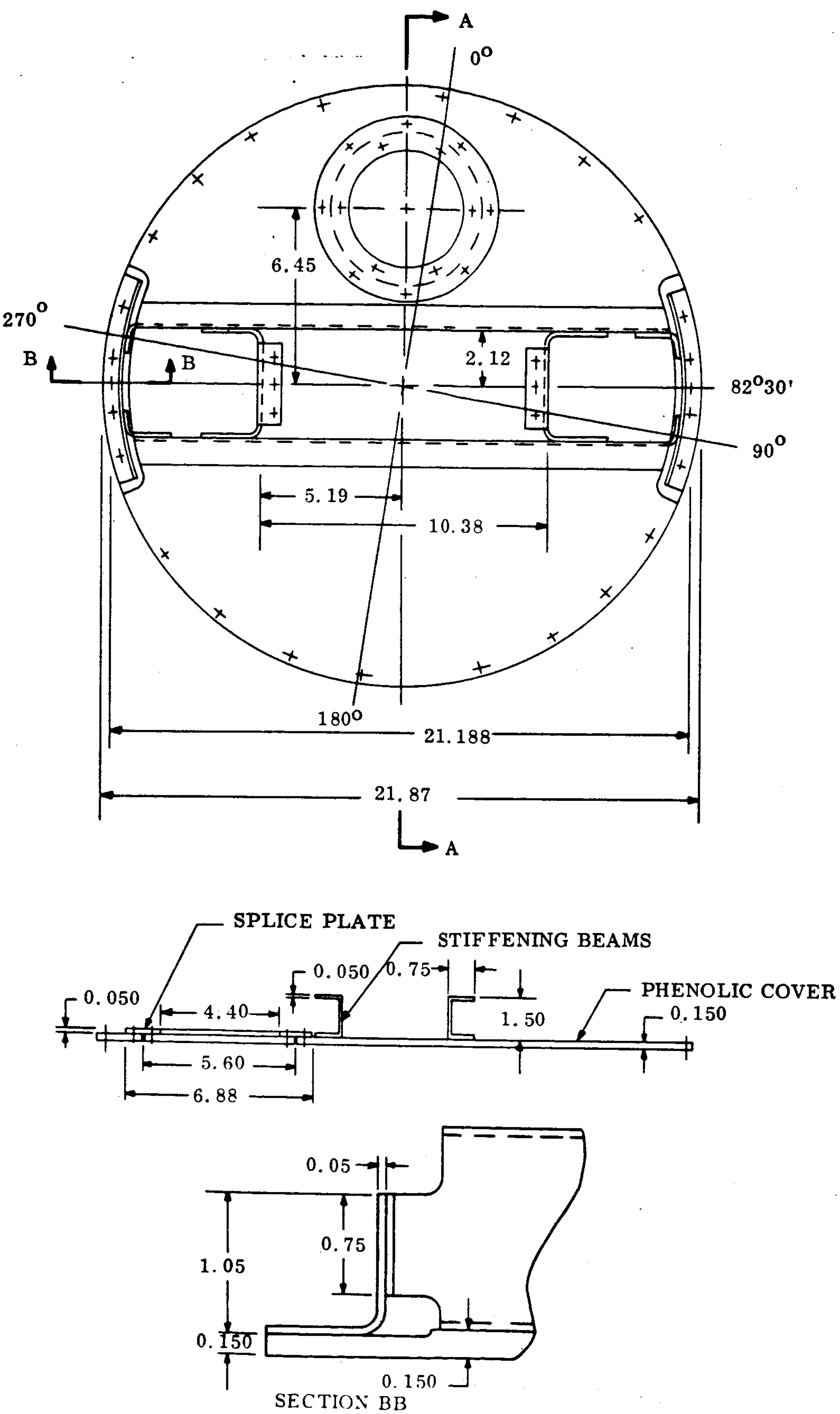

Figure 42. Aft Cover Details

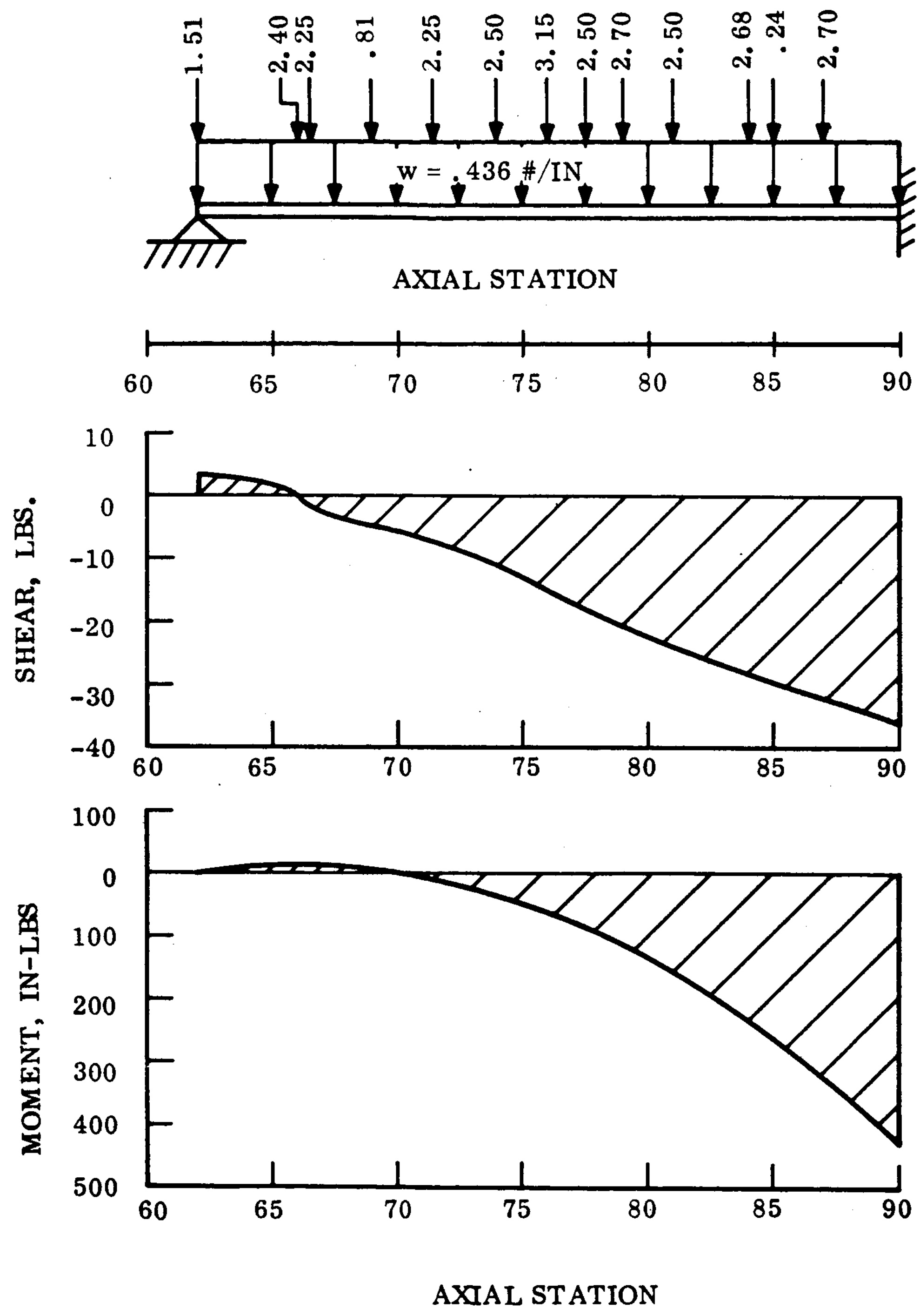

Figure 43. Equipment Package Unit Load Factor Shear and Moment Diagrams

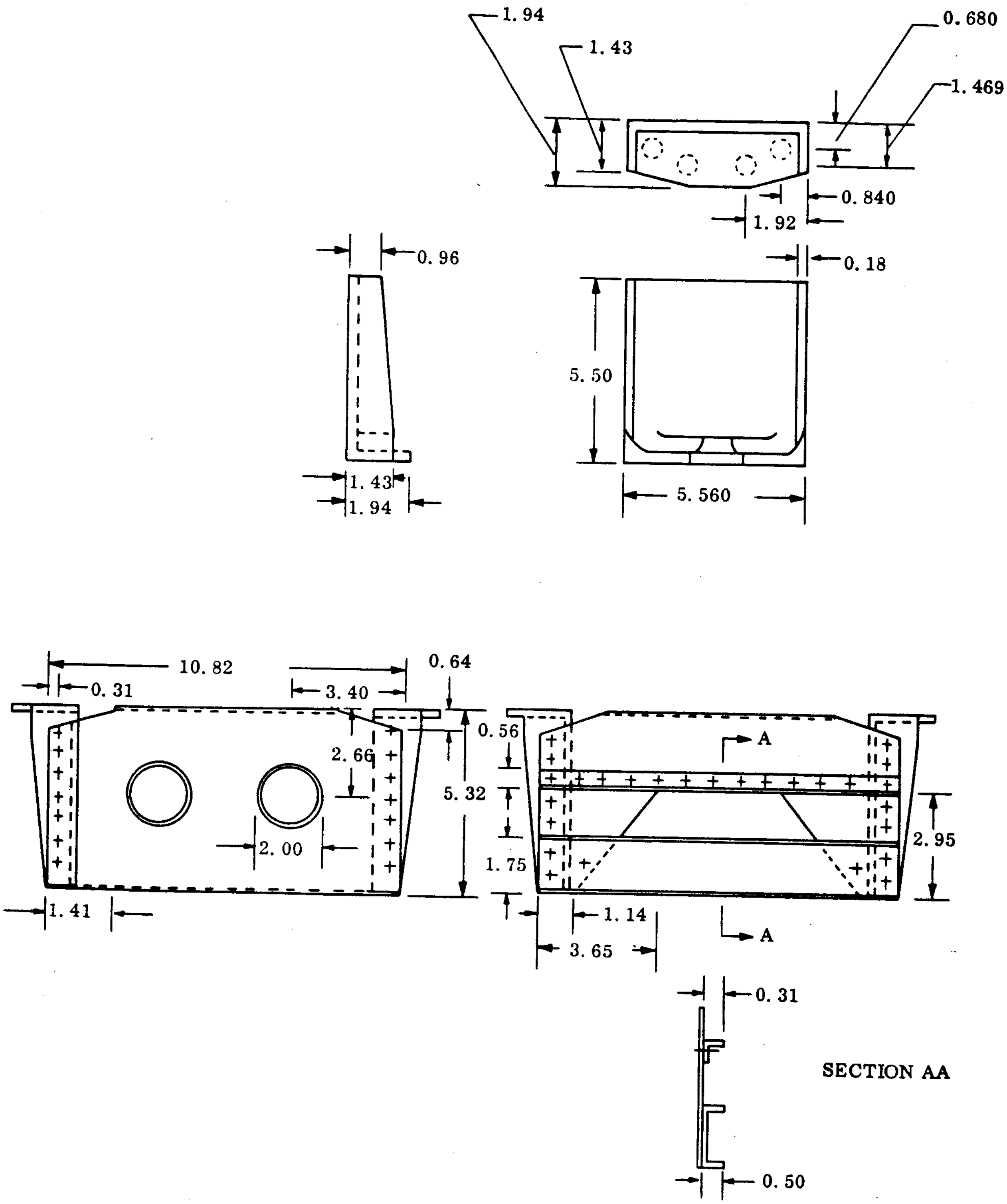

Figure 44. Battery Support Details

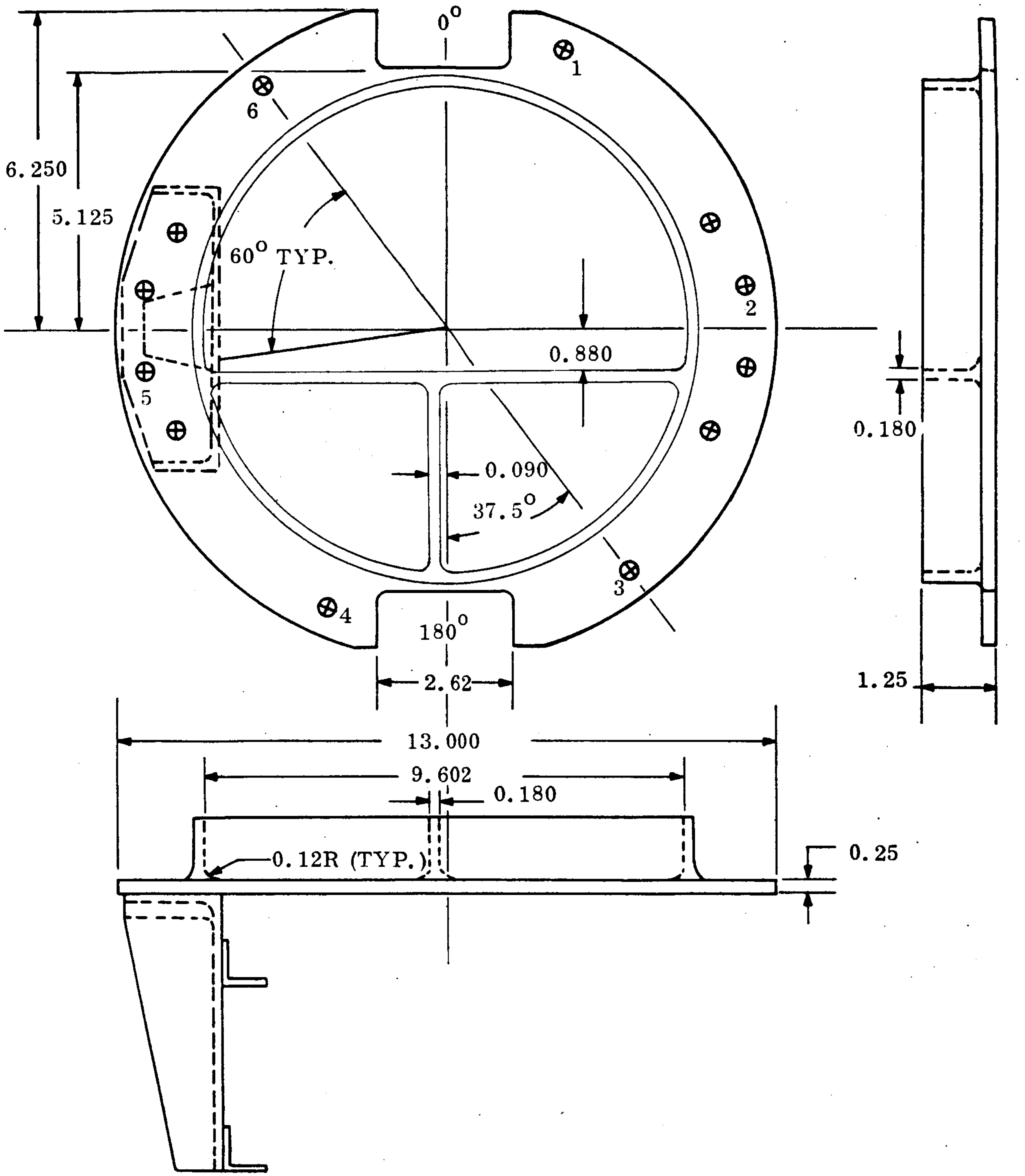

Figure 45. Equipment Package - Aft Bulk-Head

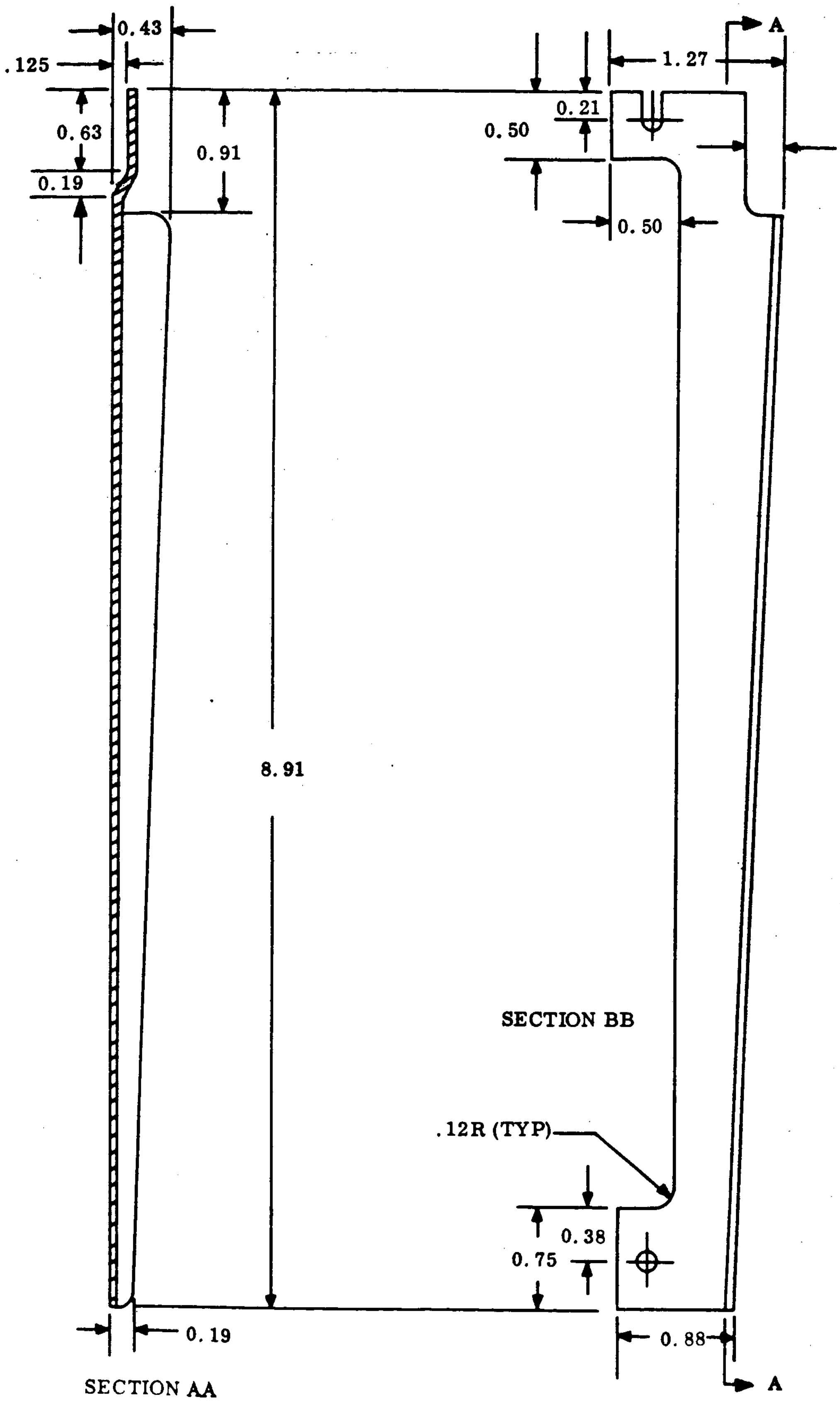

Figure 46. Equipment Package Guide

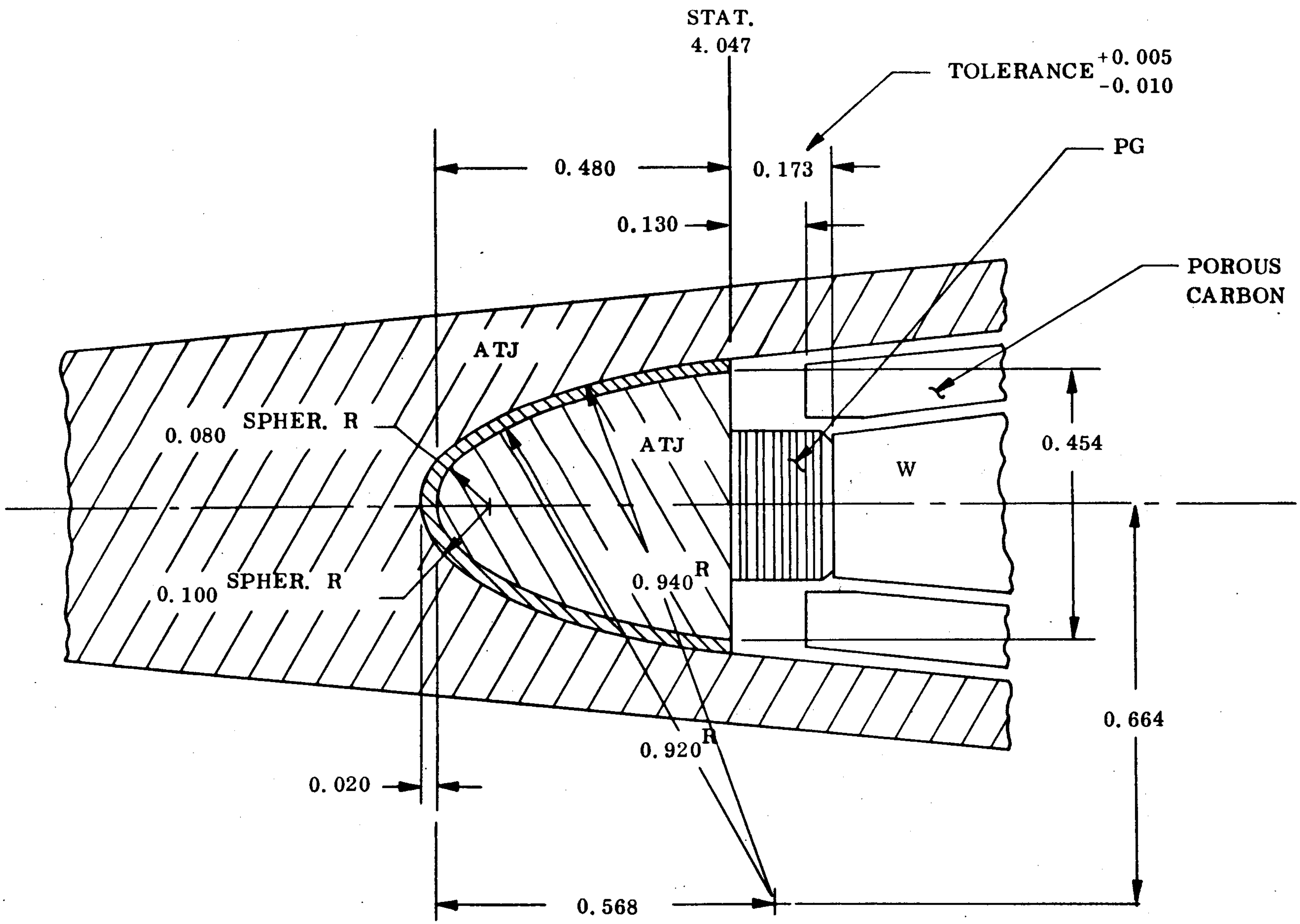

Figure 47. Details of Graphite Plug for Nose Tip

178

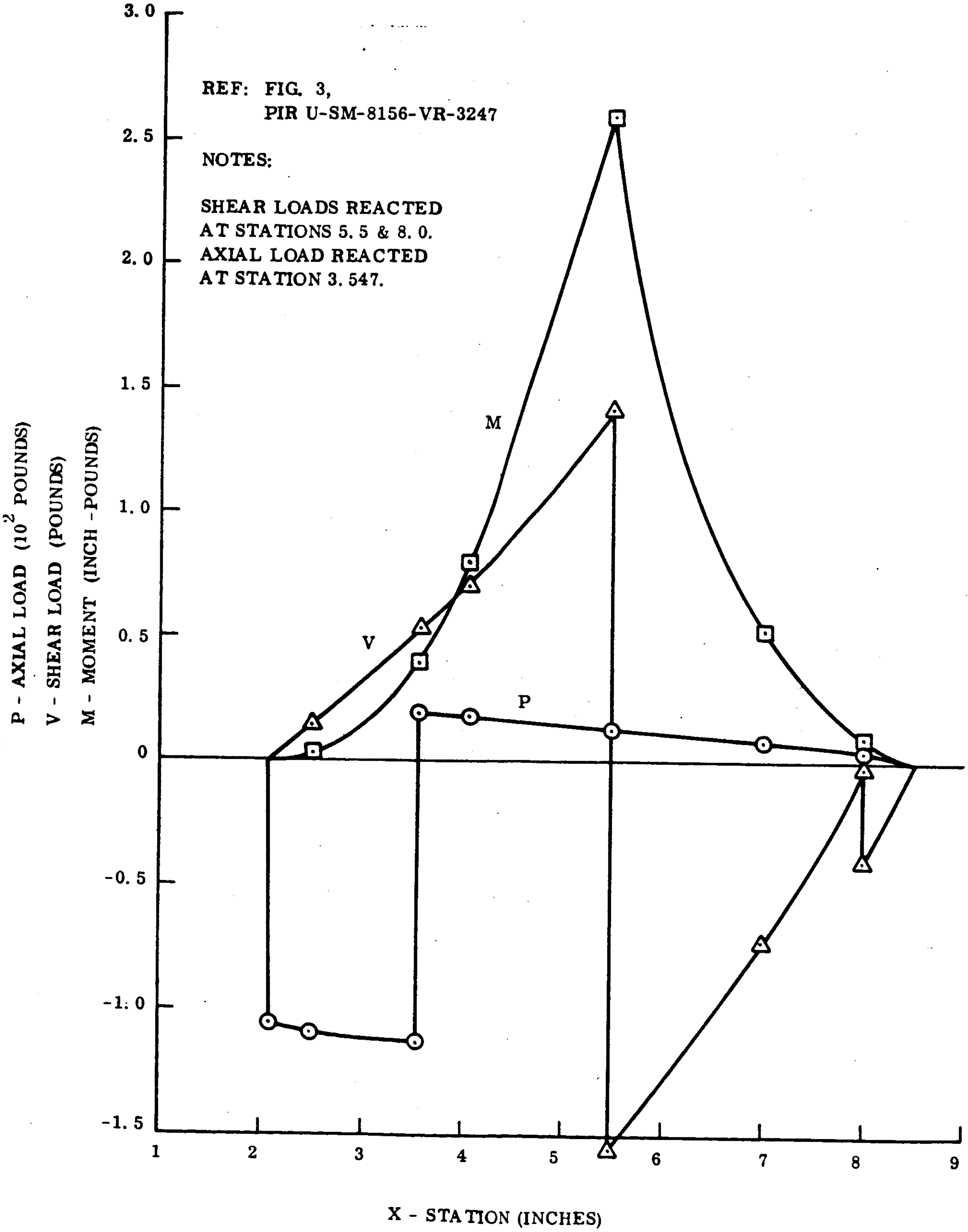

Figure 48. Re-entry Loads in ATJ Nose for C-10 Bond Failure

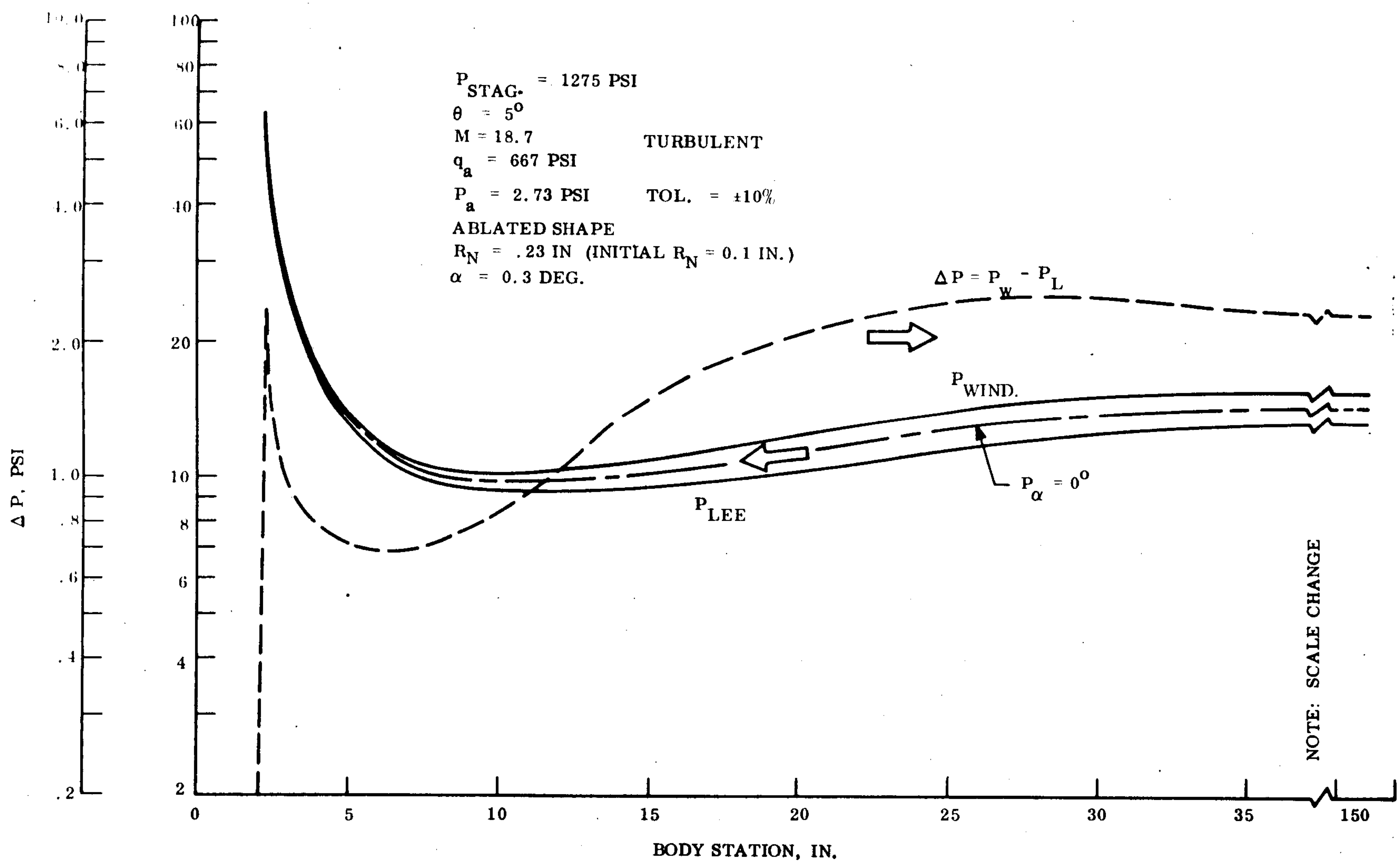

Figure 49. Re-Entry Pressure Distribution

180

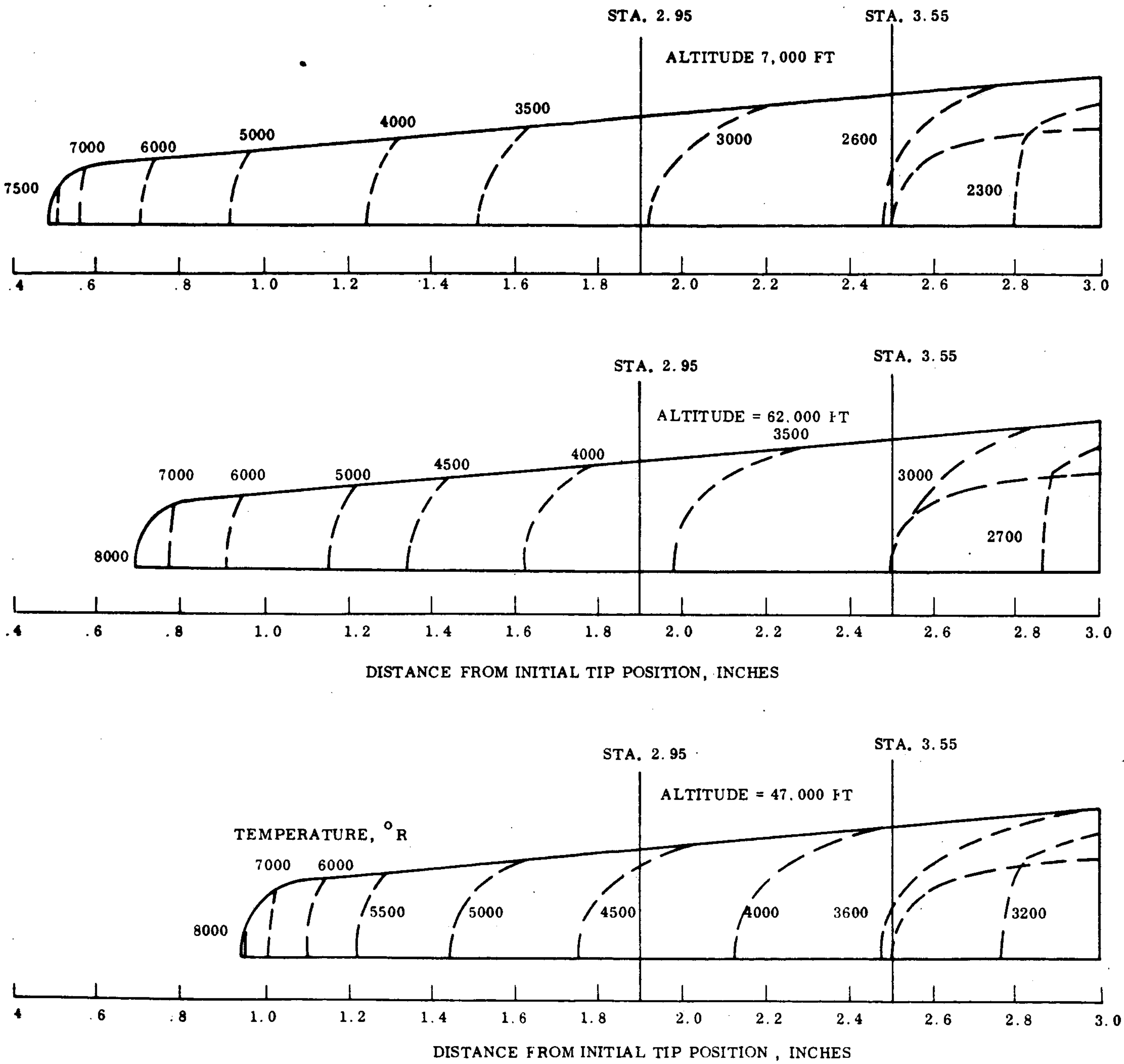

Figure 50. ATJ Shell Thermal Gradient Profiles

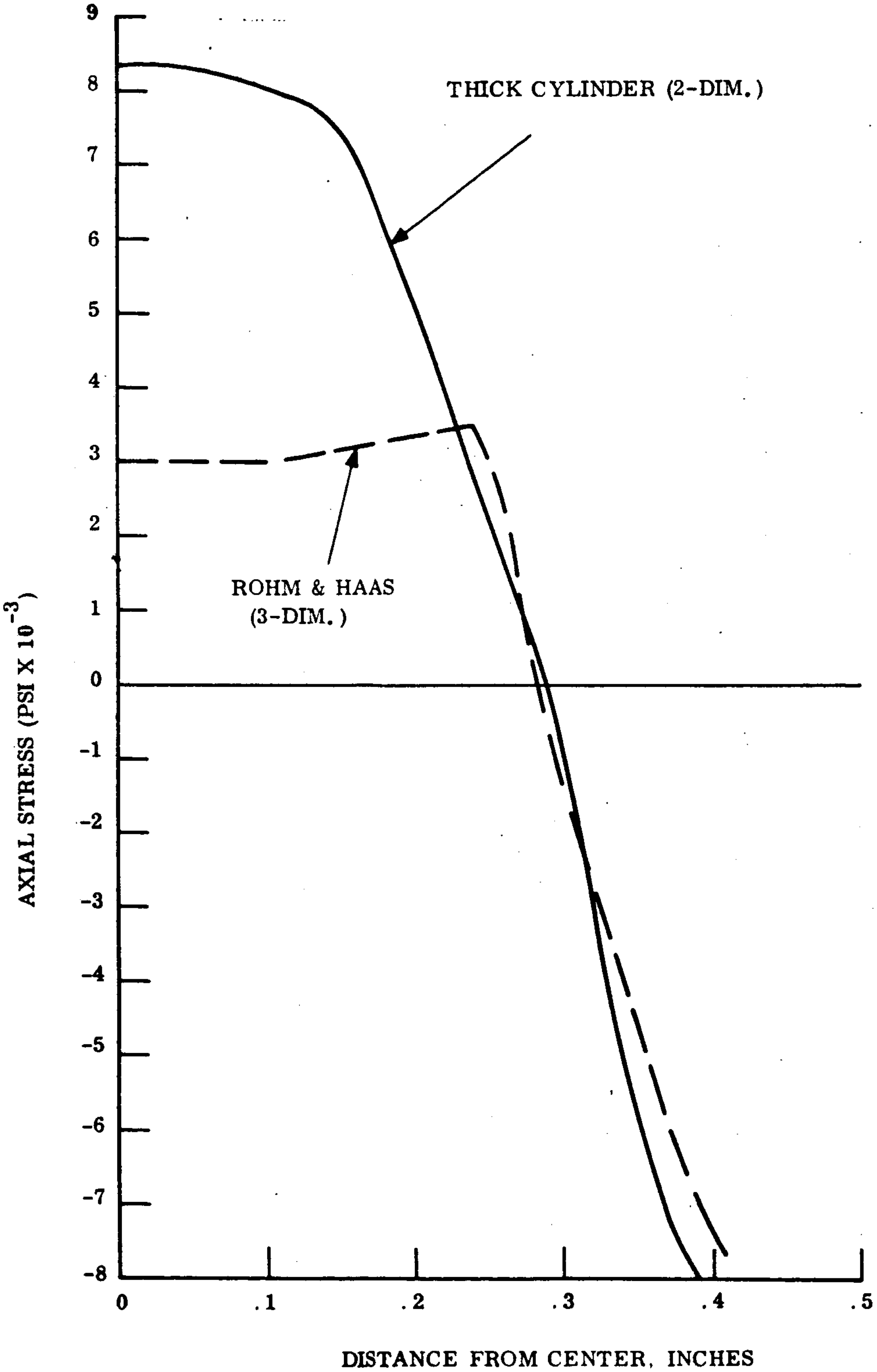

Figure 51. Axial Stress Distribution Thick Cylinder vs. Rohm & Haas Sta. 4.6 On 3.6 In. Orig. Stag. Depth Transition Section

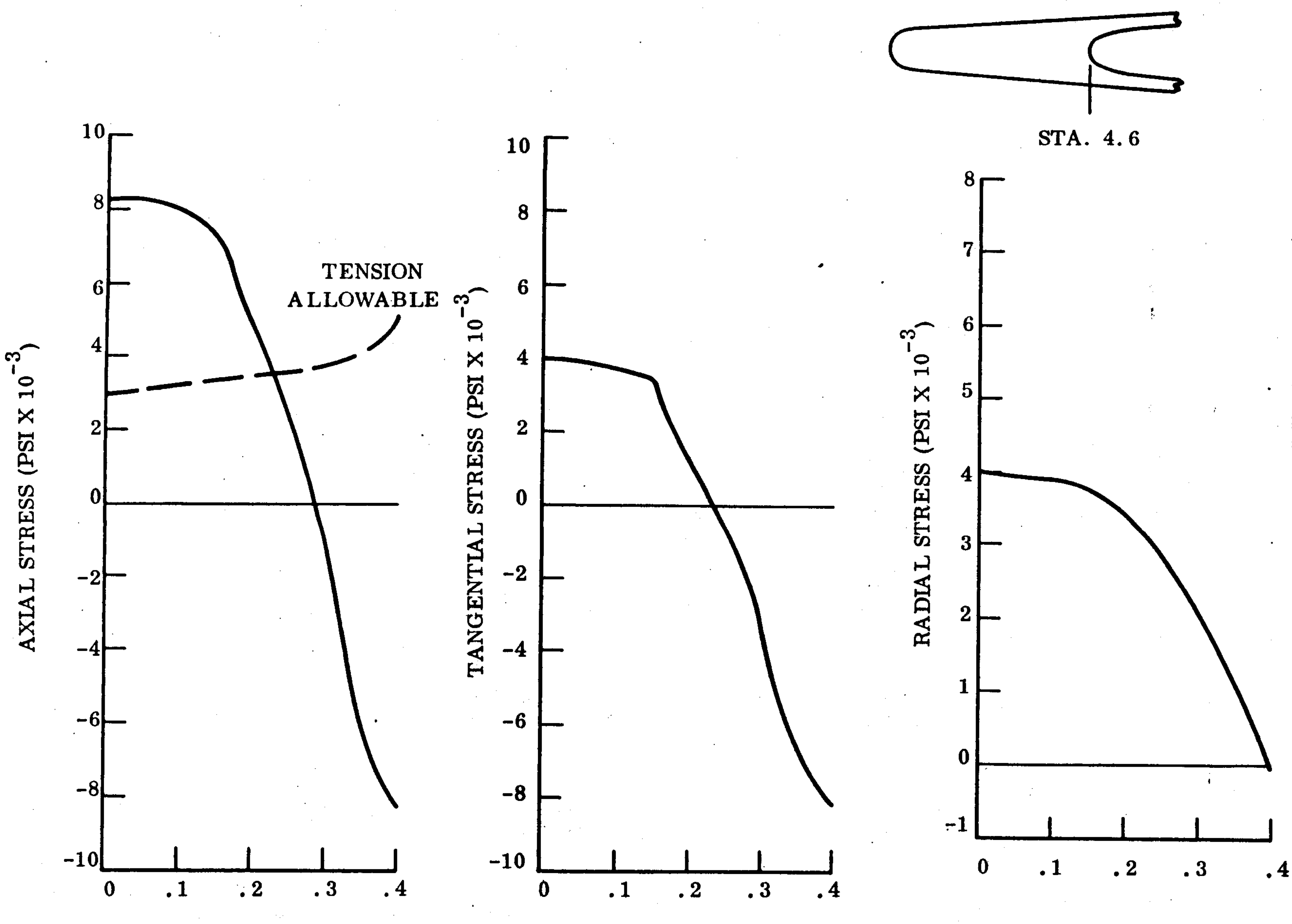

Figure 52. The Re-entry F Stress Distribution ATJ Nose at Sta. 4.6-40,000 Ft. 3.6 In. Orig. Stag. Depth

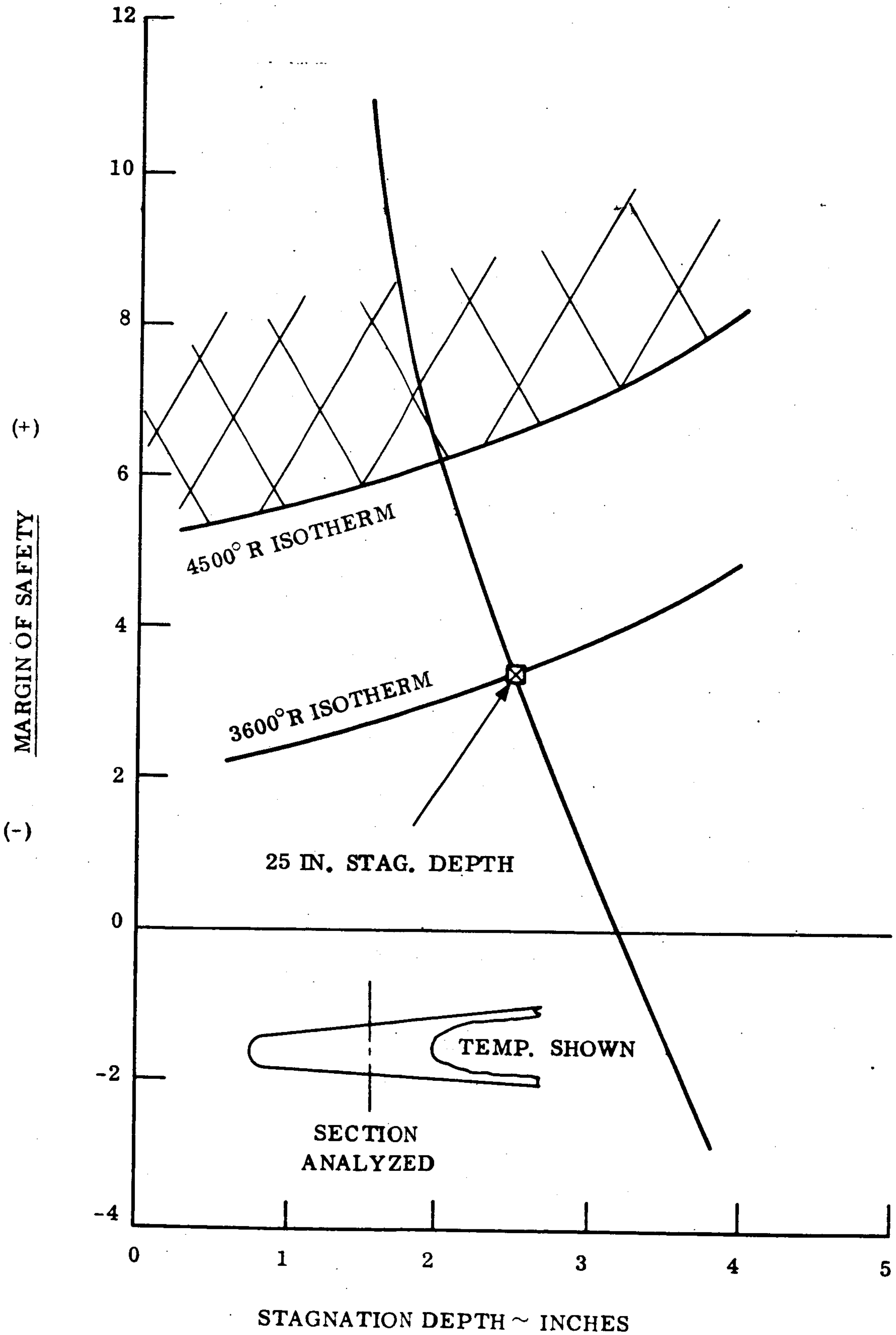

Figure 53. Margin of Safety vs. Stagnation Depth for Re-entry F Nose Design

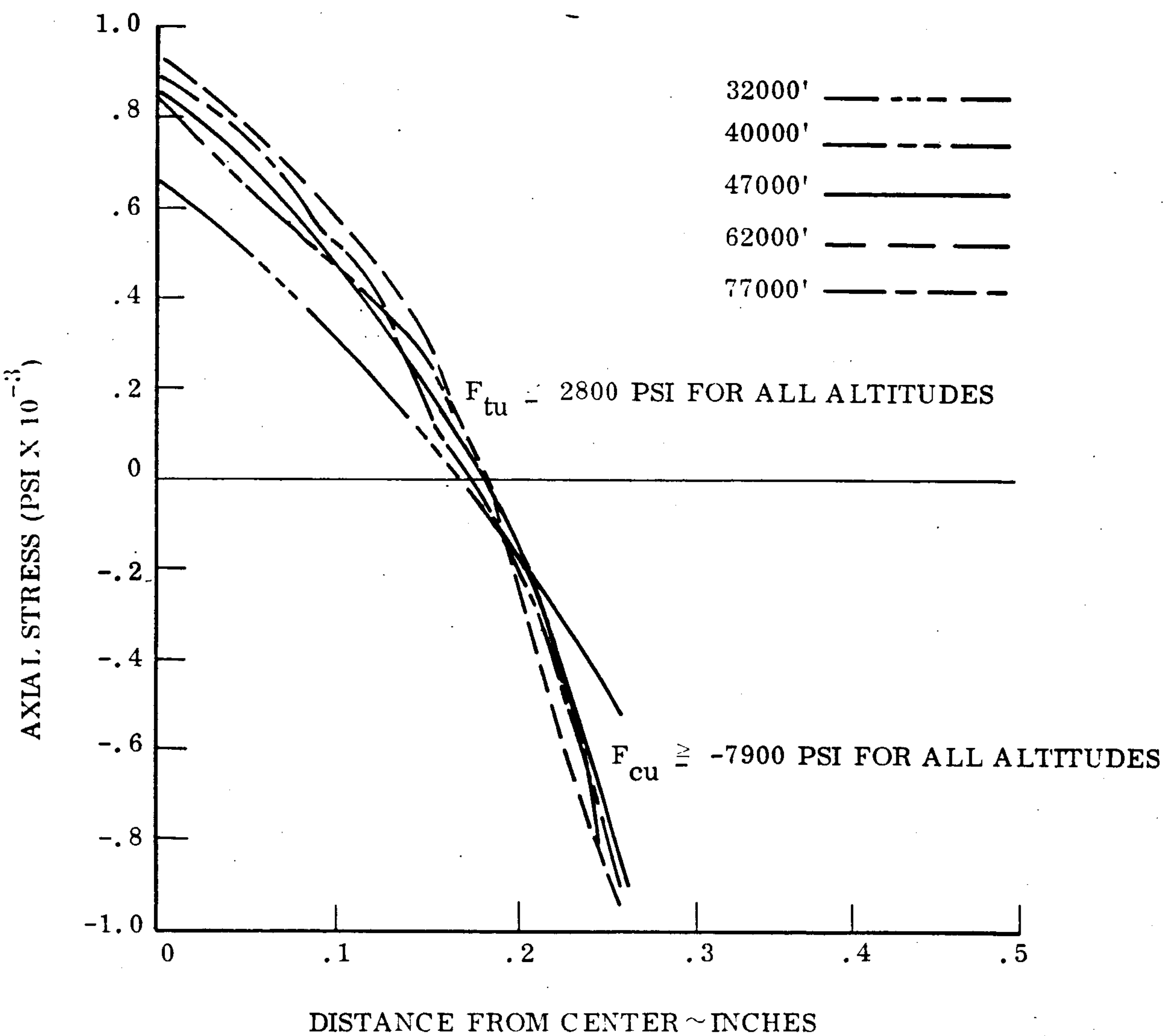

Figure 54. Axial Stress Distribution ATJ Nose at Sta. 2.95 on 2.5 In. Stag. Depth Design

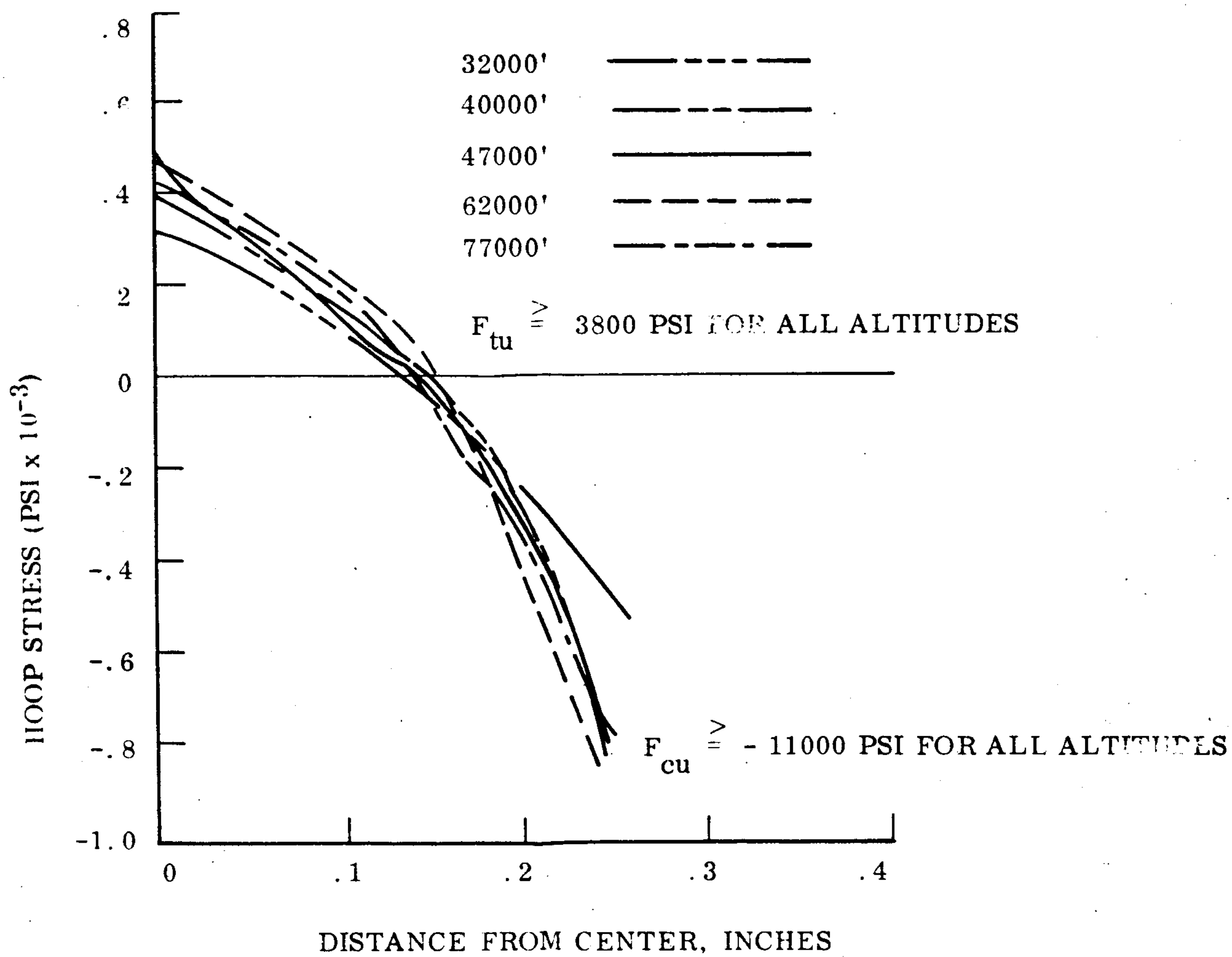

Figure 55. Hoop Stress Distribution ATJ Nose at Sta. 2.95 on 2.5 In. Stag. Depth Design

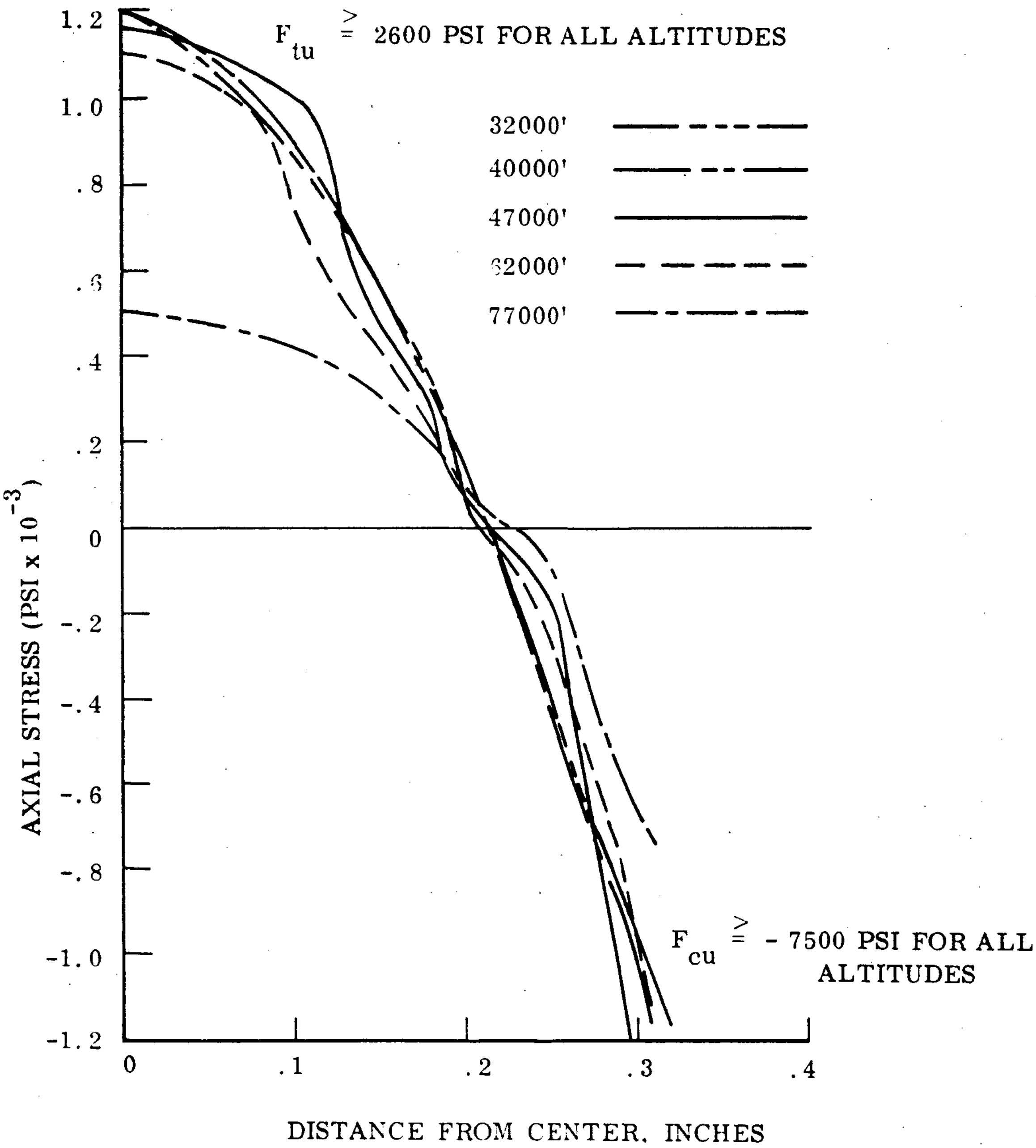

Figure 56. Axial Stress Distribution ATJ Nose at Sta. 3.55 on 2.5 In. Stag. Depth Design

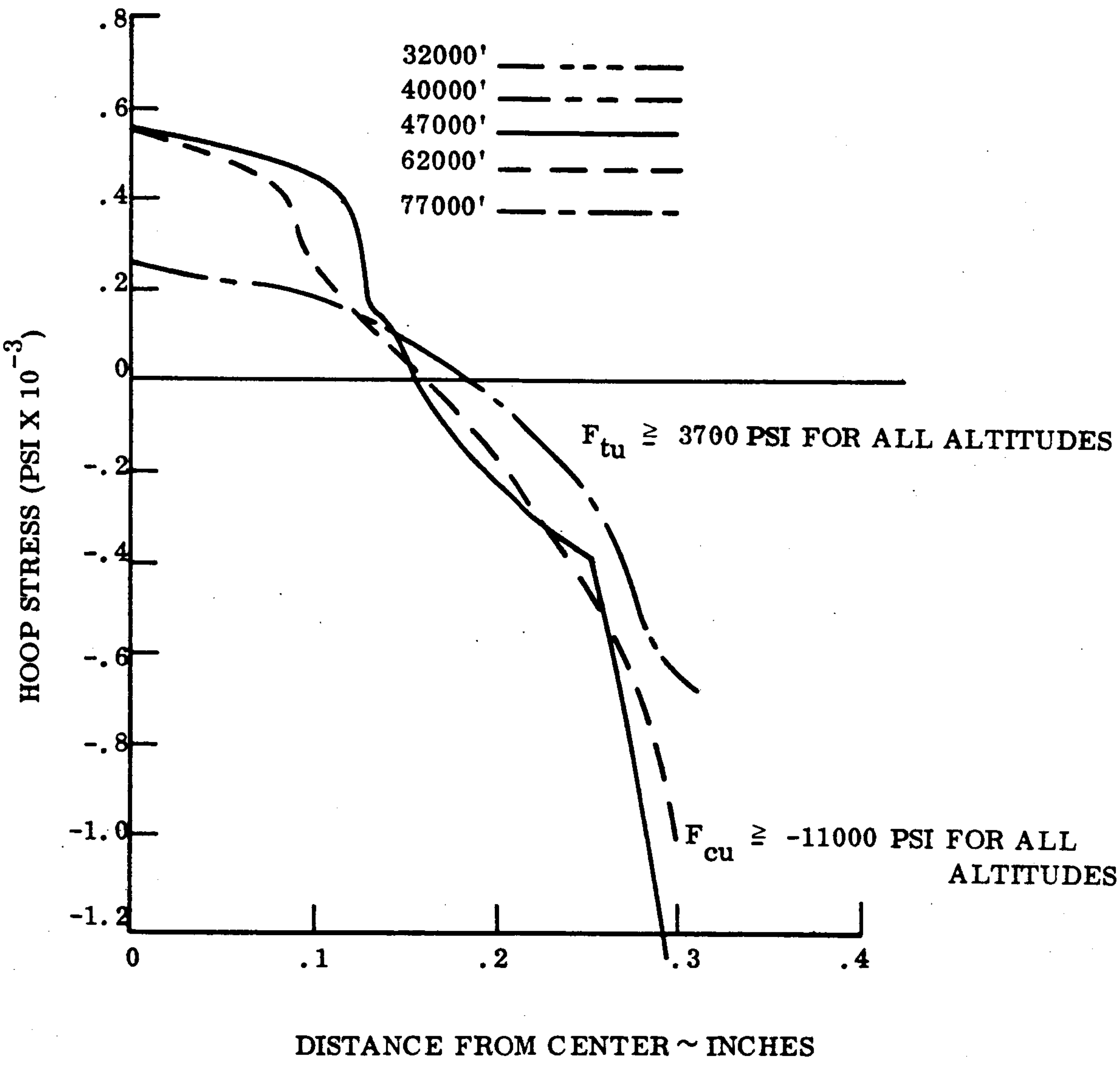

Figure 57. Hoop Stress Distribution ATJ Nose at Sta. 3.55 on 2.5 In. Stag. Depth Design

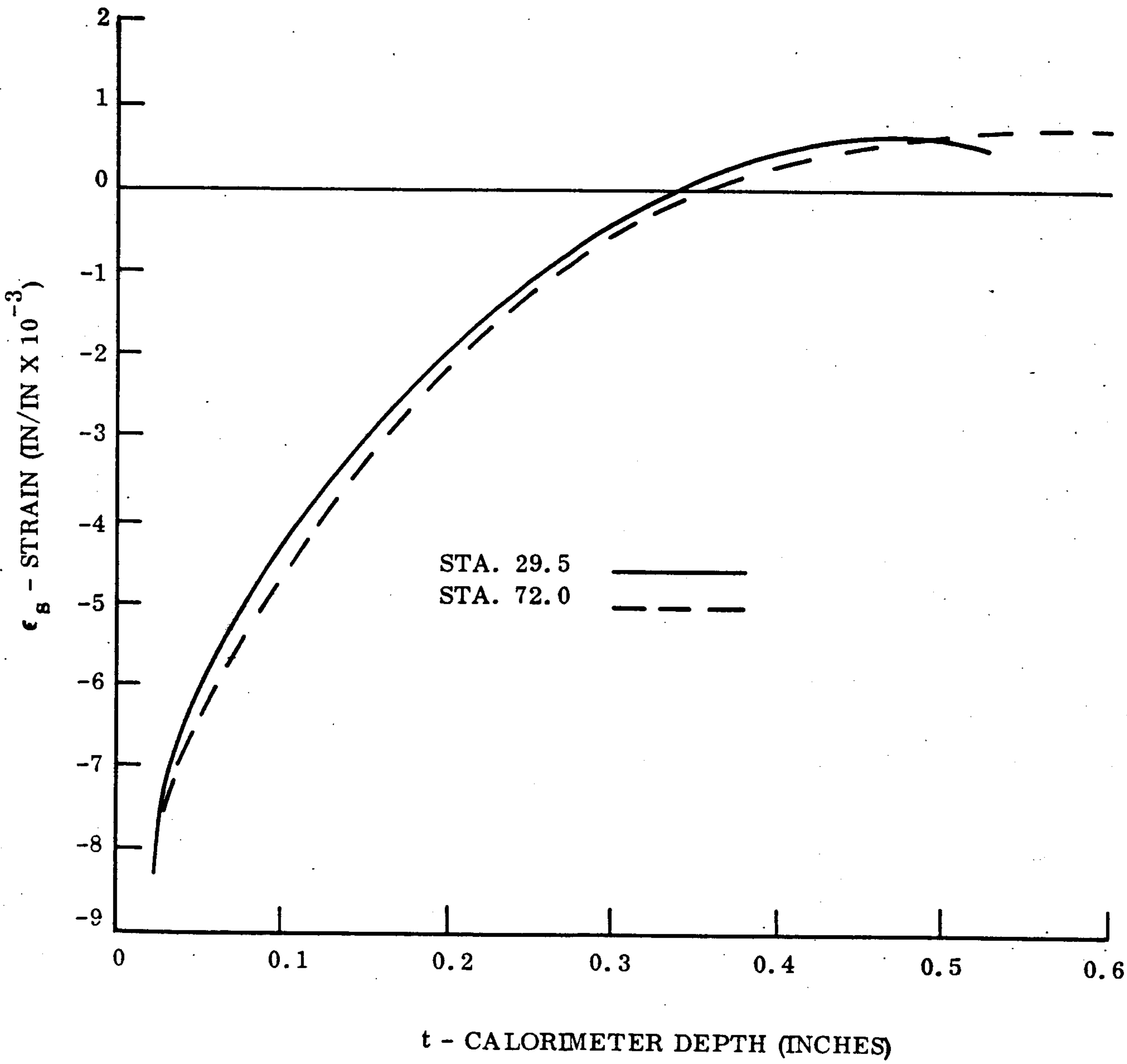

Figure 58. Calorimeter Thermal Strain Re-entry F - Time = 35.5 Secs., 46.3K Feet Altitude

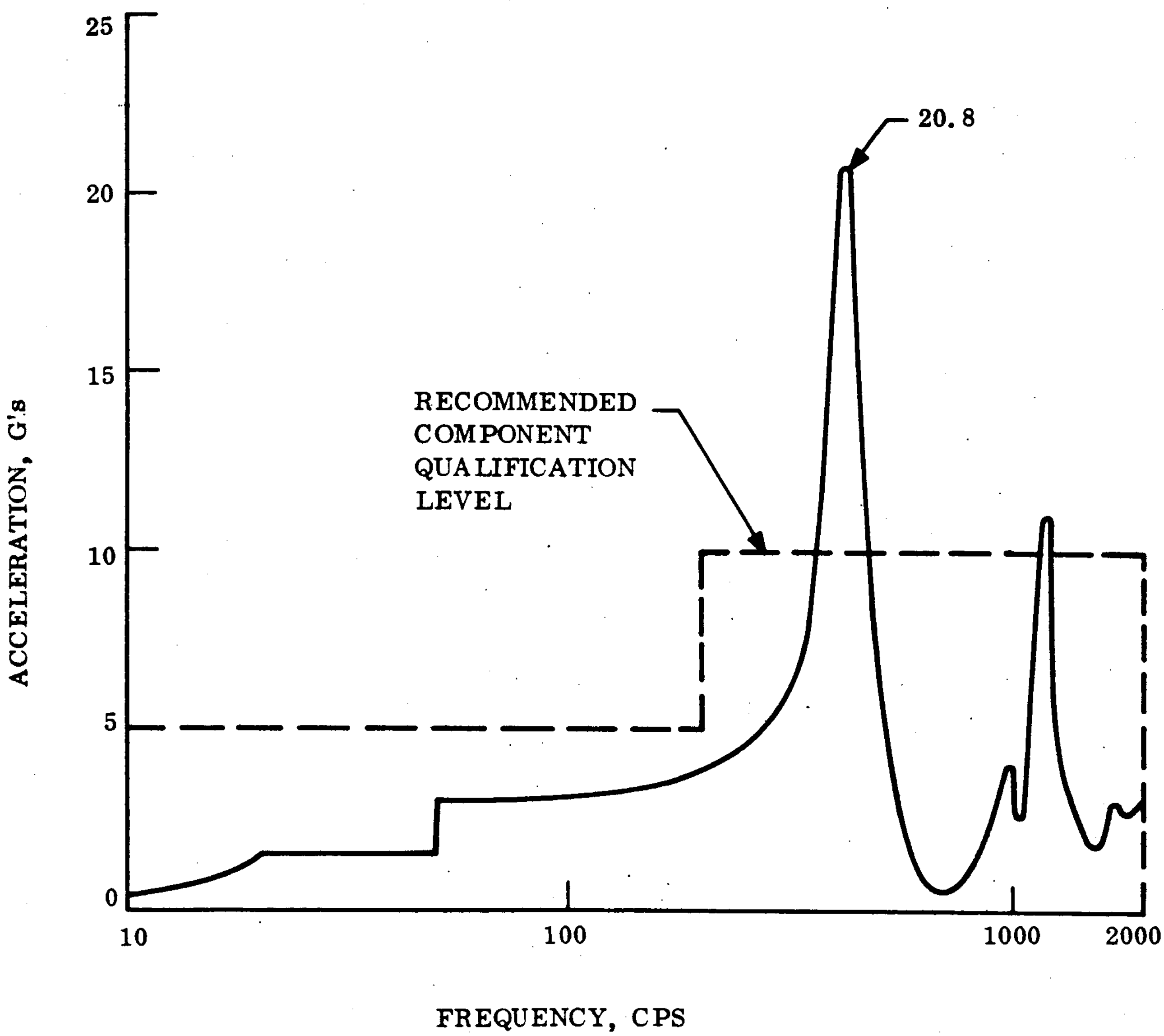

Figure 59. Response at Mass 13 to Axial Sinusoidal System Test

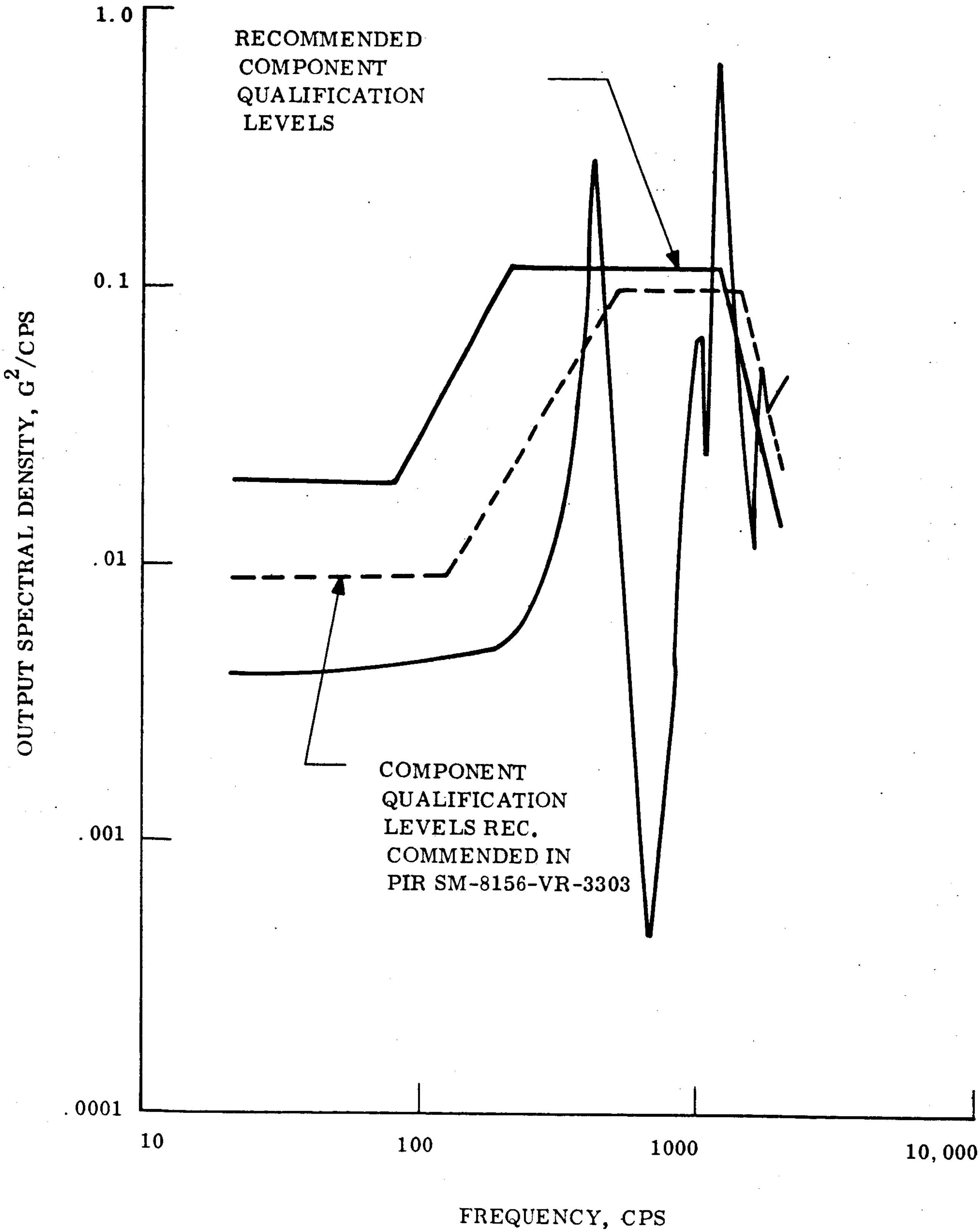

Figure 60. Response at Mass 13 to Axial Random System Test

DISTRIBUTION LIST

J. Bailey		U1235 VF
J. Berman		U3225 VF
W. Castle		7370 EC
E. Cameron		3476 CH
T. Camp		5837 CH
L. Chaump		U1235 VF
P. Cline		U1217 VF
J. Donato		U1235 VF
C. Droms		1026 B CCF #1
H. Eagle		U1226 VF
A. Farnese		3721 CH
R. Fellman		U8632 VF
A. Garbet	(3)	U1235 VF
W. Gunnis		3936 CH
A. Hecht		U1211 VF
M. Herbert		3875 CH
T. Hess		U1226 VF
J. Kallmeyer		3426 CH
G. Kachadourian		U1235 VF
O. Klima		U7211 VF
A. Komisar		5726 CH
F. Lehman		2515M VF
K. Liehr		7370 EC
R. MacIntyre		3491 CH
J. Marron	(5)	7370 EC
D. McGurk		2525B CCF #2
J. McMullen		U1235 VF
R. Newton		U7039 VF
J. Owens		5829 CH
D. Pedicone		3907 CH
D. Podietz		6078 CH
R. Quake		10334 EC
E. Richardson	(20)	3491 CH
G. Ritchie		7370 EC
M. Rosen		6616 CH
J. Sarcinello		6875 CH
C. Seyler		5411 CH
S. Smith	(5)	U3035 VF
J. Stewart		U3035 VF
J. Turner		10331 EC
H. Van Dusen		6026 CCF #1
P. Versage		3907 CH
M. White		8342 EC
R. Williams		8342 EC
J. Yocum		8342 EC
M. O'Connor	(tissue + 3)	7322 EC